INVESTIGATION OF THE EFFECT OF SEMI-GEODESIC WINDING ON THE VIBRATION CHARACTERISTICS OF FILAMENT WOUND SHELLS OF REVOLUTION

A THESIS SUBMITTED TO
THE GRADUATE SCHOOL OF NATURAL AND APPLIED SCIENCES
OF
MIDDLE EAST TECHNICAL UNIVERSITY

BY

CAN SERKAN İBRAHİMOĞLU

IN PARTIAL FULFILLMENT OF THE REQUIREMENTS
FOR
THE DEGREE OF MASTER OF SCIENCE
IN
AEROSPACE ENGINEERING

SEPTEMBER 2010

Approval of the thesis:

INVESTIGATION OF THE EFFECT OF SEMI-GEODESIC WINDING ON THE VIBRATION CHARACTERISTICS OF FILAMENT WOUND SHELLS OF REVOLUTION

submitted by **CAN SERKAN İBRAHİMOĞLU** in partial fulfillment of the requirements for the degree of **Master of Science in Aerospace Engineering Department, Middle East Technical University** by,

Prof. Dr. Canan Özgen
Dean, Graduate School of **Natural and Applied Sciences** _____

Prof. Dr. Ozan Tekinalp
Head of Department, **Aerospace Engineering** _____

Assoc. Prof. Dr. Altan Kayran
Supervisor, **Aerospace Engineering Dept., METU** _____

Examining Committee Members:

Prof. Dr. Yavuz Yaman
Aerospace Engineering Dept., METU _____

Assoc. Prof. Dr. Altan Kayran
Aerospace Engineering Dept., METU _____

Asst. Prof. Dr. Melin Şahin
Aerospace Engineering Dept., METU _____

Asst. Prof. Dr. Demirkan Çöker
Aerospace Engineering Dept., METU _____

Asst. Prof. Dr. Gökhan O. Özgen
Mechanical Engineering Dept., METU _____

Date: 03/09/2010

I hereby declare that all information in this document has been obtained and presented in accordance with academic rules and ethical conduct. I also declare that, as required by these rules and conduct, I have fully cited and referenced all material and results that are not original to this work.

Name, Last name :

Signature :

ABSTRACT

INVESTIGATION OF THE EFFECT OF SEMI-GEODESIC WINDING ON THE VIBRATION CHARACTERISTICS OF FILAMENT WOUND SHELLS OF REVOLUTION

İbrahimoğlu, Can Serkan
M.S., Department of Aerospace Engineering
Supervisor: Assoc. Prof. Dr. Altan Kayran

September 2010, 118 pages

In this thesis, the effect of semi-geodesic winding on the free vibration characteristics of filament wound composite shells of revolution with variable radii of curvature is studied. The analysis is performed by a semi-analytical solution method which is based on the numerical integration of the finite exponential Fourier transform of the fundamental shell of revolution equations. The governing equations for the free vibration analysis are initially obtained in terms of fundamental shell variables, and they are reduced to a system of first order ordinary differential equations by the application of finite exponential Fourier Transform, resulting in a two point boundary value problem. The boundary value problem is then reduced to a series of initial value problems, and the multisegment numerical integration technique is used in combination with the frequency trial method in order to extract the natural frequencies and determine the mode shapes within a given range of natural frequencies. Previous studies on geodesic winding is extended such that the effect of semi-geodesic winding which rely on the preset friction between the fiber and the mandrel surface on the stiffness and vibration characteristics of filament wound shells of revolution is investigated. Additionally, finite element analysis is employed to compare the results obtained from semi-analytical model solved by numerical integration and finite element model solved by finite element method. Sample results are obtained for filament wound truncated conical and spherical shells of revolution and the effect of the winding pattern on the vibration characteristics of shells of revolution is investigated thoroughly.

Keywords: Filament Winding, Free Vibrations, Composite Shells, Shells of Revolution, Semi-geodesic Winding

ÖZ

FİLAMENT SARGI İLE ÜRETİLEN DÖNEL KABUK YAPILARDA YARI-JEODEZİK SARIMIN KABUK YAPILARININ TİTREŞİM ÖZELLİKLERİNE OLAN ETKİSİNİN İNCELENMESİ

İbrahimoğlu, Can Serkan
Yüksek Lisans, Havacılık ve Uzay Mühendisliği Bölümü
Tez Yöneticisi: Doç. Dr. Altan Kayran

Eylül 2010, 118 sayfa

Bu tezde, filament sargı yöntemi ile üretilmiş olan kompozit dönel kabuk yapılarda yarı-jeodezik sarımın kabuk yapılarının serbest titreşim özelliklerine etkisi incelenmiştir. Analiz, sonlu üstel Fourier dönüşüm metodu uygulanmış ana dönel kabuk denklemlerinin sayısal entegrasyonunu temel alan yarı-analitik bir çözüm metoduna dayanır. Ana denklemler temel kabuk değişkenleri ile formüle edilmiş kısmi diferansiyel denklem sistemine dönüştürülmüştür. Sonra bu denklemler iki noktalı sınır değer problemi olacak şekilde sonlu üstel Fourier dönüşüm metodu uygulanarak birinci dereceden adi diferansiyel denklemlere dönüştürülmüştür. Sınır değeri problemi bir grup başlangıç değer problemine dönüştürülmüş ve verilen doğal frekans aralığındaki kritik modlar frekans deneme metodu ile bütünleşik çok parçalı sayısal integrasyon metodu kullanılarak bulunmuştur. Filament sargı işlemi sırasında fiber ve mandrel yüzeyi arasındaki sürtünmeye bağlı olan yarı-jeodezik sarımın filament sargı metodu ile üretilen dönel kabuk yapılarının sertlik ve serbest titreşim özelliklerine etkisi incelenerek, önceden jeodezik sarım üzerine yapılmış araştırmalar genişletilmiştir. Ayrıca seçilmiş yapılar için sonlu elemanlar analizi gerçekleştirilerek yarı-analitik sayısal entegrasyon metodu sonuçları ile karşılaştırılmıştır. Örnek sonuçlar kesik kompozit konik ve küresel dönel kabuk yapılar için elde edilmiş ve sarım paterninin dönel kabuk yapıların titreşim özelliklerine olan etkisi derinlemesine incelenmiştir.

Anahtar kelimeler: Filament Sargı, Serbest Titreşim, Kompozit Kabuklar, Dönel Kabuklar, Yarı-jeodezik Sarım

ACKNOWLEDGEMENTS

The author wishes to express his deepest gratitude to his supervisor *Assoc. Prof Dr. Altan Kayran* for his guidance, advice, tireless help and encouragement.

The author would also like to thank his friends and parents for supporting him.

TABLE OF CONTENTS

LIST OF TABLES

TABLES

LIST OF FIGURES

FIGURES

LIST OF SYMBOLS

1, 2, 3	: Principal material coordinates
A_1, A_2	: Lamé parameters for a shell.
A_ϕ, A_θ	: Lamé parameters for a shell of revolution.
A_{ij}	: Extensional stiffness matrix which relates the in-plane stress resultants to the reference surface strains where (i,j=1,2,6).
A_{12}	: Extension-extension coupling
A_{i6}	: Extension-shear couplings (i=1,2)
As_{45}	: Transverse shear coupling between the shear strain in the $\phi-\zeta$ plane and shear strain in the $\theta-\zeta$ plane.
As_{ij}	: Transverse shear stiffness matrix which relates the transverse shear resultants to transverse shear strains where (i,j=4,5).
$\vec{b}$	: The binormal vector.
B_{ij}	: Bending-stretching coupling matrix which relates the in-plane stress resultants and bending and twisting moment resultants to curvature and twist changes of the reference surface where (i,j=1,2,6).
B_{i6}	: Extension-twist and bending-shear coupling (i=1,2)
$\vec{c}$	: The unit curvature vector
$\boldsymbol{C}_M$	: The characteristic matrix in order to calculate the natural frequencies obtained after the application of boundary conditions with the multisegment numerical integration method in combination with the frequency trial method.

C_{ijkl} : Stiffness tensor or the material coefficients.

D_{ij} : Bending stiffness matrix which relates the bending and twisting moments to curvature and twist changes of the reference surface where (i,j=1,2,6).

D_{i6} : Bending-twist coupling (i=1,2)

E_1 : The Young's modulus in the 1-direction.

E_2 : The Young's modulus in the 2-direction.

E_3 : The Young's modulus in the 3-direction.

$\vec{f}_t$: The fiber tension.

$\vec{f}_r$: Change in the fiber tension per unit length of the mandrel surface.

$\vec{f}_n$: The normal component of $\vec{f}_r$.

$\vec{f}_b$: The transverse component of $\vec{f}_r$.

fst : The preset slippage tendency.

$\vec{\Gamma}(s)$: A fiber path on the surface of a shell of revolution.

G_{23} : The Shear Modulus in the 2-3 direction.

G_{13} : The Shear Modulus in the 1-3 direction.

G_{12} : The Shear Modulus in the 1-2 direction.

h : Total thickness of the laminate of the shell.

i : Imaginary quantity where it equals to $\sqrt{-1}$.

$\boldsymbol{K}(\phi)$: The 20x20 coefficient matrix whose elements are given in Appendix F.

n : The wave number in the circumferential direction of the shell.

M_ϕ, $M_{\phi\theta}$: Normal and twisting moment resultants in the fundamental variables.

$\vec{n}$: Normal vector to the fiber path.

N_ϕ, $N_{\phi\theta}$: Normal and shear force resultants in the fundamental variables.

Q_{ij} : The reduced stiffnesses.

$\overline{Q}_{ij}$: The transformed reduced stiffnesses.

Q_{ξ_1} : The shear force resultant per unit length acting on the face perpendicular to the ξ_1 coordinate and is parallel to ζ -direction.

Q_{ξ_2} : The shear force resultant per unit length acting on the face perpendicular to the ξ_2 coordinate and is parallel to ζ -direction.

Q_ϕ : Transverse force resultant in the fundamental variables.

R : The mean radius of the shell of revolution at a specific meridional location

R_1 : The mean radius of the shell of revolution at the location where the filament winding process is initiated.

$\vec{S}(x,\theta)$: Surface definition of a shell of revolution.

$\vec{S}_x$: The normalized basis vector in the x direction.

$\vec{S}_\theta$: The normalized basis vector in the θ direction.

t : The thickness of a single ply at the axial location .

t_1 : The thickness of a single ply at one edge of the shell where the radius is R_1 .

t : Time.

$\vec{t}$: The tangent vector to the fiber path

$\boldsymbol{T}(\phi)$: The transfer matrix of the shell, and it depends only on the geometric and material properties of the shell given by the coefficient matrix $\boldsymbol{K}(\phi)$.

$\boldsymbol{T}^i(\phi)$: The 10x10 partitioned matrix of $T(\phi)$.

$\boldsymbol{T}_i(\phi)$: The transfer matrix of a segment i.

u^0, v^0, w^0 : The displacements of a point on the reference surface of the shell in ξ_1, ξ_2, ζ coordinates, respectively.

$w^0, u_\phi^0, u_\theta^0$: Displacements in the fundamental variables.

α : The fiber orientation angle.

α_1 : The initial winding angle of the fibers.

β_1 : The rotation of a transverse normal about the ξ_2 -curvilinear coordinate.

β_2 : The rotation of a transverse normal about the ξ_1 -curvilinear coordinate.

β_ϕ, β_θ : Rotations in the fundamental variables.

γ_{12} : The inplane shearing strain.

$\gamma_{1\zeta}$: The transverse shear strain whose normal is in 1-direction.

$\gamma_{2\zeta}$: The transverse shear strain whose normal is in 2-direction.

γ_i^0 : Shearing strains of the reference surface of the shell (i=1-2).

ε_1 : The inplane normal strain component in 1-direction.

ε_2 : The inplane normal strain component in 2-direction.

ε_i^0 : Normal strains of the reference surface of the shell (i=1-2).

ζ : The thickness coordinate of a shell of revolution.

θ : The tangential coordinate of a shell of revolution.

κ_i : The curvature changes of the reference surface of the shell (i=1-2).

ν_{ij} : Poisson's ratio.

ξ_1, ξ_2, ζ : The orthogonal curvilinear coordinate system of a doubly curved shell.

ρ : The overall density of the composite laminate of the shell.

ϕ : The meridional coordinate of a shell of revolution.

ϕ, θ, ζ : The orthogonal curvilinear coordinate system of the reference surface of a shell of revolution.

$\boldsymbol{\psi}$: The column vector of fundamental variables.

ω : Dimensional natural frequency.

Ω : Non-dimensional natural frequency $\left(= \omega h \sqrt{\rho / E_1}\right)$.

CHAPTER 1

INTRODUCTION

1.1 BACKGROUND

The word composite in the term of composite material signifies that two or more materials are combined on a macroscopic scale to form a useful third material. The key is the macroscopic examination of a material wherein the components can be identified by the naked eye. Composite materials have a long history of usage. Their precise beginnings are unknown, but all recorded history contains references to some form of composite material. For example, straw was used to strengthen mud bricks by many civilizations. Plywood was used by the ancient Egyptians when they realized that wood could be rearranged to achieve superior strength and resistance to thermal expansion as well as to swelling caused by the absorption of moisture. Medieval swords and shields were constructed with layers of different metals. [1]

Filament wound pressure vessels using glass fibers were the first strength critical application for modern composites. After those, boron filaments were developed in the 1960`s which started many programs to promote various aircraft structures made of composite components [2].

After 1986, when an all composite airplane set the world record in non-stop flight around the world, composite technology gained acceleration. This plane, designed and built by Burt Rutan and his coworkers, was not only a demonstration of an ultra light structure, but also a proof of toughness and resilience of the composite structures. The improved technology of composites has spurred applications outside the aerospace industry. Sporting goods industry became a major industry for composites. Thousands tons of composites are used for tennis and squash rackets, golf shafts, bicycles, oars for rowing and other equipments where weight, stiffness and strength are important [2](Figure1.2). Currently, range of applications is very large; they are used in electronics (insulation and support, boxes and covers, antennas and radomes, etc.), buildings (chimneys, concrete molds, furniture, windows, etc.), transports (body components, transmission shafts, trailers, seats, wagons, boats, etc.), and in many other general mechanical applications [3].

Today, composite materials refer to materials having strong fibers –continuous or non continuous- surrounded by a weaker matrix material. The matrix serves to distribute the fibers and also transmit the load to the fibers.

Fibers consist of thousands of filaments, each filament having a diameter of between 5 and 15 micrometers, allowing them to be producible using textile machines [3].

Principal fiber materials are:

- Glass
- Aramid or Kevlar® (very light)
- Carbon (high modulus or high strength)
- Boron (high modulus or high strength)
- Silicon Carbide (high temperature resistance)

In forming fiber reinforcement, the assembly of fibers to make fiber forms for the fabrication of composite material can take different forms, leading to different structural characteristics (Figure 1.1). Materials created using one-directional tows, yarns, tapes are called unidimensional; using two-directional woven or nonwoven fabrics (felts or mats) are called bidimensional, and using multi-directional fabrics (>2) are called tridimensional.

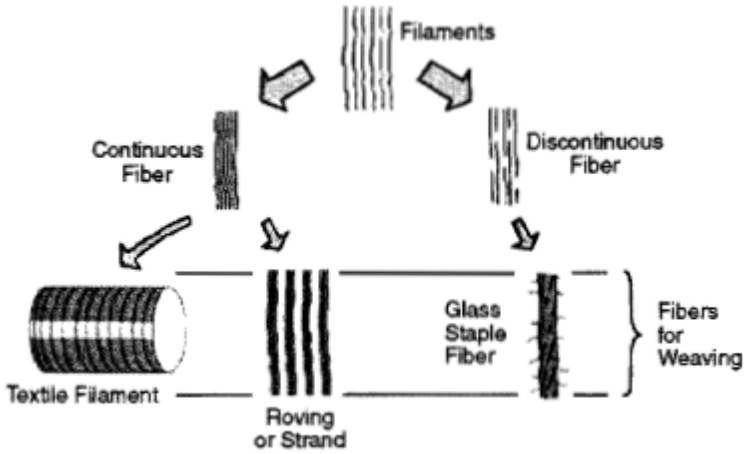

Figure 1.1 Different fiber forms [2]

Matrix materials include the following:

- Polymeric matrix: thermoplastic resins (polypropylene, polyphenylene sulfone, polyamide, polyetheretherketone, etc.) and thermoset resins (polyesters, phenolics, melamines, silicones, polyurethanes, epoxies). Their principal physical properties can be found in [3].
- Mineral matrix: silicon carbide, carbon. They can be used at high temperatures.
- Metallic matrix: aluminum alloys, titanium alloys, oriented eutectics.

Apart from the remarkable weight advantage of composite materials, there are other superiorities of composite materials which make their use favorable [3]:

- Composite materials do not yield (their elastic limit correspond to the rupture limit)
- Composite materials are very fatigue resistant
- Composite materials age subject to humidity (epoxy resin can absorb water by diffusion up to 6% of its mass; the composite of reinforcement/resin can absorb up to 2%) and heat.
- Composite materials do not corrode, except in the case of "aluminum with carbon fiber" in which case galvanic phenomenon creates rapid corrosion.
- Composite materials are not sensitive to the common chemicals used in engines: grease, oils, hydraulic liquids, paints and solvents, petroleum. However, paint thinners attack the epoxy resins.
- Composite materials have medium to low level impact resistance (inferior to that of metallic materials).
- Composite materials have excellent fire resistance as compared with the light alloys with identical thicknesses. However, the smokes emitted from the combustion of certain matrices can be toxic.

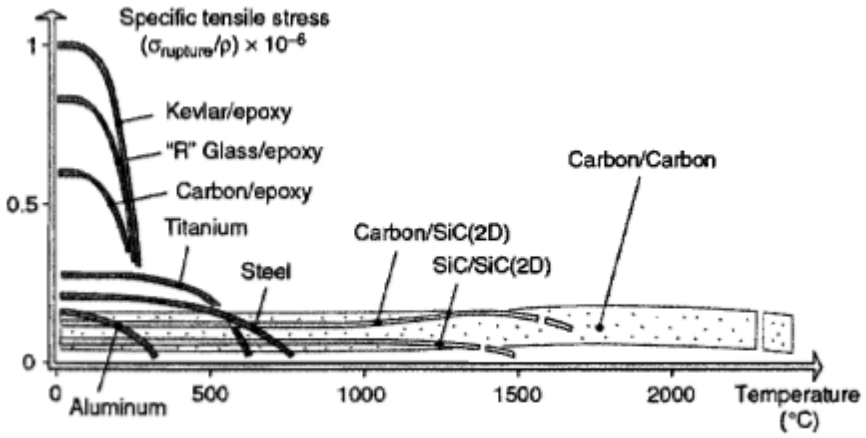

Figure 1.2 Specific strength of different composites [3]

There are many manufacturing techniques which are selected considering the respective ease for a specific part. Some of the most used techniques are given below. More detailed information on those techniques can be found in [3], as well as in other composite materials reference books. In this study, only filament winding method will be analyzed to a further depth, as presented analysis is applicable for filament wound structures.

- Bulk molding compound
- Centrifugation
- Contact molding
- Filament winding
- Compression molding
- Autoclave molding
- Pultrusion
- Reinforced-reaction injection molding
- Structural-reaction injection molding
- Resin transfer molding
- Sheet molding compound
- Reinforced thermoplastics
- Reinforced stamped thermoplastics
- etc.

Traditional filament winding was one of the earliest fabrication processes used for producing continuous filament composites. In the laboratory this process can be used to form controlled composites in two optional formats. In the first, the fibers are pre-impregnated by passing them through a suitable matrix, while the second option requires winding the fibers onto a mandrel and impregnating the total assembly. When a sufficient number of layers of fibers have been appropriately laid down, the impregnated windings are cured. Alternately, if the second process is used, the mandrel is impregnated and allowed to furnace cool following a programmed procedure [4].

The basic elements of traditional filament winding are a mandrel and a spool. The mandrel spins fiber off the spool as the spool moves parallel to it. The fiber can be wound in helical, hoop (or circumferential), and polar patterns around the mandrel, as seen in Figure 1.4. [5]

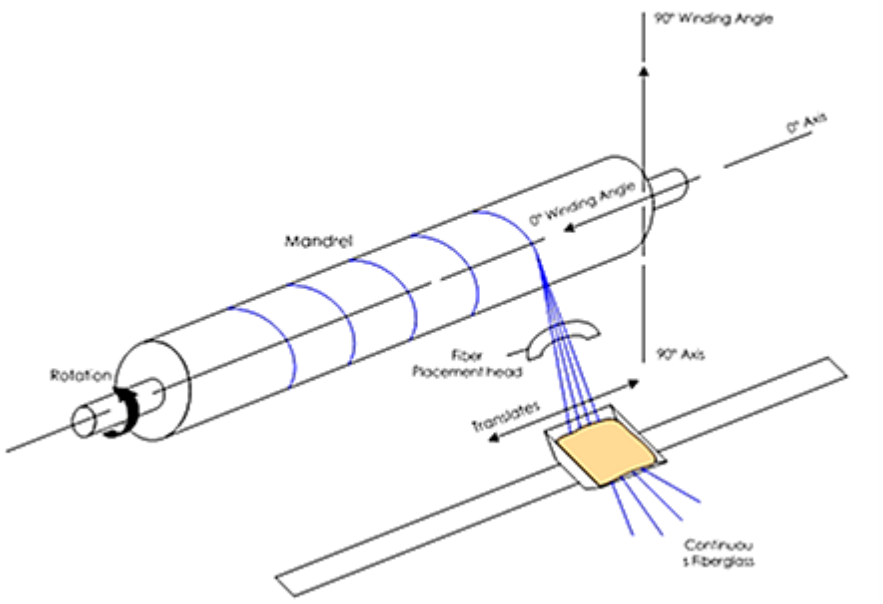

Figure 1.3 Traditional filament winding method.[1]

1. www.thaicomposites.com/technology.php

Filament winding machines operate on the principles of controlling machine motion through various axes of motion. The most basic motions are the spindle or mandrel rotational axis, the horizontal carriage motion axis and the cross or radial carriage motion axis (Figure 1.3). Additional axes may be added, typically a rotating eye axis or a yaw motion axis, and when the pattern calls for more precise fiber placement further additional axes may be added.

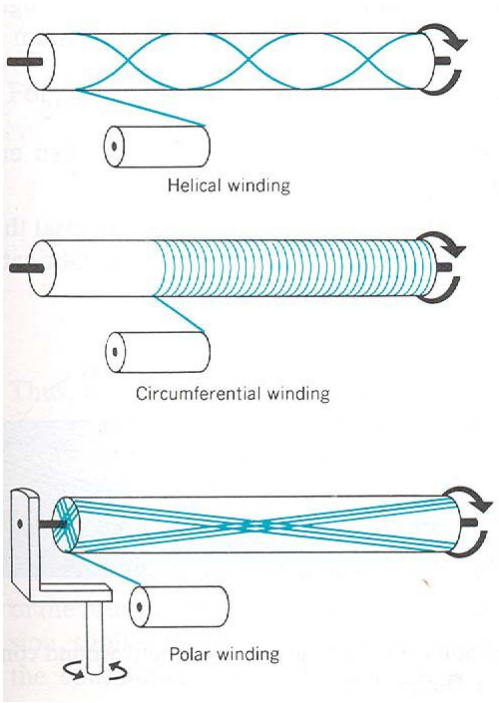

Figure 1.4 Helical, circumferential (or hoop), and polar winding patterns.[2]

The strongest and lightest arrangement for composites is when they are made with continuous and aligned fiber reinforcements. Filament winding is a composites manufacturing process that keeps the fibers continuous and aligned throughout each part. This process winds from spools of fiber continuously so that the fibers can remain uncut through the entire manufacturing process.

Using filament winding technique, generally shell structures are generated. A shell is a thin walled body, just as a beam or plate is, whose middle surface is curved in at least one direction. For instance, cylindrical and conical shells have only one direction in which the middle surface is curved. On the other hand, in a spherical shell there is curvature in both directions. Shell theory is greatly complicated compared to beam and plate theory because of this curvature. Then, to complicate shell theory with all of the material complexities associated with laminated composite materials makes shell theory of composite materials a great challenge [4].

2. Callister, 1997, p.537

"…When designing filament-wound components, one obviously has to cope with the possibilities and limitations inherent to filament winding technology. Design and manufacturing interact with one another in the sense that feasible component complexity depends on the available winding equipment. On the other hand, there is the winding machine itself, with its dimensions, degrees of freedom and control capacity determining the possible component geometry and size; the more degrees of freedom, the more complex the component may be but also the more complex control will become. When conceiving mandrel geometry, the designer must realize that sharp edges cause the tensioned fibre to cut in at the edges and that flat surfaces result in poor consolidation. Furthermore, mandrel geometry must allow for the fibre to be returned at the ends. In many applications the mandrel must be removable, requiring either a collapsible or segmented mandrel configuration, or a soluble or meltable mandrel material. Also important is that mandrel and composite are both subjected to the same temperature cycle during cure, making the final part dimensions dependant on the thermal expansion of the mandrel material. Finally, there is also the surface quality of the component; if important, either vacuum bagging or an external mould must be used…" [6]. Laminate lay-up design considerations and fiber trajectories are the main topic of this study; thus their design will be discussed extensively in the following sections.

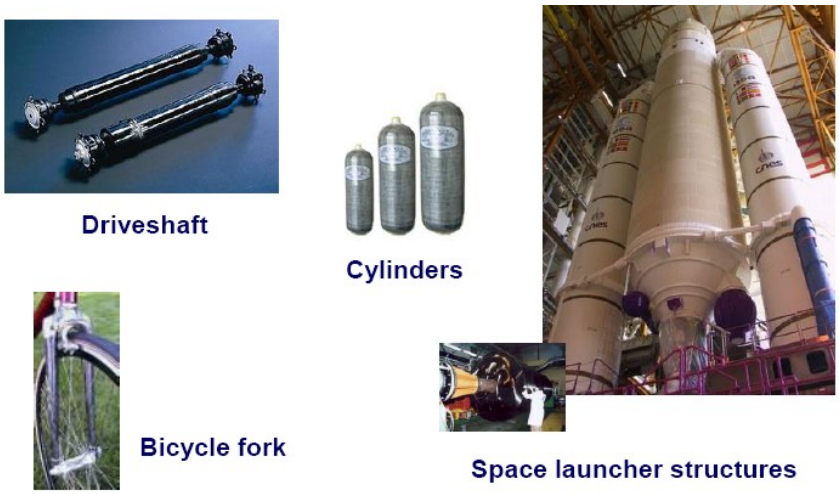

Figure 1.5 Carbon fiber applications [16]

Fiber-reinforced composites are widely used in aircrafts, rockets and automotive structures for their low weight with high strength and stiffness. Good corrosion and chemical resistance of composites allow them to be used in storage and transport of fluid and gases for rockets and automobiles (Figures 1.5 and 1.6). In addition, a designer can utilize the anisotropy produced by building up a laminate from plies with a properly selected fiber-resin combination and orientation-stacking sequence to meet the performance requirements. Filament winding is one of the fabrication techniques for high performance composites. Continuous filaments are the economical and excellent form of fiber reinforcement and can be oriented to match the direction of the stresses loaded in a

structure. Filament winding also allows the placement of fibers with a highly reproducible degree of precision [7].

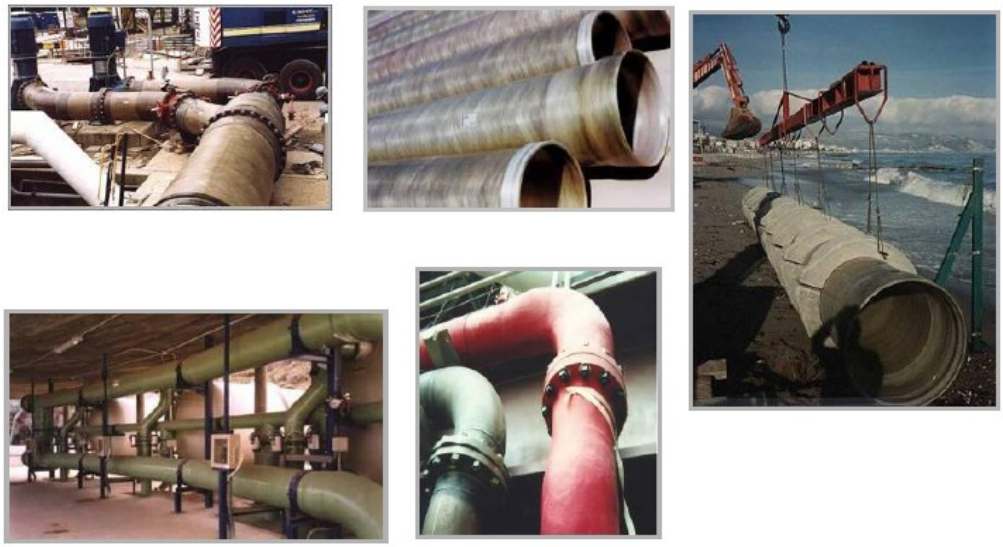

Figure 1.6 Glass fiber applications in chemical, oil and water industries [16]

Non-traditional filament winding is less well known. The concept here is basically the inverse of traditional filament winding. In non-traditional filament winding the spools rotate around the mandrel [5]. Most famous application of this system was used to seismically retrofit bridge columns in USA [8, 9].

"… A major problem in the construction industry is building a structure that can withstand cyclic axial and cyclic lateral loads during an earthquake. Typically, steel retrofits are used to improve flexural and shear strength of a RC column because steel has established structural design allowables and properties. However, steel reinforcements corrode over time and require periodic maintenance. Although the material cost for purchasing the steel to be used in these retrofits is low, installation and regular maintenance is laborious and costly. Reinforced concrete (RC) columns, which carry the largest load in many RC structures, are particularly vulnerable to failure during seismic activity. One solution to protect these columns from earthquakes is to retrofit the RC columns using fiber-reinforced plastic (FRP) composites. The company XXsys Technologies has developed a speedy method for applying a FRP composite wrap to RC columns. XXsys designed a machine called the Robo-Wrapper that constructs a hoop-wrapped jacket around a RC column using tows of continuous carbon fiber pre-impregnated with resin (Figure 1.7). The Robo-Wrapper is a programmable two-axis machine that can wrap pre-preg tow to precise dimensions around highway and bridge columns. The machine rotates around the column while it moves up and or down, encasing the entire column with carbon fiber pre-preg. Because the carbon fiber is continuous, the wrap created provides uniform confinement of the concrete. This ensures there are no weak spots

where the shear strength and flexural strength would be low. XXsys also designed a radiant heat oven, which cures the resin at high temperatures (Figure 1.8). During the cure, the resin cross-links and forms a hard shell. The resin also acts as an adhesive and bonds to the concrete forming a tight structure around the entire cross section of the column.

Figure 1.7 The ROBO-Wrapper I™. A freeway column retrofit filament winder. [8]

Figure1.8 XXsys'curing system. [8]

Two main machines, the Robo-I and the Robo-II, are used to retrofit RC columns of all sizes. The Robo-I, shown in Figure 1.7, can complete a composite wrap for an average freeway circular column, four feet in diameter and 20 feet high, in 8 to 12 hours. The Robo-II has the capability of wrapping two 22 foot tall circular columns per day, which includes machine set-up, the actual wrapping, and then removing the equipment from the site. The Robo-I uses up to six spools of pre-preg tow while the Robo-II uses twice as many spools and can wind 4 to 5 times faster. The XXsys' wrap system is well equipped for handling seismic retrofits of structurally deficient bridge columns. A typical retrofit process would follow three general steps: column preparation, operation of the Robo-Wrapper, and the curing system. During the first step the columns surface area is cleaned of dirt and dust. All defects in the concrete are fixed to ensure as close to a contamination-free surface as possible. The less contamination on the surface the better the composite wrap will bond to the concrete column. The second step involves assembling the Robo-Wrapper machine, programming the machine, and wrapping the column. The Robo-Wrapper is made up of two segments that are lifted to the appropriate location and bolted together. Once in place, the machine is programmed and then activated. The final step is the curing system. The curing system, shown in Figure 1.8, is constructed after each column is wrapped. The curing oven is made up of radiant curing panels that are bolted together around an eight-foot section of the column. The panels are

insulated and the power source is a diesel electric generator. The cables shown in the same figure are the electric power cables connecting the generator to the curing panels. Thermocouples are used to measure the actual temperature of the part accurately. When the job is finished a detailed report showing what was done, such as jacket thickness in specific areas, etc., can be reviewed. The XXsys method of FRP composite application is an example of non-traditional filament winding method…" [9].

Another example for non-traditional winding process is a machine manufacturing CompTether™ tendons which are used to tether Tension Leg Platforms to the ocean floor. Carbon fiber rods are wound helically around these very long tendons). In the case of the manufacturing process from DeepWater Composites, seen in Figure 1.9, the CompTether™ tendon moves through the center of the rotating shuttle that holds the spools [5].

Composite materials offer several attractive attributes for offshore service; high specific strength along with high corrosion resistance, good thermal insulation, excellent damping and fatigue performance, and high specific stiffness. These properties combined with the unmatched tailorability of fiber reinforcements along load paths have motivated the industry to promote the use of composites in several critical load bearing applications, particularly for risers, spoolable tubulars and tethers. Latest design innovations are also addressing embedding fiber optics, strain sensors and electrical conductors into the composite part to monitor structural integrity and loads during service, and to obtain operational conditions from remote locations. Metrics for success will be in the development of data bases, terminations, process automation, standards/certification testing and criteria for maintenance, repair and/or replacement decisions [10].

Figure 1.9 Carbon fiber rods are wound helically around these very long tendons.[3]

3. www.ivt.ntnu.no

Although there is extensive industry experience with the design, installation and operation of tension leg platforms (TLPs) with steel risers, the concept is currently becoming out of favor for deepwater for two primary reasons: (i) its current steel tether design cannot be extended beyond about 1500-m; (ii) steel risers at such depths are heavy and require high axial tension mechanisms which can only be accommodated by building a bigger platform. It is commonly acknowledged that the introduction of composite riser and tether technology can extend the current range of TLP applicability to beyond 3000-m water depth with 37% reduction in total installed cost. These savings are derived from reduced top tension requirements, total system weight, stacked volume and buoyancy weight providing excellent hang off performance [10].

Currently, the environment pollution and energy crisis are two important problems all around the world. Hydrogen energy is considered as a kind of advanced energy due to its advantages of clean and cyclic utilization. The economic, safe, efficient hydrogen storage technique is a key to the practicality of the hydrogen utilization. Carbon fiber/epoxy composites have been increasingly used to develop the lightweight high pressure hydrogen vessel in areas of the hydrogen fuel cell vehicle because they exhibit many advantages such as high strength/stiffness-to-weight ratio and excellent resistance to fatigue and corrosion [11]. Due to limited space available on the vehicle, the hydrogen storage system is critically required to reach the lightweight, small volume, low cost, and excellent safety performance so that the continuous and safe run of vehicle can be satisfied [12]. This creates a great need for improvements in terms of high efficiency and high strength pressure vessels.

Another possible future application for the filament wound conical shells is the wind turbine tower production. During last 20 years wind turbine manufacturers took the path of building larger machines to generate more electricity (Figure 1.10). However, the bigger the size got, the more material was required to support the loads, leading to a great weight increase. For the market, more weight and bigger size mean new manufacturing techniques and design with several pieces to be able to transport, bigger cranes and more labor. If one also considers the practical difficulties while transferring the product, such as height of bridges on the way, available roads wide enough without sharp corners, enclosure of the roads to traffic during transport, police escort to trucks, etc.(Figure 1.11). As a result, new methods are great importance nowadays for the future of wind turbine market.

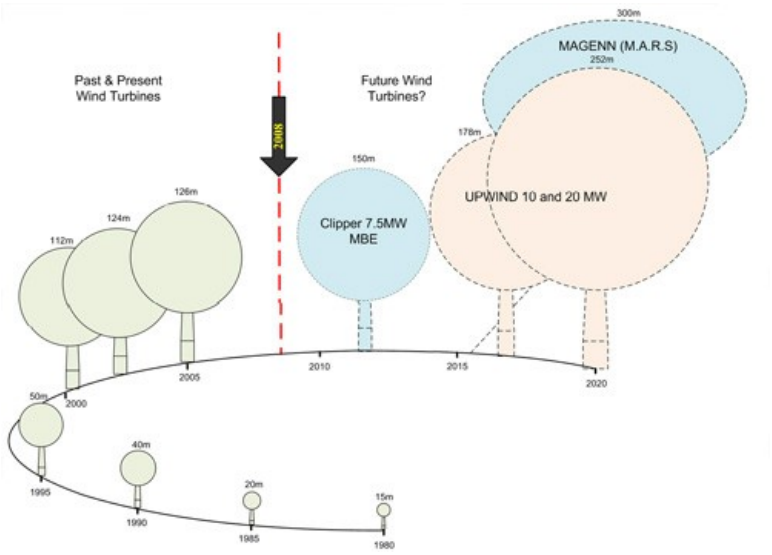

Figure 1.10 Evolution of wind turbines.[4]

Figure 1.11 Transport of a segment of wind turbine tower.[5]

Figure 1.12 Cranes to install offshore turbines.[6]

4. www.wind-energy-the-facts.org/en/executive-summary/part-i-technology.html
5. truckstop.truckismo.com
6. www.siemens.com/innovation

Lately, cement and steel hybrid towers are designed for towers higher than 100m. For steel towers, 100m hub height is normally the limit, because a larger height requires a tower diameter of more than the 4.3m, which cannot be transported anymore because of bridge passage. The height of the tower is extremely critical as the higher hub heights mean higher wind speeds and higher energy generation, especially for the low wind regions such as most of Turkey. A Dutch company called Advanced Tower Systems recently designed and built a 133m tower using this hybrid idea and claims 18% increase in the energy generation. The lower section of the tower consists of narrow concrete pre-fabricated parts, the upper section of conventional steel components [13]. As the industry faces new challenges, new structural solutions may become available for the wind generator superstructures, using advanced composite materials technology and employing their advantages, such as prolonged life, improved dynamic damping characteristics, extended fatigue life, reduced maintenance cost and reduced logistic costs for installation as a consequence of smaller size and weight.

According to European Wind Power Association (EWEA), off-shore wind farms will dominate the next 20 years of the wind energy market (Table 1.1) [15]. Improvements in the manufacturing methods and extended research on the topic could be very beneficial for off-shore market. In the case of the composite material tower made by the filament winding method welding is no longer necessary and the cost of labor is reduced due to simplification of bolting and drilling. And, as there is no need for welding, there is no roughness of the surface by welding [14]. Application of traditional or non-traditional winding method on the field instead of manufacturing the tower on the land and transporting to off-shore might be another critical improvement for the industry. Those simplifications, especially in terms of weight and labor, are highly critical for off-shore applications where the working conditions are far from ideal and the transportation is expensive (Figure 1.12).

Table 1.1 Forecast of offshore wind energy installations 2000-2030 by EWEA [15]

Year	Cumulative capacity (MW)	Annual installations (MW)	Wind energy production (TWh)	Wind energy's share of electricity demand (EC ref. scenario)	Wind energy's share of electricity demand (EC New Energy Policy)	Annual offshore wind power investments (€ billion)	CO_2 avoided annually (Mt)
2000	35.35	3.8	0	0.0%	0.0%	0.007	0
2001	85.85	50.5	0	0.0%	0.0%	0.089	0
2002	255.85	170	1	0.0%	0.0%	0.306	1
2003	515.05	259.2	2	0.1%	0.1%	0.480	1
2004	604.75	89.7	2	0.1%	0.1%	0.175	2
2005	694.75	90	3	0.1%	0.1%	0.185	2
2006	895.25	200.5	3	0.1%	0.1%	0.431	2
2007	1,105.25	210	4	0.1%	0.1%	0.483	3
2008	1,471.33	366.08	5	0.2%	0.2%	0.879	4
2009	1,901	430	7	0.2%	0.2%	1.032	4
2010	3,001	1,099	11	0.3%	0.3%	2.529	7
2011	4,501	1,500	16	0.5%	0.5%	3.300	10
2012	6,459	1,958	24	0.6%	0.7%	3.916	15
2013	8,859	2,400	32	0.9%	0.9%	4.320	20
2014	11,559	2,700	42	1.1%	1.2%	4.320	26
2015	14,659	3,100	54	1.4%	1.6%	4.573	33
2016	18,259	3,605	67	1.7%	2.0%	5.047	40
2017	22,375	4,116	82	2.1%	2.4%	5.557	49
2018	27,240	4,865	101	2.5%	2.9%	6.315	59
2019	33,090	5,852	122	3.0%	3.6%	7.526	71
2020	40,000	6,915	148	3.6%	4.3%	8.810	85
2021	47,700	7,717	177	4.3%	5.2%	9.779	100
2022	56,200	8,500	209	5.0%	6.1%	10.713	117
2023	65,500	9,303	244	5.8%	7.1%	11.662	135
2024	75,600	10,100	282	6.6%	8.2%	12.593	155
2025	86,500	10,904	323	7.5%	9.5%	13.521	176
2026	98,100	11,650	366	8.5%	10.8%	14.367	198
2027	110,400	12,470	413	9.5%	12.2%	15.293	221
2028	123,200	13,059	461	10.6%	13.6%	15.927	244
2029	136,400	13,290	511	11.7%	15.1%	16.118	268
2030	150,000	13,690	563	12.8%	16.7%	16.510	292

Nowadays, researchers are working on the new solutions for the adaptability of the molds to build filament wound composite materials. One recent trend is the reusable mandrels with shape memory polymers. Shape memory polymer (SMP) resin is an integral component of a shape memory composite system. A shape memory composite acquires some SMP characteristics, making it a unique material for use in dynamic structures and other applications requiring both load strength and "shape-shifting" flexibility. Under thermal controls, shape memory composites can be temporarily softened, reshaped, and rapidly hardened to function as structures in a variety of configurations.[7]

7. www.crgrp.com/technology/overviews/smp1.shtml

In this method, mandrel is placed in a clamshell mold, heated above its transition temperature and blown into its complex shape under air pressure. Still under air pressure, the mandrel is cooled in its new shape. Once cooled, it is removed from the mold and installed on a winder. The rigid mandrel is filament-wound. After the part cures, the mandrel is heated above its transition temperature to return to its initial tubular shape. Then, the composite part is completed (Figure 1.13) [16].

Figure 1.13 Reusable mandrels with shape memory polymers [16]

However, one of the problems with filament winding is that the trajectory of the fiber path and the corresponding fiber angles cannot be chosen freely because of the fiber path stability requirement. Initially, using geodesic path was the easiest and applicable solution, but requirements of the industry improved as the new technologies are presented to the market. Mentioned requirement pushed engineers to research for application of fiber paths other than the geodesic trajectories.

1.2 THESIS STATEMENT AND METHOD

One of the main advantages of composite materials is the freedom in the design. Composite designer is able to construct his/her material, having stiffness only in the required direction(s) and saving weight by not having an unnecessary isotropic behavior. The stiffness coefficients of laminated shells of revolutions are usually assumed to be constant for avoiding the exhausting and complicated calculations resulting from the varying stiffness coefficients as a function of the longitudinal coordinate. For a shell of revolution, for which its radius change along the longitudinal axis, fiber orientations and thicknesses change along that axis, which ultimately influences the stiffness coefficients.

Geodesic fiber trajectories are the most frequently used trajectories in the filament winding operation due to the fact that filaments wound along geodesic paths do not require any friction to be stable. For conical shells of revolution it has been shown that geodesic winding causes the winding angle and the thickness to vary along the meridian of the shell of revolution [17][18]. The starting edge of the winding operation, whether small radius edge or large radius edge, also affects the variation of the winding angle and the thickness of the shell of revolution along the meridian of the shell of revolution, and this in turn causes continuous meridional variation of the stiffness coefficients.

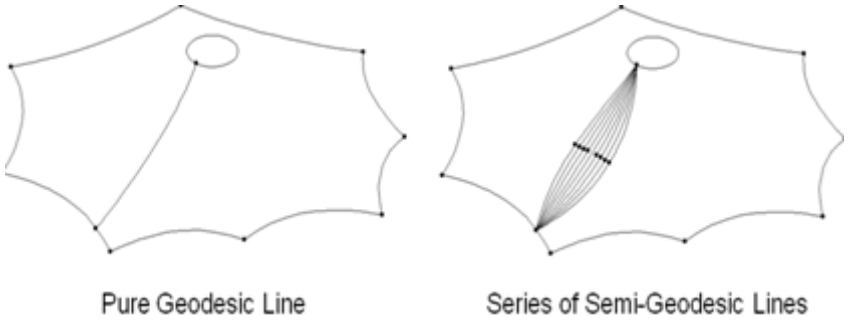

Figure 1.14 Geodesic and semi-geodesic fiber paths

In filament winding operation filaments must not necessarily be wound along geodesic paths to be stable. The so-called semi-geodesic fiber paths slightly deviate from the geodesic paths counting on friction to keep the fiber in its proper position (Figure 1.14) [19]. In case of semi-geodesic fiber path the tensile force in the fiber also has force component transverse to the fibers, and this transverse force component can cause fibers to slip if enough friction is not available. The ratio of the transverse force to the normal force on the fiber is defined as the slippage tendency which must be less than the maximum friction coefficient [20][21]. In case of preset constant slippage tendency the winding law can be expressed by a differential equation, which is more complex than the winding law for geodesic winding [20]. Numerical integration is necessary in particular geometries to define the continuous meridional variation of the winding angle, thickness and the stiffness coefficients, due to semi-geodesic winding process.

This thesis will compare the free vibration characteristics of conical and spherical shells of revolution, which are wound along geodesic and semi-geodesic fiber paths.For the mentioned task, derivation of the winding angle along the longitudinal direction for conical and spherical shells of revolution, which are wound along semi-geosesic paths, is realized.For a conical shell of revolution the winding angle can be calculated analytically by using the derived formula; however for the spherical shell of revolution the final form is an ordinary differential equation and requires a numerical integration solution to determine the fiber orientation at each meridional location.

Semi-geodesic winding presents alternative fiber paths which can be exploited for theoretical reasons and especially for optimization purposes. Semi-geodesic winding analysis will be performed for different slippage tendencies between fiber and mandrel surface, which is usually determined experimentally.

The effect of geodesic and semi-geodesic winding patterns on the free vibration characteristics of composite shells of revolution is investigated by means of a semi-analytical solution method which is based on the numerical integration of the finite exponential Fourier transform of the fundamental shell of revolution equations. For the semi-geodesic winding the effect of the preset constant slippage tendency on the vibration characteristics is particularly analyzed.

Sample results are obtained for filament wound truncated conical and spherical shells of revolution and the effect of the geodesic and semi-geodesic winding patterns on the free vibration characteristics of composite shells of revolution is investigated thoroughly.

1.3 LITERATURE SURVEY

Laminated composite shells of revolution are widely encountered structures in many applications such as pressure vessels, rocket nozzles, fuselage frames, external stores, antenna etc. The axisymmetric composite shells of revolution are typically manufactured by the filament winding process either by winding organic or inorganic filaments or tapes over a mandrel of required shape. During the filament winding process, the filaments are placed in arbitrary orientation with respect to the geometric axis of the shell of revolution with the fundamental requirement that filaments must be slip-free [22]. Geodesic fiber trajectories are the most frequently used trajectories in the filament winding operation due to the fact that filaments wound along geodesic paths do not require any friction to be stable. For conical shells of revolution it has been shown that geodesic winding causes the winding angle and the thickness to vary along the meridian of the shell of revolution [18][23]. The starting edge of the winding operation, whether small radius edge or large radius edge, also affects the variation of the winding angle and the thickness of the shell of revolution along the meridian of the shell of revolution, and this in turn causes continuous meridional variation of the stiffness coefficients.

In filament winding operation filaments must not necessarily be wound along geodesic paths to be stable. The so-called semi-geodesic fiber paths slightly deviate from the geodesic paths counting on friction to keep the fiber in its proper position [25]. In case of semi-geodesic fiber path the tensile force in the fiber also has force component transverse to the fibers, and this transverse force component can cause fibers to slip if enough friction is not available. The ratio of the transverse force to the normal force on the fiber is defined as the slippage tendency which must be less than the maximum friction coefficient [22][25]. In case of preset constant slippage tendency the

winding law can be expressed by a differential equation, which is more complex than the winding law for geodesic winding [22]. Semi-geodesic winding presents alternative fiber paths which can be exploited especially for optimization purposes.

A rather complete analysis of composite material shells, both utilizing classical shells including transverse and shear deformation has been compiled by Vinson and Chou [26]. In 1975, Wilkins and Love [27] examined the combined compression and shear buckling behavior of laminated composite cylindrical shells characteristics of fuselage structures. Compression-shear interaction curves were obtained for sample shells. Compared to classical buckling theory the actual compression buckling values were 65% of the theoretical value. The disparity was attributed to imperfections. Good agreement between theory and experiment were realized for shear.

The free vibration of laminated orthotropic cylindrical shells using classical theory has been studied by White [28], Dong [29], Bert [30], and Tasi [31] [32]. Misky [33] [34] included transverse shear deformation and transverse normal strain of orthotropic homogenous cylindrical shells. Dong and Tso [35] analyzed the vibration of layered orthotropic homogenous cylinders including transverse shear deformation. Sun and Whitney [36] studied the axially symmetric vibration of laminated composite cylindrical shell including transverse shear deformation, transverse normal stress and strain, rotator inertia and higher order stiffness and inertia terms.

Most of the previous work on the study of the vibration characteristics of composite shells of revolution has been performed by taking constant stiffness coefficients or on shells of revolution, with constant radii of curvature, for which the stiffness coefficients and thickness remain constant along the meridian of the shell of revolution. Some examples of these studies include the work of Noor and Peters [37], who used a combination of Fourier series representation in the circumferential direction, three-field mixed finite element model for the discretization in the meridional direction, and analyzed cylindrical and toroidal shells of revolution. A semi-analytical study of the composite shells of revolution has been performed by Xi et al. [38], who used conical finite elements and included transverse shear deformation in their analysis. A finite element semi-analytical model for laminated axisymmetric shells is presented by Correia et al. [39]. Ferreria et.al. [40] presented a meshless method based on multiquadric radial basis functions for the solution of natural frequencies of cross-ply composite shells. Nguyen-Van et.al. [41] investigated the free vibration analysis of laminated shell structures based on FSDT with a novel quadrilateral finite element.

A typical study of the effect of the variation of the stiffness coefficients due to geodesic winding on the buckling behavior of filament wound conical shells has been performed by Goldfield and Arbocz [18]. Korjakin et.al [42] investigated the damped vibrations of laminated conical shells by finite element analysis, and incorporated the effect of the variation of the winding angle and thickness due to geodesic winding on the natural frequencies of laminated conical shells. Park et.al [43] considered the variation of the winding angle in the longitudinal and thickness direction in the

dome part of a cylindrical pressure vessel due to semi-geodesic winding and performed finite element analysis of the pressure vessel subject to internal pressure. Recently, Kayran and Yavuzbalkan [44] studied the effect of the variation of stiffness coefficients due to geodesic winding on the free vibration characteristics of filament wound shells of revolution by a semi-analytical method.

It was concluded by Baruch et al. [23] that the stiffness coefficients needed for the analysis of a laminated structure have to be calculated only after taking into account the manufacturing process which can be used to build the structure. Based on the examples presented about the studies performed on the dynamics of composite shells of revolution, it is assessed that the effect of winding patterns on the dynamic characteristics of filament wound shells of revolutions has not received enough attention in the literature. Therefore, the main aim of the present thesis is to study the effect of winding patterns on the free vibration characteristics of filament wound composite shells of revolution. Specifically, at first the effect of the initial winding angle, the starting edge of the winding, geodesic and semi-geodesic winding patterns on the variation of the winding angle, thickness and stiffness coefficients is investigated.

By introducing the preset slippage tendency during the winding process, it is aimed to investigate its influence on the free vibration characteristics and mode shapes. This information has a potential to provide a new parameter to control the dynamic characteristics of the shell structure and increase the design options for optimization of the structure.

1.4 THESIS ORGANISATION

The remaining chapters of this thesis are organized as follows:

Chapter 2 presents the governing equations of free vibration analysis of anisotropic laminated composite shells of revolution and the multisegment method is briefly explained as the method of solution. Described solution technique and presented governing equations are very well known from literature and have been used for rotationally symmetrical shells of revolutions wound by using geodesic fiber paths.

Chapter 3 explains the filament winding laws for geodesic winding and semi-geodesic winding. In the case of introduction of preset slippage tendency, the winding law is expressed by a differential equation. The variation of winding angle for a conical and spherical shell of revolution is derived in this chapter for a semi-geodesic winding process. Derived fiber orientation and thickness equations enabled the calculation of stiffness coefficients along the shell and also to determine the dynamic characteristics of the shell. Semi-geodesic winding laws are integrated to the available

computer code which is developed to calculate the natural frequencies for the shells of revolution wound by using geodesic fiber paths.

Chapter 4 presents a verification study conducted by using the finite element analysis (FEA), which is a different solution method compared to the semi-analytical model solved by numerical integration. For this comparison study, commercially available PATRAN/NASTRAN software is employed. This verification study was required due to the limited references in the literature and its purpose is to check the proper integration of the semi-geodesic fiber path to the multi-segment numerical integration method, rather than verification of the accuracy of the two different solution approaches.

Chapter 5 summarizes the numerical results obtained for a truncated conical shell and spherical shell of revolution. Introduction of preset slippage tendency and its effect on stiffness coefficients and free vibration characteristics is the main research topic in this study. The effect of semi-geodesic winding on stiffness coefficients, natural frequencies and mode shapes for both shell structures are investigated throughout this chapter. Moreover, for a conical shell of revolution, the effect of the cone angle is also investigated as it is the main geometrical parameter altering the cone geometry and dynamic properties.

Finally, conclusions are summarized and recommendations for future work are discussed in Chapter 6.

CHAPTER 2

GOVERNING EQUATIONS OF FILAMENT WOUND SHELLS OF REVOLUTION AND METHOD OF SOLUTION

This thesis investigates the effect of semi-geodesic winding on the free vibration characteristics of filament wound composite shells of revolution. The vibration resulting from the action of forcing upon a system is known as forced vibration, and the one resulting from initial conditions is called free vibration. An elastic structure displaced from its equilibrium position and thereafter allowed to oscillate with no further imposed force is considered as exhibiting free vibration.

Theory of shells is examined under the theory of elasticity in two parts: two-dimensional and three-dimensional shell theories. Two-dimensional shell theories are derived from three-dimensional elasticity theory employing assumptions concerning the kinematics of deformation through the thickness of the shell. Two-dimensional shell theories include thin and thick; shallow and deep; linear and non-linear shell theories defined considering the thickness of the shell, the span length or radii of curvatures, and the magnitude of linear and rotational displacements [45].

In this thesis, thin elastic shell theory is employed. Thin elastic shell theory assumes small elastic deformations under the influence of loads. Small deformation assumption allows the usage of the equilibrium conditions for deformed elements same as if they were not deformed. The behavior of thin elastic shells is based upon the equations of the theory of linear elasticity. However, three-dimensional equations of elasticity in rectangular coordinate system do not assure the analytical solutions of thin elastic shells. Two main “difficulty factors” involved in achieving an analytical solution of the boundary value problem using the three-dimensional elasticity theory is stated clearly in [45].

"…The first of these factors deals with the "degree of the geometrical complexity" of the shells, for example prescribed in the circular coordinate system. The number of boundaries in the shell geometry can lead to difficulties in the application of boundary conditions. The second "difficulty factor" involved in the solution of the three-dimensional equations of motion and the strain-displacement relations of shells in the circular coordinate system deals with the "degree of material complexity". In fact, the most general form of the constitutive equations, do not have analytical solutions available in the literature. Therefore, almost all shell theories for thin elastic shells reduce the three-dimensional elasticity problem into a two-dimensional problem by making suitable assumptions. This is usually done by eliminating the coordinate normal to the shell surface in the development of the two-dimensional shell theories…" [45].

There exist a number of theories for thin homogenous elastic shells which describe the deformations of a thin elastic shell. The linear differential equations of classical shell theories have some differences considering the assumptions made about the form of small terms and the order of terms. The classical shell theories are based on the Love- Kirchhof assumptions which states:

- Straight lines normal to the undeformed reference surface remain straight and normal to the deformed reference surface;
- The normal stresses perpendicular to the reference surface can be neglected in the stress-strain relation (plane stress condition in the two-dimensional elasticity);
- The transverse displacement is independent of the thickness coordinate (the transverse normal of the reference surface is inextensible).

"…The classical shell theories are expected to yield sufficiently accurate results when (i) the lateral and/or longitudinal dimension, or the radii of curvature-to-thickness ratio is large (thin elastic shell); (ii) the dynamic excitations are within the low-frequency range (in the scope of small deformations); (iii) the material anisotropy (isotropic or orthotropic) is not severe. However, the application of Love-Kirchhoff assumptions based theories to laminated composite shells could lead to errors in deflections, stresses, buckling loads and natural frequencies. These errors occur due to the anisotropy and heterogeneity of the materials of different layers and the existence of layers which exhibit weak resistance to transverse shear and normal deformations. A remedy for decreasing errors to some extent is to account for transverse shear deformations in two-dimensional shells theories for the laminated composite shell analysis. As a matter of fact that the experiments have revealed that neglecting transverse shear strains in the modeling leads to underestimations of deflection and overestimates of natural frequencies and buckling loads. In the case of plates and shells made of advanced laminated composite materials such as graphite-epoxy and boron-epoxy, where the ratio of elastic in-plane moduli to transverse shear moduli are very great (i.e., of the order 25-40 instead of 2.6 for isotropic materials), the transverse shear deformation becomes significant. Actually, as pointed out by Koiter [46], refinement of Love-Kirchhoff assumptions based theory,

namely classical shell theory, of thin elastic shells is meaningless unless the effects of transverse shear and normal stresses are taken into consideration. Transverse shear deformation plays a very important role in reducing the effective flexural stiffness of anisotropic and laminated plate and shell structures than in corresponding isotropic plate and shell structures…"[47]. This analysis led to development of refined shell theories and computational models to obtain sufficiently accurate results for response and failure characteristics of anisotropic and laminated composite shells. "…Roughly, they can be splitted into three categories: the three-dimensional elasticity models, the quasi-three-dimensional models, and the two-dimensional shear-flexible models. In the three-dimensional elasticity models, the 15 unknowns (3 displacements, 6 normal and shear stresses, and 6 normal and shear strains) are tried to be found out directly by 15 available equations of elasticity (3 equilibrium equations, 6 stress-strain relations, and 6 strain-displacement relations) without any assumptions whereas in quasi-three-dimensional models, simplifying assumptions are made regarding the stress (or strain) state in the shell (or in the individual layers), but no a priori assumptions are made about the distribution of the different response quantities in the thickness direction. The use of both three-dimensional and quasi-three-dimensional models for predicting the response characteristics of anisotropic and laminated composite shells with complicated geometry is computationally cumbersome; therefore, they are only applied to shells with simple geometries, loading and boundary conditions. On the other hand, the two-dimensional shell theories are adequate and practical for predicting the gross response characteristics such as natural frequencies, buckling loads, and average through-the-thickness displacements and rotations of anisotropic and laminated composite shells. But they are not adequate for the precise accurate prediction of the transverse stresses and deformations. There are four approaches for constructing two-dimensional shell theories for laminated composite shells which can be listed as: Method of hypotheses; method of expansion; asymptotic integration technique; iterative methods and methods of successive corrections.

The first approach is an extension of the Kirchhoff-Love approach and is based on introducing a priori plausible kinematic or static assumptions regarding the variation of displacements, strains and/or stresses in the thickness direction. The simplest of these hypotheses is the linear variation of the displacement components used in conjunction with first-order shear deformation theories. Although the method of hypotheses has the advantages of physical clarity and simplicity of applications, it has the drawback of not providing an estimate of the error in the response predictions.

The second approach is based on a series expansion, in terms of the thickness coordinate for displacements and/or stresses. It also includes the method of initial functions in which the displacements and stresses are expanded in a Taylor series in the thickness coordinate. The relations between the higher-order derivatives of each of the displacements and stresses and their lower-order derivatives are obtained by successive differentiation of the three-dimensional elasticity relations.

In the third approach, appropriate length scales are introduced in the three-dimensional elasticity equations for the different response quantities, followed by parametric (asymptotic) expansions of these quantities in power series in terms of a small thickness parameter. The three-dimensional elasticity equations are thereby reduced to recursive sets of two-dimensional equations, governing the interior and edge zone responses of the shell. The edge zone (or boundary layer) is produced by self-equilibrated boundary stresses in the thickness direction. The lowest-order system of two-dimensional equations, depending on the choice of the length of scales, corresponds to the thin-shell assumptions. The higher-order systems introduce thickness correction effects in a systematic and consistent manner.

The fourth approach includes various iterative approximations of the three-dimensional elasticity equations, and predictor-corrector procedures based on a single correction or successive corrections of the two-dimensional equations…" [48].

This thesis employs a two-dimensional shell theory including shear deformation based on the method of hypotheses in association with the smeared continuum approach. "…The smeared continuum approach is defined with the simplifying assumption of laminated anisotropy which is often used in applying two-dimensional theory to plates and shells consisting of layers of composite materials. In this approach, the individual properties of composite constituents, the fibers and the matrix, are "smeared" and thus each lamina is treated as an orthotropic material…"[47]. Similar to classical shell theories laminated composite shell theories including shear deformation vary among themselves considering the different assumptions. These assumptions are listed in [48] as:

- global through-the-thickness, or piecewise, layer-by-layer, approximations;
- purely kinematic assumptions (on displacements and strains), or a hybrid combination of kinematic and stress assumptions;
- linear or nonlinear, through-the-thickness, variation of the response of quantities;
- including or neglecting the transverse normal strains.

The equivalent single-layer theories are developed by assuming the form of the displacement field or stress field as a linear combination of unknown functions and the thickness coordinate:

$$\varphi_i(x,y,z,t) = \sum_{j=0}^{N} (z)^j \varphi_i^j(x,y,t) \tag{2.1}$$

where φ_i is the i^{th} component of displacement or stress, (x,y) are the in-plane coordinates, z is the thickness coordinate, t denotes the time, and φ_i^j are functions to be determined [49].

The following assumptions and considerations are made during the derivation of governing equations using Reissner-Naghdi's thin elastic shell theory for the free vibration analysis of anisotropic laminated composite, thin, doubly curved shells:

- The shell is considered to be thin when the ratio of the shell thickness to the wavelength of the deformation mode and/or radii of curvature is less than 1/10.
- The thickness is constant throughout the shell.
- The shell undergoes geometrical linear deformation. In other words, all the displacement terms and their derivatives are linear in the kinematic relations.
- There is no change in the temperature of the shell during the analysis (isothermal state).
- The shell is to be linear elastic.
- The displacements are prescribed with the assumed displacement field using consistent two-dimensional shell theory.
- The system of curvilinear coordinates (ξ_1, ξ_2, ξ) is chosen in a manner that at each point the elastically equivalent directions coincide with coordinate directions, noting that, infinitesimally small elements defined at different points of the body by three pairs of coordinate surfaces, being anisotropic possess identical elastic properties.
- The doubly curved shell has mutually orthogonal curvilinear coordinate system. The two of the curvilinear coordinates ξ_1 and ξ_2 coincides with the orthogonal lines of principal curvature of its reference surface. The third coordinate, the thickness coordinate, is normal to the reference surface at that point.
- The normal stresses perpendicular to the reference surface of the shell are small when compared to other stress so that they can be neglected in the stress-strain relation. This leads to plane stress elasticity problem.
- A linear element normal to the undeformed reference surface undergoes at most a translation and a rotation and suffers no extension. Thus, a linear element normal to the reference surface before deformation remains linear but does not necessarily remain normal to the reference surface after the deformation of the shell. This phenomena results in the inclusion of the shear deformation effects in the formulation whereas this does not exist in the classical shell theory. In addition to shear deformation, the rotary inertias are included in the formulation. In this study, the first-order shear deformation theory is used.
- The assumed displacement field does not satisfy the transverse shear boundary conditions on the top and bottom surfaces of the shell since a constant shear angle through the thickness is assumed, and plane sections remain plane. Therefore, shear correction factors are usually required for equilibrium consideration. The shear correction factors are only functions of lamination parameters (number of layers, stacking sequence, degree of orthotropy and fiber orientation in each layer).

- The transverse normals of the shell are considered to be inextensible. This results in zero transverse normal strain. In other words, the transverse displacement of the shell is independent of the thickness.
- The laminated composite shell is replaced by an equivalent single-layer which is statically and dynamically in equilibrium.
- The reference surface of the laminated composite doubly curved shell is taken at the middle of the laminate.
- An anisotropic body is one which has different values of a material property in different directions at a point; namely, material properties are directionally dependent, the functions of position. In laminated anisotropic shells, the individual layers are, in general, anisotropic and/or orthotropic depending on the fiber orientation angle, and the principal axes of material symmetry of the individual layers coincide with only one of the principal coordinates of the shell (the thickness normal coordinate).
- The layers of the lamination are assumed to be perfectly bonded. The perfectly bonding between layers exists when there is no gap of flaw between layers, no lamina can slip relative to another, and the laminate acts as a single lamina with special integrated properties.
- The material properties of the equivalent single-layer are constant along ξ_1 and ξ_2 directions, or ϕ and θ directions for doubly curved shells or shells of revolution, respectively.
- The shell structure is physically linear; that is, there are no discontinuities and complexities such as holes, stiffeners or being crack-free and invariable cross-sectional area in any direction. However, shells with circumferential stiffeners or rings can be considered in the further analysis.

In the following sections, the differential element and the curvilinear coordinate system are defined for doubly curved shells at first. In addition, the expressions studied in the differential geometry section are presented for an arbitrary point on the surface located ξ away up with respect to the reference surface in the shell space. Then, the field equations of doubly curved shell are derived. Subsequently, these derived equations are manipulated to obtain the fundamental system of equations of a shell of revolution.

2.1 GOVERNING EQUATIONS OF ANISOTROPIC SHELLS OF REVOLUTION

Figure 2.1 shows the geometry notation used for a shell of revolution. In Figure 2.1, R_θ and R_ϕ denote the radii of curvature of the middle surface of the shell in the tangential (θ) and meridional (ϕ) directions, respectively. R denotes the distance of the shell mid surface from the axis of revolution ($R = R_\theta \sin\phi$).

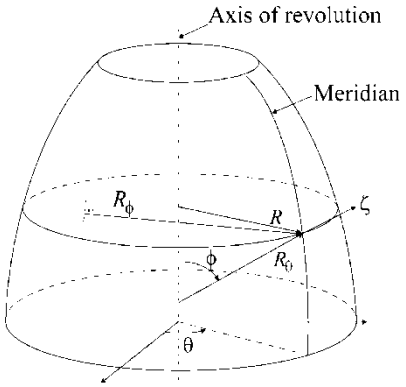

Figure 2.1 Geometry and coordinate system of the shell of revolution

In accordance with the first order transverse shear deformation theory, the displacement field is approximated as

$$U_\phi(\phi,\theta,\zeta,t) = u_\phi^0(\phi,\theta,t) + \zeta\,\beta_\phi(\phi,\theta,t) \tag{2.2}$$

$$U_\theta(\phi,\theta,\zeta,t) = u_\theta^0(\phi,\theta,t) + \zeta\,\beta_\theta(\phi,\theta,t) \tag{2.3}$$

$$W(\phi,\theta,\zeta,t) = w^0(\phi,\theta,t) \tag{2.4}$$

where U_ϕ, U_θ, W represent the displacement of a general point in the shell thickness in meridional, tangential and thickness directions, respectively. In Eqs. (2.2)-(2.4), $u_\phi^0, u_\theta^0, w^0$ represent the mid surface displacements at $\zeta = 0$, and β_ϕ and β_θ represent the rotations of a transverse normal about θ and ϕ curvilinear coordinates, respectively. Based on Reissner shell theory [50], utilizing the displacement field given by Eqs. (2.2) - (2.4), membrane and bending strain expressions for a general shell of revolution with radii of curvatures R_ϕ and R_θ become

$$\varepsilon_{\phi\phi}^0 = \frac{1}{R_\phi}\left[\frac{\partial u_\phi^0}{\partial\phi} + w^0\right] \tag{2.5}$$

$$\varepsilon_{\theta\theta}^{0}=\frac{1}{R_\theta \sin\phi}\left[u_\phi^0\cos\phi+\frac{\partial u_\theta^0}{\partial\theta}+w^0\sin\phi\right] \tag{2.6}$$

$$\gamma_{\phi\theta}^{0}=\frac{1}{R_\theta \sin\phi}\frac{\partial u_\phi^0}{\partial\theta}+\frac{1}{R_\phi}\frac{\partial u_\theta^0}{\partial\phi}-\frac{\cot\phi}{R_\theta}u_\theta^0 \tag{2.7}$$

$$\kappa_{\phi\phi}^{0}=\frac{1}{R_\phi}\frac{\partial\beta_\phi}{\partial\phi} \tag{2.8}$$

$$\kappa_{\theta\theta}^{0}=\frac{1}{R_\theta \sin\phi}\left[\beta_\phi\cos\phi+\frac{\partial\beta_\theta}{\partial\theta}\right] \tag{2.9}$$

$$\kappa_{\phi\theta}^{0}=\frac{1}{R_\theta \sin\phi}\frac{\partial\beta_\phi}{\partial\theta}+\frac{1}{R_\phi}\frac{\partial\beta_\theta}{\partial\phi}-\frac{\cot\phi}{R_\theta}\beta_\theta \tag{2.10}$$

$$\gamma_{\phi\zeta}=\beta_\phi-\frac{u_\phi^0}{R_\phi}+\frac{1}{R_\phi}\frac{\partial w^0}{\partial\phi} \tag{2.11}$$

$$\gamma_{\theta\zeta}=\beta_\theta-\frac{u_\theta^0}{R_\theta}+\frac{1}{R}\frac{\partial w^0}{\partial\theta} \tag{2.12}$$

Eqs. (2.11) and (2.12) give the transverse shear strains in terms of rotations of the mid-surface normal, and mid-surface displacements. For the first order shear deformation theory, the rotation terms β_ϕ and β_θ are also unknowns.

Full anisotropic form of the constitutive equations relating the stress resultants to mid surface strains ($\varepsilon_{\phi\phi}^0,\varepsilon_{\theta\theta}^0,\gamma_{\phi\theta}^0$) and curvatures ($\kappa_{\phi\phi},\kappa_{\theta\theta},\kappa_{\phi\theta}$) are given in matrix form as [51]

$$\begin{bmatrix}N_{\phi\phi}\\N_{\theta\theta}\\N_{\phi\theta}\\M_{\phi\phi}\\M_{\theta\theta}\\M_{\phi\theta}\end{bmatrix}=\begin{bmatrix}A_{11}&A_{12}&A_{16}&B_{11}&B_{12}&B_{16}\\A_{12}&A_{22}&A_{26}&B_{12}&B_{22}&B_{26}\\A_{16}&A_{26}&A_{66}&B_{16}&B_{26}&B_{66}\\B_{11}&B_{12}&B_{16}&D_{11}&D_{12}&D_{16}\\B_{12}&B_{22}&B_{26}&D_{12}&D_{22}&D_{26}\\B_{16}&B_{26}&B_{66}&D_{16}&D_{26}&D_{66}\end{bmatrix}\begin{bmatrix}\varepsilon_{\phi\phi}^0\\\varepsilon_{\theta\theta}^0\\\gamma_{\phi\theta}^0\\\kappa_{\phi\phi}\\\kappa_{\theta\theta}\\\kappa_{\phi\theta}\end{bmatrix} \tag{2.13}$$

where N_{ij} terms represent force per unit length, and M_{ij} terms represent moment per unit length. The stiffness coefficients are expressed in the usual manner as [51]

$$\left(A_{ij},B_{ij},D_{ij}\right)=\sum_{k=1}^{N_L}\int_{h_{k-1}}^{h_k}\overline{Q}_{ij}^{(k)}\left(1,\zeta,\zeta^2\right)d\zeta\qquad\left(i,j=1,2,6\right) \tag{2.14}$$

In Eq. (2.14), $\overline{Q}_{ij}$ are the transformed reduced stiffness coefficients, N_L denotes the total number of layers, and h_k and h_{k-1} denote the vector distance of the outer and inner surface of the k^{th} lamina measured from the mid plane of the shell wall, respectively. Integration of the transverse shear stresses across the thickness of the shell yields the transverse shear stress resultants as

$$\begin{bmatrix} Q_\theta \\ Q_\phi \end{bmatrix} = \begin{bmatrix} As_{44} & As_{45} \\ As_{45} & As_{55} \end{bmatrix} \begin{bmatrix} \gamma_\theta^0 \\ \gamma_\phi^0 \end{bmatrix} \tag{2.15}$$

where the transverse shear stiffness coefficients are given by

$$\begin{gathered} \left(As_{44}, As_{45}, As_{55}\right) = \sum_{k=1}^{N_L} \int_{h_{k-1}}^{h_k} \left(\overline{Q}_{44}^{(k)}, \overline{Q}_{45}^{(k)}, \overline{Q}_{55}^{(k)}\right) f(\zeta) d\zeta \\ f(\zeta) = \frac{5}{4}\left[1 - 4\left(\frac{\zeta}{h}\right)^2\right] \end{gathered} \tag{2.16}$$

In Eq. (2.16), it is assumed that the transverse shear stress has a parabolic distribution across the shell wall. A factor of 5/4 multiplies the distribution function used by Whitney [52] so that the shear factor calculated for the layered anisotropic shell wall can be consistent with the established shear factor from the previous work of Reissner [50] and Mindlin [53] for the homogenous case.

Governing equations for free vibration analysis of macroscopically anisotropic, laminated, doubly curved shells of revolution can be obtained through the use of Hamilton's Principle. Application of Hamilton's principle results in five partial differential equations, with the independent variables being time, and meridional (ϕ) and circumferential (θ) coordinates. These are Eqns. (2.17-2.21) [54]

$$\frac{\partial N_{\phi\phi}}{\partial \phi} R_\theta \sin\phi + (N_{\phi\phi} - N_{\theta\theta}) R_\phi \cos\phi + \frac{\partial N_{\phi\theta}}{\partial \theta} R_\phi + Q_\phi R_\theta \sin\phi = \rho h \ddot{u}_\phi^0 R_\theta R_\phi \sin\phi \tag{2.17}$$

$$\frac{\partial N_{\phi\theta}}{\partial \phi} R_\theta \sin\phi + 2N_{\phi\theta} R_\phi \cos\phi + \frac{\partial N_{\theta\theta}}{\partial \theta} R_\phi + Q_\theta R_\phi \sin\phi = \rho h \ddot{u}_\theta^0 R_\theta R_\phi \sin\phi \tag{2.18}$$

$$\frac{\partial Q_\theta}{\partial \theta} R_\phi + \frac{\partial Q_\phi}{\partial \phi} R_\theta \sin\phi + Q_\phi R_\phi \cos\phi - N_{\theta\theta} R_\phi \sin\phi - N_{\phi\phi} R_\theta \sin\phi = \rho h \ddot{w}^0 R_\theta R_\phi \sin\phi \tag{2.19}$$

$$\frac{\partial M_{\phi\phi}}{\partial \phi} R_\theta \sin\phi + \frac{\partial M_{\phi\theta}}{\partial \theta} R_\phi + (M_{\phi\phi} - M_{\theta\theta}) R_\phi \cos\phi - Q_\phi R_\phi R_\theta \sin\phi = \frac{1}{12} \rho h^3 \ddot{\beta}_\phi R_\theta R_\phi \sin\phi \tag{2.20}$$

$$\frac{\partial M_{\phi\theta}}{\partial \phi} R_\theta \sin\phi + \frac{\partial M_{\theta\theta}}{\partial \theta} R_\phi + 2M_{\phi\theta} R_\phi \cos\phi - Q_\theta R_\phi R_\theta \sin\phi = \frac{1}{12} \rho h^3 \ddot{\beta}_\theta R_\theta R_\phi \sin\phi \tag{2.21}$$

In Eqs. (2.17) - (2.19), the terms on the right hand side of the equality sign represent the inertia terms related to the translation of the mid shell surface, and double dot sign indicates differentiation with respect to time twice. In Eqs. (2.20) - (2.21), the terms on the right hand side represent rotary inertia terms. For a hybrid composite shell wall, the mass density ρ is calculated as an average across the thickness. Application of Hamilton's principle also generates conditions on the boundary displacements, and boundary stress resultants applied on the constant meridional coordinate (ϕ=constant) for a shell of revolution. For the free vibration problem boundary conditions are given by [54]

$$\text{Either} \quad N_{\phi\phi} \text{ or } \quad u_\phi^0 = 0 \tag{2.22}$$

$$\text{Either} \quad N_{\phi\theta} \text{ or } \quad u_\theta^0 = 0 \tag{2.23}$$

$$\text{Either} \quad Q_\phi \quad \text{or} \quad w^0 = 0 \tag{2.24}$$

$$\text{Either} \quad M_{\phi\phi} \text{ or } \quad \beta_\phi = 0 \tag{2.25}$$

$$\text{Either} \quad M_{\phi\theta} \text{ or } \quad \beta_\theta = 0 \tag{2.26}$$

Eqs. (2.5) - (2.26) are the governing equations of free vibration for anisotropic shells of revolution, with arbitrary shape of the meridian, based on the Reissner-Naghdi shell theory.

2.2 DERIVATION OF FUNDAMENTAL SYSTEM OF EQUATIONS

The order of the system of Eqs. (2.5) - (2.26) is ten with respect to the meridional coordinate ϕ. Consequently, it is possible to reduce Eqs. (2.5) - (2.26) to ten partial differential equations which are first order in ϕ. The essential point in the derivation of these equations is the definition of the unknowns, as exactly those quantities that enter into the appropriate boundary conditions on a rotationally symmetric edge of the shell of revolution. These unknowns are called as the fundamental variables, and they are defined in the fundamental variable vector $\boldsymbol{\psi}$ as

$$\boldsymbol{\psi}(\phi,\theta,t) = \left[w^0, u_\phi^0, u_\theta^0, \beta_\phi, \beta_\theta, Q_\phi, N_{\phi\phi}, N_{\phi\theta}, M_{\phi\phi}, M_{\phi\theta} \right]^T \tag{2.27}$$

Fundamental system of equations is obtained by deriving expressions for the first derivative of the fundamental variables with respect to meridional coordinate ϕ. For the free vibration analysis,

the time dependence of each quantity in synchronous motion appears in a factor $e^{i\omega t}$, where ω is the natural frequency. Thus, time variable can be eliminated, and in that case the translatory and rotary inertia terms in Eqs. (2.17) - (2.21) would include the natural frequency ω. All the first derivatives of the fundamental variables when collected in matrix format would appear as

$$\frac{d\boldsymbol{\psi}(\phi,\theta)}{d\phi} = f\left(\boldsymbol{\psi}(\phi,\theta), \frac{\partial}{\partial\theta}\left(\boldsymbol{\psi}(\phi,\theta)\right), \frac{\partial^2}{\partial^2\theta}\left(\boldsymbol{\psi}(\phi,\theta)\right)\right) \tag{2.28}$$

The first expression $\dfrac{\partial w^0}{\partial\phi}$ in Eq. (2.28) can be obtained by substituting the transverse shear strain expressions given by Eqs. (2.11) and (2.12) in the second expression of Eq. (2.15), which gives the transverse shear stress resultant Q_ϕ. After the manipulation of the terms, the first fundamental equation can be determined.

$$\frac{\partial w^0}{\partial\phi} = cp_{11}\frac{\partial w^0}{\partial\theta} + c_{12}u_\phi^0 + c_{13}u_\theta^0 + c_{14}\beta_\phi + c_{15}\beta_\theta + c_{16}Q_\phi \tag{2.29}$$

In Eq. (2.29), the coefficients $cp_{11}, c_{12}, c_{13}, c_{14}, c_{15}$ and c_{16} are given in compact form by Kayran and Yavuzbalkan [57]. In the following, all the coefficients of the fundamental system of equations are given in compact form in [57]. Since the coefficients are too lengthy, they are not repeated in this thesis. Readers are referred to Yavuzbalkan [44] for the explicit expressions of the coefficients.

The expressions for the first ϕ derivatives of the mid surface displacements u_ϕ^0, u_θ^0 and rotation terms β_ϕ and β_θ can be determined simultaneously from the constitutive relations given by Eq. (2.13). After substituting the strain displacement relations given by Eqs. (2.5) - (2.10) into the expressions for $N_{\phi\phi}, N_{\phi\theta}$, and $M_{\phi\phi}$, $M_{\phi\theta}$ given in Eq. (2.13), we get four equations involving the first ϕ derivatives of $u_\phi^0, u_\theta^0, \beta_\phi$ and β_θ. These equations can be expressed in compact form as a matrix equation in Eq. (2.30).

$$\mathbf{h}\,\mathbf{d} = \mathbf{j} \tag{2.30}$$

where $$\mathbf{d} = \left[\frac{\partial u_\phi^0}{\partial\phi} \quad \frac{\partial u_\theta^0}{\partial\phi} \quad \frac{\partial\beta_\phi}{\partial\phi} \quad \frac{\partial\beta_\theta}{\partial\phi}\right]^T, \quad \mathbf{j} = \begin{bmatrix} j_1 & j_2 & j_3 & j_4 \end{bmatrix}^T$$

In Eq. (2.30), the components of the 4X4 coefficient matrix $\mathbf{h}$ depend on stiffness coefficients (A_{ij}, B_{ij}, D_{ij}; $i, j = 1,2,6$)), and radii of curvature of the shell (R_ϕ, R_θ). The

components of the vector $\mathbf{j}$ on the right hand side of Eq. (2.30) comprise of the fundamental variables, θ derivatives of the fundamental variables, meridional coordinate ϕ, stiffness coefficients (A_{ij}, B_{ij}, D_{ij} ; $i, j = 1,2,6$), and radii of curvature of the shell (R_ϕ, R_θ). Eq. (2.30) is solved symbolically by Matlab for the first ϕ derivatives of $u_\phi^0, u_\theta^0, \beta_\phi$ and β_θ, and they are given in simplified form by Eqs. (2.31) - (2.34).

$$\frac{\partial u_\phi^0}{\partial \phi} = c_{21}w^0 + c_{22}u_\phi^0 + cp_{22}\frac{\partial u_\phi^0}{\partial \theta} + c_{23}u_\theta^0 + cp_{23}\frac{\partial u_\theta^0}{\partial \theta} + c_{24}\beta_\phi + cp_{24}\frac{\partial \beta_\phi}{\partial \theta} + c_{25}\beta_\theta + cp_{25}\frac{\partial \beta_\theta}{\partial \theta} + c_{27}N_{\phi\phi} + c_{28}N_{\phi\theta} + c_{29}M_{\phi\phi} + c_{210}M_{\phi\theta} \tag{2.31}$$

$$\frac{\partial u_\theta^0}{\partial \phi} = c_{31}w^0 + c_{32}u_\phi^0 + cp_{32}\frac{\partial u_\phi^0}{\partial \theta} + c_{33}u_\theta^0 + cp_{33}\frac{\partial u_\theta^0}{\partial \theta} + c_{34}\beta_\phi + cp_{34}\frac{\partial \beta_\phi}{\partial \theta} + c_{35}\beta_\theta + cp_{35}\frac{\partial \beta_\theta}{\partial \theta} + c_{37}N_{\phi\phi} + c_{38}N_{\phi\theta} + c_{39}M_{\phi\phi} + c_{310}M_{\phi\theta} \tag{2.32}$$

$$\frac{\partial \beta_\phi}{\partial \phi} = c_{41}w^0 + c_{42}u_\phi^0 + cp_{42}\frac{\partial u_\phi^0}{\partial \theta} + c_{43}u_\theta^0 + cp_{43}\frac{\partial u_\theta^0}{\partial \theta} + c_{44}\beta_\phi + cp_{44}\frac{\partial \beta_\phi}{\partial \theta} + c_{45}\beta_\theta + cp_{45}\frac{\partial \beta_\theta}{\partial \theta} + c_{47}N_{\phi\phi} + c_{48}N_{\phi\theta} + c_{49}M_{\phi\phi} + c_{410}M_{\phi\theta} \tag{2.33}$$

$$\frac{\partial \beta_\theta}{\partial \phi} = c_{51}w^0 + c_{52}u_\phi^0 + cp_{52}\frac{\partial u_\phi^0}{\partial \theta} + c_{53}u_\theta^0 + cp_{53}\frac{\partial u_\theta^0}{\partial \theta} + c_{54}\beta_\phi + cp_{54}\frac{\partial \beta_\phi}{\partial \theta} + c_{55}\beta_\theta + cp_{55}\frac{\partial \beta_\theta}{\partial \theta} + c_{57}N_{\phi\phi} + c_{58}N_{\phi\theta} + c_{59}M_{\phi\phi} + c_{510}M_{\phi\theta} \tag{2.34}$$

The first derivatives of Q_ϕ, $N_{\phi\phi}$, $N_{\phi\theta}$, $M_{\phi\phi}$ and $M_{\phi\theta}$ with respect to ϕ are determined from the equilibrium Eqs. (2.19), (2.17), (2.18), (2.20) and (2.21), respectively. After placing the required ϕ derivative of the fundamental variables to the left hand side of the equations, the terms remaining on the right hand side are expressed in terms of fundamental variables, through the use of constitutive Eqs. (2.13) and (2.15), and ϕ derivatives of the mid surface displacements and rotations given by Eq. (2.29) and Eqs. (2.31) - (2.34). The simplified expressions of the derivatives of stress resultants which are obtained by this process are given in Eqs. (2.35) - (2.39).

$$\frac{\partial Q_\phi}{\partial \phi} = c_{61}w^0 + cdp_{61}\frac{\partial^2 w^0}{\partial \theta^2} + c_{62}u_\phi^0 + cp_{62}\frac{\partial u_\phi^0}{\partial \theta} + c_{63}u_\theta^0 + cp_{63}\frac{\partial u_\theta^0}{\partial \theta} + c_{64}\beta_\phi + cp_{64}\frac{\partial \beta_\phi}{\partial \theta} + c_{65}\beta_\theta + cp_{65}\frac{\partial \beta_\theta}{\partial \theta} + c_{66}Q_\phi + cp_{66}\frac{\partial Q_\phi}{\partial \theta} + c_{67}N_{\phi\phi} + c_{68}N_{\phi\theta} + c_{69}M_{\phi\phi} + c_{610}M_{\phi\theta} \tag{2.35}$$

$$\frac{\partial N_{\phi\phi}}{\partial \phi} = c_{71}w^0 + c_{72}u_\phi^0 + cp_{72}\frac{\partial u_\phi^0}{\partial \theta} + c_{73}u_\theta^0 + cp_{73}\frac{\partial u_\theta^0}{\partial \theta} + c_{74}\beta_\phi + cp_{74}\frac{\partial \beta_\phi}{\partial \theta} + c_{75}\beta_\theta + cp_{75}\frac{\partial \beta_\theta}{\partial \theta} + c_{76}Q_\phi + c_{77}N_{\phi\phi} + c_{78}N_{\phi\theta} + cp_{78}\frac{\partial N_{\phi\theta}}{\partial \theta} + c_{79}M_{\phi\phi} + c_{710}M_{\phi\theta} \tag{2.36}$$

$$\frac{\partial N_{\phi\theta}}{\partial \phi} = cp_{81}\frac{\partial w^0}{\partial \theta} + c_{82}u_\phi^0 + cp_{82}\frac{\partial u_\phi^0}{\partial \theta} + cdp_{82}\frac{\partial^2 u_\phi^0}{\partial \theta^2} + c_{83}u_\theta^0 + cp_{83}\frac{\partial u_\theta^0}{\partial \theta} + cdp_{83}\frac{\partial^2 u_\theta^0}{\partial \theta^2} + c_{84}\beta_\phi + cp_{84}\frac{\partial \beta_\phi}{\partial \theta} + cdp_{84}\frac{\partial^2 \beta_\phi}{\partial \theta^2} + c_{85}\beta_\theta + cp_{85}\frac{\partial \beta_\theta}{\partial \theta} + cdp_{85}\frac{\partial^2 \beta_\theta}{\partial \theta^2} + c_{86}Q_\phi + cp_{87}\frac{\partial N_{\phi\phi}}{\partial \theta} + c_{88}N_{\phi\theta} + cp_{88}\frac{\partial N_{\phi\theta}}{\partial \theta} + cp_{89}\frac{\partial M_{\phi\phi}}{\partial \theta} + cp_{810}\frac{\partial M_{\phi\theta}}{\partial \theta} \tag{2.37}$$

$$\frac{\partial M_{\phi\phi}}{\partial \phi} = c_{91}w^0 + c_{92}u_\phi^0 + cp_{92}\frac{\partial u_\phi^0}{\partial \theta} + c_{93}u_\theta^0 + cp_{93}\frac{\partial u_\phi^0}{\partial \theta} + c_{94}\beta_\phi + cp_{94}\frac{\partial \beta_\phi}{\partial \theta} + c_{95}\beta_\theta + cp_{95}\frac{\partial \beta_\theta}{\partial \theta} + c_{96}Q_\phi + c_{97}N_{\phi\phi} + c_{98}N_{\phi\theta} + c_{99}M_{\phi\phi} + c_{910}M_{\phi\theta} + cp_{910}\frac{\partial M_{\phi\theta}}{\partial \theta} \tag{2.38}$$

$$\frac{\partial M_{\phi\theta}}{\partial \phi} = cp_{101}\frac{\partial w^0}{\partial \theta} + c_{102}u_\phi^0 + cp_{102}\frac{\partial u_\phi^0}{\partial \theta} + cdp_{102}\frac{\partial^2 u_\phi^0}{\partial \theta^2} + c_{103}u_\theta^0 + cp_{103}\frac{\partial u_\theta^0}{\partial \theta} + cdp_{103}\frac{\partial^2 u_\theta^0}{\partial \theta^2} + c_{104}\beta_\phi + cp_{104}\frac{\partial \beta_\phi}{\partial \theta} + cdp_{104}\frac{\partial^2 \beta_\phi}{\partial \theta^2} + c_{105}\beta_\theta + cp_{105}\frac{\partial \beta_\theta}{\partial \theta} + cdp_{105}\frac{\partial^2 \beta_\theta}{\partial \theta^2} + c_{106}Q_\phi + cp_{107}\frac{\partial N_{\phi\phi}}{\partial \theta} + cp_{108}\frac{\partial N_{\phi\theta}}{\partial \theta} + cp_{109}\frac{\partial M_{\phi\phi}}{\partial \theta} + c_{1010}M_{\phi\theta} + cp_{1010}\frac{\partial M_{\phi\theta}}{\partial \theta} \tag{2.39}$$

Eq. (2.29) and Eqs. (2.31) - (2.39) are the fundamental system of partial differential equations in ϕ and θ. In the following, reduction of these equations to first order system of ordinary differential equations will be discussed. The reduction process makes use of the rotational symmetry of the shell of revolution.

2.2.1 Classical Fourier decomposition of the fundamental variables

For the classical shell theory, when the full anisotropic form of constitutive relations given by Eqs. (2.13) and (2.15) are utilized, the uncoupling of the governing equations describing the symmetric and antisymmetric responses, with respect to circumferential coordinate, cannot be achieved by the classical Fourier decomposition of the fundamental shell variables. Therefore, multisegment numerical integration technique cannot be employed due to the existence of coupling stiffness coefficients with subscripts 16 and 26 in the constitutive relations, Eq. (2.13), and shear coupling stiffness coefficients with subscript 45 in Eq. (2.15). The same restriction also exists for the first order shear deformation shell theory [55]. Vanishing of coupling stiffness coefficients with subscripts 16, 26, and 45 imply laminates with specially orthotropic layers. Thus, with the classical Fourier decomposition of the fundamental variables in the circumferential direction, it is not possible

to treat shells of revolution with full anisotropic constitutive relations, which allow for arbitrary orientation of fibres with respect to the curvilinear coordinate system of the shell of revolution.

2.2.2 Finite exponential Fourier transform of the fundamental variables

When the full anisotropic form of constitutive relations given by Eqs. (2.13) and (2.15) are utilized, each fundamental variable, in Eq. (2.28), can be expanded in complex Fourier series in an attempt to generate a new fundamental system of equations. The aim is to uncouple of the governing equations, describing the symmetric and antisymmetric responses with respect to circumferential coordinate θ. Complex Fourier series representation of the fundamental variable vector $\boldsymbol{\psi}$ can be shown as

$$\boldsymbol{\psi}(\phi,\theta)=\sum_{-\infty}^{+\infty}\boldsymbol{\psi}_n(\phi)e^{\mathrm{i}n\theta} \tag{2.40}$$

$$\boldsymbol{\psi}_n(\phi)=\frac{1}{2\pi}\int_0^{2\pi}\boldsymbol{\psi}(\phi,\theta)e^{-\mathrm{i}n\theta}=\boldsymbol{\psi}_{nc}(\phi)-\mathrm{i}\,\boldsymbol{\psi}_{ns}(\phi) \tag{2.41}$$

where

$$\boldsymbol{\psi}_{nc}(\phi)=\frac{1}{2\pi}\int_0^{2\pi}\boldsymbol{\psi}(\phi,\theta)\cos n\theta\, d\theta \tag{2.42}$$

$$\boldsymbol{\psi}_{ns}(\phi)=\frac{1}{2\pi}\int_0^{2\pi}\boldsymbol{\psi}(\phi,\theta)\sin n\theta\, d\theta \tag{2.43}$$

It is clearly seen in Eq. (2.41) that application of finite exponential Fourier transform results in doubling of the number of fundamental variables. In this study, conversion of the system of partial differential equations, Eq.(2.29) and Eqs. (2.31) - (2.39), to the system of ordinary differential equations is accomplished through the use of finite exponential transform given by Eq. (2.41). Application of finite exponential transform to first fundamental equation (Eq. (2.29)) will be demonstrated to explain the conversion procedure. Application of finite exponential transform to each term in Eq. (2.29) results in

$$\begin{aligned}\frac{\mathrm{d}w_{nc}^{0}}{\mathrm{d}\phi}-\mathrm{i}\frac{\mathrm{d}w_{ns}^{0}}{\mathrm{d}\phi}=&cp_{11}\mathrm{i}n\left(w_{nc}^{0}-\mathrm{i}\,w_{ns}^{0}\right)+c_{12}\left(u_{\varphi nc}^{0}-\mathrm{i}u_{\varphi ns}^{0}\right)+c_{13}\left(u_{\theta nc}^{0}-\mathrm{i}u_{\theta ns}^{0}\right)+c_{14}\left(\beta_{\phi nc}-\mathrm{i}\,\beta_{\phi ns}\right)\\&+c_{15}\left(\beta_{\theta nc}-\mathrm{i}\,\beta_{\theta ns}\right)+c_{16}\left(Q_{\varphi nc}-\mathrm{i}Q_{\varphi ns}\right)\end{aligned} \tag{2.44}$$

It should be noted that during the application of the finite exponential transform to the θ derivative of the lateral displacement w^0 in Eq. (2.29), the definite integral is taken by applying integration by parts. Since all variables are periodic with a period of 2π in the circumferential direction, the first term of the integral, which includes the difference of the boundary values of w^0 at 0 and 2π vanishes. The same argument also holds for higher order θ derivatives of all fundamental

variables. Thus, after the real and imaginary parts of Eq. (2.44) are separately written, two first order ordinary differential equations are obtained.

$$\frac{\mathrm{d}\, w_{nc}^{0}}{\mathrm{d}\,\phi} = n\, cp_{11}\, w_{ns}^{0} + c_{12}\; u_{\phi nc}^{0} + c_{13}\; u_{\theta nc}^{0} + c_{14}\; \beta_{\phi nc} + c_{15}\; \beta_{\theta nc} + c_{16}\; Q_{\phi nc} \tag{2.45}$$

$$\frac{\mathrm{d}\, w_{ns}^{0}}{\mathrm{d}\,\phi} = -n\; cp_{11}\, w_{nc}^{0} + c_{12}\; u_{\phi ns}^{0} + c_{13}\; u_{\theta ns}^{0} + c_{14}\; \beta_{\phi ns} + c_{15}\; \beta_{\theta ns} + c_{16}\; Q_{\phi ns} \tag{2.46}$$

45)

Application of the finite exponential Fourier transform to the remaining fundamental partial differential equations (Eqs. (2.31) - (2.39)), results in a system of 20 first order ordinary differential equations, which is represented by the following matrix equation.

$$\frac{d\boldsymbol{\psi}}{d\phi} = \frac{d}{d\phi}\begin{bmatrix}\boldsymbol{\psi}^{(1)}(\phi)\\ \boldsymbol{\psi}^{(2)}(\phi)\end{bmatrix} = \mathbf{K}(n,\omega,\phi)\begin{bmatrix}\boldsymbol{\psi}^{(1)}(\phi)\\ \boldsymbol{\psi}^{(2)}(\phi)\end{bmatrix} \tag{2.47}$$

where n is the circumferential wave number and

$$\boldsymbol{\psi}^{(1)}(\phi) = \left[w_{nc}^{0}, w_{ns}^{0}, u_{\phi nc}^{0}, u_{\phi ns}^{0}, u_{\theta nc}^{0}, u_{\theta ns}^{0}, \beta_{\phi nc}, \beta_{\phi ns}, \beta_{\theta nc}, \beta_{\theta ns}\right]^{T} \tag{2.48}$$

$$\boldsymbol{\psi}^{(2)}(\phi) = \tag{2.49}$$

$$\left[Q_{\phi nc}, Q_{\phi ns}, N_{\phi\phi nc}, N_{\phi\phi ns}, N_{\phi\theta nc}, N_{\phi\theta ns}, M_{\phi\phi nc}, M_{\phi\phi ns}, M_{\phi\theta nc}, M_{\phi\theta ns}\right]^{T}$$

The elements of the coefficient matrix **K** are given by Kayran and Yavuzbalkan [57].

The variables used in the fundamental system of equations, Eq. (2.47), are not the actual physical variables, but they are the transformed variables given by Eqs. (2.42) and (2.43). Therefore, the boundary conditions, Eqs. (2.22) – (2.26), specified at the two constant meridional coordinates should also be expressed in terms of the transformed variables. If the exponential transform is applied to the fundamental variables at the boundary of the shell of revolution, then for the free vibration problem the following equality holds.

$$\boldsymbol{\psi}_{n}(\phi) = \frac{1}{2\pi}\int_{0}^{2\pi} \boldsymbol{\psi}(\phi,\theta) e^{-\mathrm{i}n\theta} = \boldsymbol{\psi}_{nc}(\phi) - \mathrm{i}\,\boldsymbol{\psi}_{ns}(\phi) = 0 \tag{2.50}$$

Eq. (2.50) implies that both the real and imaginary parts have to be equal to zero. Thus, the boundary conditions expressed in terms of the transformed fundamental variables can be represented as

$$\text{Either}\quad (N_{\phi\phi nc}, N_{\phi\phi ns}) \text{ or } \quad (u_{\phi nc}^{0}, u_{\phi ns}^{0}) = 0 \tag{2.51}$$

$$\text{Either } (N_{\phi\theta nc}, N_{\phi\theta ns}) \text{ or } (u^0_{\theta nc}, u^0_{\theta ns}) = 0 \tag{2.52}$$

$$\text{Either } (Q_{\phi nc}, Q_{\phi ns}) \text{ or } (w^0_{nc}, w^0_{ns}) = 0 \tag{2.53}$$

$$\text{Either } (M_{\phi\phi nc}, M_{\phi\phi ns}) \text{ or } (\beta_{\phi nc}, \beta_{\phi ns}) = 0 \tag{2.54}$$

$$\text{Either } (M_{\phi\theta nc}, M_{\phi\theta ns}) \text{ or } (\beta_{\theta nc}, \beta_{\theta ns}) = 0 \tag{2.55}$$

Fundamental system of equations, Eq. (2.47), together with the boundary conditions, Eqs. (2.51) – (2.55), specified at the two boundary edges of an anisotropic shell of revolution form an eigenvalue problem for the eigenvectors which are the transformed displacements, and stress resultants. Eigenvalues are the natural frequencies, ω.

2.3 METHOD OF SOLUTION

2.3.1 Multisegment numerical integration

The solution of Eq. (2.47) together with the boundary conditions, Eqs. (2.51) – (2.55), for the natural frequencies and the transformed displacements, and stress resultants, in principle follows the multisegment numerical integration technique. However, due to the application of finite exponential Fourier transform to handle the full anisotropic form of the constitutive relations, eigenvalue extraction process differs from the technique proposed by Kalnins [56].

In the multisegment numerical integration technique, the shell is divided into M number of segments in the meridional direction, and the solution to Eq. (2.47) can be written as

$$\boldsymbol{\psi}(\phi) = \mathbf{T}_i(n, \omega, \phi)\boldsymbol{\psi}(\phi_i) \qquad (i = 1,2,...M) \tag{2.56}$$

where the transfer matrices $\mathbf{T}_i$ are obtained from the initial value problems defined in each segment *i* by

$$\frac{\mathrm{d}\,\mathbf{T}_i(n, \omega, \phi)}{\mathrm{d}\,\phi} = \mathbf{K}(n, \omega, \phi)\,\mathbf{T}_i(n, \omega, \phi) \tag{2.57}$$

with the initial conditions

$$\mathbf{T}_i(n, \omega, \phi_i) = \mathbf{I} \tag{2.58}$$

where **I** is the identity matrix.

Continuity requirements of the fundamental variables at the end points of the segments, lead from Eq. (2.56) to the following partitioned matrix equation

$$\begin{bmatrix} \boldsymbol{\psi}^{(1)}(\phi_{i+1}) \\ \boldsymbol{\psi}^{(2)}(\phi_{i+1}) \end{bmatrix} = \begin{bmatrix} \mathbf{T}^{(1)}(\phi_{i+1}) & \mathbf{T}^{(2)}(\phi_{i+1}) \\ \mathbf{T}^{(3)}(\phi_{i+1}) & \mathbf{T}^{(4)}(\phi_{i+1}) \end{bmatrix}_i \begin{bmatrix} \boldsymbol{\psi}^{(1)}(\phi_i) \\ \boldsymbol{\psi}^{(2)}(\phi_i) \end{bmatrix} \qquad (i = 1,2,...M) \qquad (2.59)$$

When the boundary conditions given by (2.51) – (2.55) are transformed, total of ten elements of the fundamental variable vector $\boldsymbol{\psi}$ at the each edge of the shell, ϕ_1 and ϕ_{M+1}, must be prescribed. For computational ease, the rows of the fundamental variable vector $\boldsymbol{\psi}$ at both ends of the shell, ϕ_1 and ϕ_{M+1}, are adjusted such that the first ten elements of $\boldsymbol{\psi}(\phi_1)$ and the last ten elements of $\boldsymbol{\psi}(\phi_{M+1})$ are the prescribed boundary conditions. In the following, to keep the uniformity of the notation used for the partitioned fundamental variable vector, the boundary conditions are also represented by the same vector notation defined by Eqs. (2.48) and (2.49). Therefore, boundary conditions at the ends of the shell of revolution are expressed by (2.60).

$$\boldsymbol{\psi}^{(1)}(\phi_1) = \boldsymbol{\psi}^{(2)}(\phi_{M+1}) = 0 \qquad (2.60)$$

Eq. (2.59) constitutes a system of linear homogenous matrix equation with 2M unknowns. The solution for the eigenvalue problem requires the writing out of matrix equations in each interval *i* separately, and bringing the whole equation set into an upper diagonal matrix equation by Gauss elimination. The resulting matrix equation is given by Eq.(2.61).

$$\begin{bmatrix} \mathbf{E}_1 & -\mathbf{I} & 0 & . & . & 0 \\ 0 & \mathbf{C}_1 & -\mathbf{I} & 0 & . & 0 \\ . & 0 & . & . & . & . \\ . & . & 0 & . & . & . \\ 0 & . & . & 0 & \mathbf{E}_M & -\mathbf{I} \\ 0 & . & . & 0 & 0 & \mathbf{C}_M \end{bmatrix} \begin{bmatrix} \boldsymbol{\psi}^{(2)}(\phi_1) \\ \boldsymbol{\psi}^{(1)}(\phi_2) \\ . \\ . \\ \boldsymbol{\psi}^{(2)}(\phi_M) \\ \boldsymbol{\psi}^{(1)}(\phi_{M+1}) \end{bmatrix} = 0 \qquad (2.61)$$

where, the $(10X10)$ matrices $\mathbf{E}_i$ and $\mathbf{C}_i$ are evaluated successively from

$$\mathbf{E}_1 = \mathbf{T}_1^{(2)} \qquad (2.62)$$

$$\mathbf{C}_1 = \mathbf{T}_1^{(4)} \mathbf{E}_1^{-1} \qquad (2.63)$$

$$\mathbf{E}_i = \mathbf{T}_i^{(2)} + \mathbf{T}_i^{(1)} \mathbf{C}_{i-1}^{-1} \qquad (i = 2,3,...,M) \qquad (2.64)$$

$$\mathbf{C}_i = \left(\mathbf{T}_i^{(4)} + \mathbf{T}_i^{(3)} \mathbf{C}_{i-1}^{-1} \right) \mathbf{E}_i^{-1} \qquad (i = 2,3,...,M) \qquad (2.65)$$

Natural frequencies are determined by requiring non-trivial solution of the last row of Eq. (2.61), and setting the determinant of the coefficient matrix to zero.

$$\det \mathbf{C}_M = 0 \tag{2.66}$$

Assuming that a particular natural frequency is determined from Eq. (2.66), then from the last row of Eq. (2.61), $\boldsymbol{\psi}^{(1)}(\phi_{M+1})$ is determined up to an arbitrary constant. The remaining unknown fundamental variables at each ends of the shell segments can then be calculated successively from

$$\boldsymbol{\psi}^{(2)}(\phi_M) = \mathbf{E}_M^{-1}\, \boldsymbol{\psi}^{(1)}(\phi_{M+1}) \tag{2.67}$$

$$\boldsymbol{\psi}^{(1)}(\phi_{M-i+1}) = \mathbf{C}_{M-i}^{-1}\, \boldsymbol{\psi}^{(2)}(\phi_{M-i+1}) \quad (i = 1,2,...,M-1) \tag{2.68}$$

$$\boldsymbol{\psi}^{(2)}(\phi_{M-i}) = \mathbf{E}_{M-i}^{-1}\, \boldsymbol{\psi}^{(1)}(\phi_{M-i+1}) \quad (i = 1,2,...,M-1) \tag{2.69}$$

For the specially orthotropic material model and improved shell theory, which includes first order shear deformation, the order of the characteristic matrix $\mathbf{C}_M$ is five [55]. However, the derivation process for the characteristic matrix shows that, for the macroscopically anisotropic material model and first order shear deformation theory, the order of the characteristic matrix $\mathbf{C}_M$ becomes ten.

2.3.2 Frequency trial method

The solution of natural frequencies through Eq. (2.66) requires a frequency search, because the determinant of the characteristic matrix $\mathbf{C}_M$ can only be evaluated if all the transfer matrices $\mathbf{T}_i$ are determined at each end of the shell segments. On the other hand, since the coefficient matrix **K** includes the frequency term ω, solution of the initial value problems (Eq. (2.57)) subject to initial conditions (Eq. (2.58)) can be accomplished for any particular circumferential vibration mode, only if a trial frequency is given as input. In principle, Kalnins [56] solved the natural frequencies of isotropic shells of revolution using classical shell theory by calculating the determinant of $\mathbf{C}_M$ for incremented values of the frequency ω, until a change in the sign of the determinant of $\mathbf{C}_M$ occurs. Later on Kayran and Vinson [55] used the same technique to extract the natural frequencies for the specially orthotropic shells with arbitrary number of layers using the first order shear deformation shell theory. In these studies, because the full anisotropic constitutive relations were not used, classical Fourier decomposition was applied, and it was observed that determinant of the characteristic matrix $\mathbf{C}_M$ actually changed sign at the natural frequency.

However, as the fundamental system of equations are applied by the application of finite exponential Fourier transform to the circumferentially coupled partial differential equations, the determinant of the characteristic matrix $\mathbf{C}_M$ does not change sign at the natural frequency. Variation of the determinant of the characteristic matrix for the case of exponential Fourier transform is studied by Kayran and Yavuzbalkan [57]. In the referred study, it is seen that the determinant of the

10x10 characteristic matrix of the exponential Fourier transform is exactly the square of the determinant of the 5x5 characteristic matrix of the classical Fourier decomposition.

Because the determinant of the characteristics matrix does not change sign through a natural frequency, a different algorithm is employed by Kayran and Yavuzbalkan to locate the natural frequency. The method essentially relies on checking the slope change of the determinant of the characteristic matrix, and detecting the interval where a natural frequency resides. After the extraction of the natural frequency, the transformed fundamental shell variables (Eqs. (2.42) and (2.43)) along the meridian of the shell are determined recursively from Eqs. (2.67) – (2.69) by operating on the already determined sub matrices $\mathbf{C}_i$ and $\mathbf{E}_i$ The dominant fundamental variable involved in the particular natural vibration mode is decided by looking at the normalized mode shapes along the meridian of the shell. For the particular circumferential wave number, the actual variation of the fundamental variables can be constructed by utilizing the cosine and sine parts of the fundamental shell variables, in the complex Fourier series representation Eqs. (2.40) and (2.41).

In the present study, the initial value problems defined by Eqs. (2.57) and (2.58) are solved by numerically integrating the equations by the International Mathematical and Statistical Library (IMSL) subroutine DIVPAG utilizing the Adams-Moulton numerical integration option. The initial step in the solution procedure is to integrate Eq. (2.57), subject to the initial condition Eq. (2.57), in each shell segment and store the elements of the transfer matrices at the end of each shell segment. For a particular circumferential wave number n and trial frequency ω, Eq. (2.57) is numerically integrated and the continuous meridional variation of the winding angle, thickness and the stiffness coefficients, due to semi-geodesic winding, of the shell of revolution is handled during the numerical integration process. In the current study numerical integration of Eq. (2.57) within each shell segment is performed by the IMSL subroutine DIVPAG which uses a user supplied subroutine where all the elements of the coefficient matrix K are given. Therefore, as long as continuous variation of the elements of the coefficient matrix along the meridian of the shell of revolution is coded accordingly, arbitrary meridional variation of the shell properties can be handled very accurately.

CHAPTER 3

FILAMENT WINDING LAWS

In this section filament winding laws will be briefly reviewed to aid the understanding of the variation of the winding angle and the thickness of filament wound shells of revolution along the meridian. The geometry and winding patterns are the basic parameters governing the manufacturing of a filament wound shell of revolution. Figure 3.1 shows a typical fiber path on the surface of a shell of revolution. On the surface of the shell of revolution, which is defined by $\vec{S}(x,\theta)$, fiber follows a path $\vec{\Gamma}(s)$ [43].

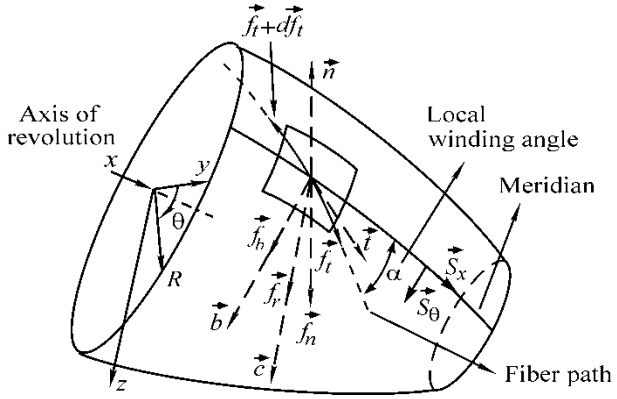

Figure 3.1 Fiber path on the surface of a shell of revolution

$$\vec{S}(x,\theta) = x\hat{\varepsilon}_1 + R(x)\cos\theta\hat{\varepsilon}_2 + R(x)\sin\theta\hat{\varepsilon}_3 \tag{3.1}$$

$$\vec{\Gamma}(s) = x(s)\hat{\varepsilon}_1 + \theta(s)\hat{\varepsilon}_\theta \tag{3.2}$$

In Eqs. (3.1) and (3.2) $\hat{\varepsilon}_1, \hat{\varepsilon}_2, \hat{\varepsilon}_3$ represent the unit vectors in the *x*, *y* and *z* directions, and $\hat{\varepsilon}_\theta$ represents the unit vector in the tangential direction θ. The change in the fiber tension $\vec{f}_t$ along the fiber path gives rise to a force $\vec{f}_r$, per unit length of the fiber on the mandrel surface.

$$\vec{f}_r = \frac{d\vec{f}_t}{ds} \tag{3.3}$$

$\vec{f}_r$ is directed towards the center of curvature of the fiber path and it can be split into a normal component $\vec{f}_n$, which is perpendicular to the surface of the shell of revolution, and a transverse force $\vec{f}_b$ which lies in the tangent plane drawn to the surface. $\vec{f}_b$ is perpendicular to the plane formed by the tangent vector to the fiber path $\vec{t}$ and the normal vector $\vec{n}$. In semi-geodesic winding terminology, it is common to define the slippage tendency "*fst*" which is defined as the ratio of the transverse force $\vec{f}_b$ and normal force $\vec{f}_n$ [6].

$$fst = \frac{\vec{f}_r.\vec{b}}{\vec{f}_r.\vec{n}} = \frac{\vec{c}.\vec{b}}{-\vec{c}.\vec{n}} \tag{3.4}$$

In Eq.(3.4) $\vec{c}$ is the unit curvature vector, and $\vec{b}$ is the binormal vector and they are defined by Eq. (3.5).

$$\vec{c} = \frac{d\vec{t}}{ds}, \quad \vec{b} = \vec{t} \text{ x } \vec{n}, \quad \vec{t} = \frac{d\vec{S}}{ds}, \quad \vec{n} = -\vec{S}_x \text{ x } \vec{S}_\theta \tag{3.5}$$

where $\vec{S}_x$ and $\vec{S}_\theta$ are the normalized basis vectors of the surface in the x and θ directions, respectively.

$$\vec{S}_x = \frac{1}{\left|\partial\vec{S}/\partial x\right|}\frac{\partial\vec{S}}{\partial x} \quad , \quad \vec{S}_\theta = \frac{1}{\left|\partial\vec{S}/\partial\theta\right|}\frac{\partial\vec{S}}{\partial\theta} \tag{3.6}$$

The tangent vector to the fiber path can also be written as in Eq.(3.7);

$$\vec{t} = \vec{S}_x \cos\alpha + \vec{S}_\theta \sin\alpha \tag{3.7}$$

where α is the local winding angle shown in Figure 3.1.

Eq. (3.4) can be manipulated and brought into the form given by Eq. (3.8) with the help of Eqs.(3.5)-(3.7). A detailed derivation of Eq. (3.8) can be found in [43].

$$\frac{d\alpha}{dx} = \frac{fst\left((1+R'^2)\sin^2\alpha - RR''\cos^2\alpha\right) - (1+R'^2)R'\sin\alpha}{R(1+R'^2)\cos\alpha} \tag{3.8}$$

In Eq. (3.8) *R'* and *R''* indicate the first and second derivatives of with respect to x which is the axial coordinate shown in Figure 3.1. Eq.(3.8) gives the variation of the winding angle along the axis of the shell of revolution. Since the slippage tendency "*fst*" is taken as non-zero, Eq. (3.8) gives

the winding pattern for a semi-geodesic fiber path on the surface of the shell of revolution. For geodesic fiber path, slippage tendency "*fst*" is taken as zero and in that case Eq. (3.8) simplifies to

$$\frac{d\alpha}{dx} = \frac{-R'}{R}\tan\alpha \tag{3.9}$$

3.1 GEODESIC WINDING

Due to the fiber path stability requirements in the filament winding, the trajectory of the fiber path and the corresponding winding angles cannot be selected freely. Fibers are wound onto the mandrel along different paths which require stability and no slippage. The trajectory connecting two points on a surface according to the shortest distance over that surface is defined as the geodesic path. As this path represents the shortest distance, a fiber placed along this line will not slip when being pulled and no friction will be required to keep the fiber stable.

For a shell of revolution with varying radii of curvature, Eq. (3.9) can be integrated from a known winding angle at one end of the shell of revolution, and the winding angle at any axial location can be calculated.

For a general shell of revolution integration of Eq. (3.9) from a known winding angle α_1 at one edge of the shell $(x_1,R_1)$to any axial location (x,R) yields Eq. (3.10).

$$\sin\alpha = \sin\alpha_1 \frac{x_1}{x} = \sin\alpha_1 \frac{R_1}{R} \tag{3.10}$$

For a truncated spherical shell of revolution $R_\phi = R_\theta = R_s$ and $R = R_s \sin\phi$ therefore, Eq. (3.10) can be expressed as

$$\sin\alpha = \sin\alpha_1 \frac{\sin\phi_1}{\sin\phi} \tag{3.11}$$

where ϕ_1 is the meridional angle of the starting edge of the winding, and ϕ is the meridional angle at any axial location.

It should be noted that with geodesic winding once the starting edge and winding angle are chosen for a given geometry the whole fiber trajectory is determined. Therefore, fiber path freedom is quite limited with geodesic winding.

3.2 SEMI-GEODESIC WINDING

Filaments are not necessarily wound geodesically to be stable. Stable non-geodesic winding, often called semi-geodesic winding, can also be performed. This requires a little deviation from the geodesic paths, depending on the required friction to hold the fiber at the desired position. Semi-geodesic winding offers more design freedom but still remains limited to the available friction during the winding process.

3.2.1 Variation of the winding angle for truncated conical shell of revolution

In case of semi-geodesic winding of conical shell of revolution, Eq. (3.8) can be simplified because R'' vanishes and R' is given by tan β where β ($\pi/2$-ϕ) is the semi-vertex angle of the truncated cone. Therefore, for a truncated conical shell with the semi-vertex angle β, as shown in Figure3.2, closed form solution to Eq. (3.8) can be found.

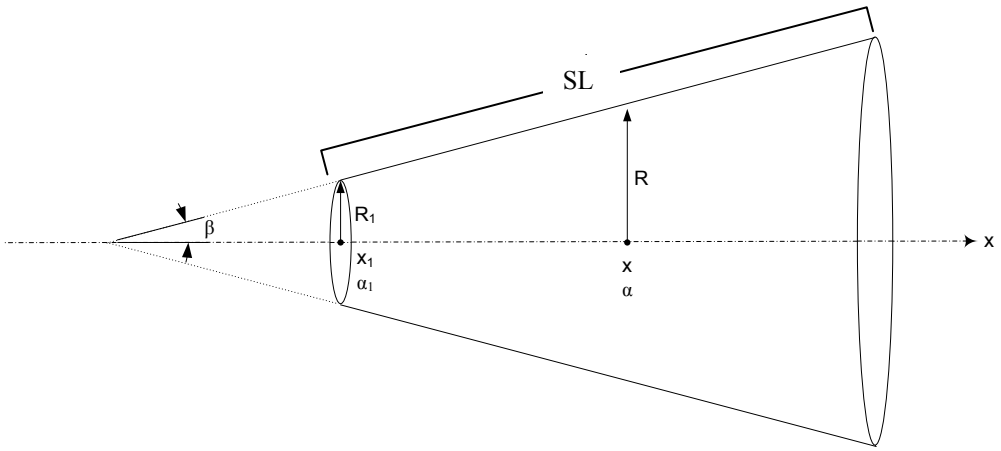

Figure3.2 Truncated conical shell of revolution geometry

Using the geometrical relations for a truncated conical shell of revolution shown in Figure 3.2, Eqs. (3.12) are derived.

$$\left\{\begin{array}{l} R = x.\tan\beta \\ R' = \tan\beta \\ R'' = 0 \end{array}\right\} \tag{3.12}$$

Substituting R, R' and R'' in Eq. (3.8) where primed terms indicate the first and second derivatives of R with respect to x, the axial coordinate, Eq. (3.13) is obtained.

$$\frac{d\alpha}{dx} = \frac{(fst.\sin\alpha - \tan\beta).\tan\alpha}{x.\tan\beta} \tag{3.13}$$

Integration of Eq.(3.13) from a known winding angle α_1 at one edge o f the shell (x_1,R_1) to any axial location (x,R) yields to Eq. (3.15). Detailed solution for the integration of Eq. (3.14) is given in the Appendix A.

$$\int_{\alpha_1}^{\alpha} \frac{\tan\beta}{(fst.\sin\alpha - \tan\beta).\tan\alpha} d\alpha = \int_{x_1}^{x} \frac{1}{x} dx \tag{3.14}$$

$$\sin\alpha = \frac{R_1 \sin\alpha_1 \ \tan\beta}{fst\ (R_1 - R)\sin\alpha_1 + R\tan\beta} \tag{3.15}$$

3.2.2 Variation of the winding angle for truncated spherical shell of revolution

For a spherical shell of revolution R_ϕ and R_θ is equal to the radius of the sphere R_s as shown in Figure3.3 and R is given by $R_s \sin\phi$.

$$\begin{Bmatrix} R_\phi = R_\theta = R_S \\ dx = ds.\sin\phi \\ ds = R_\phi.d\phi \end{Bmatrix} \tag{3.16}$$

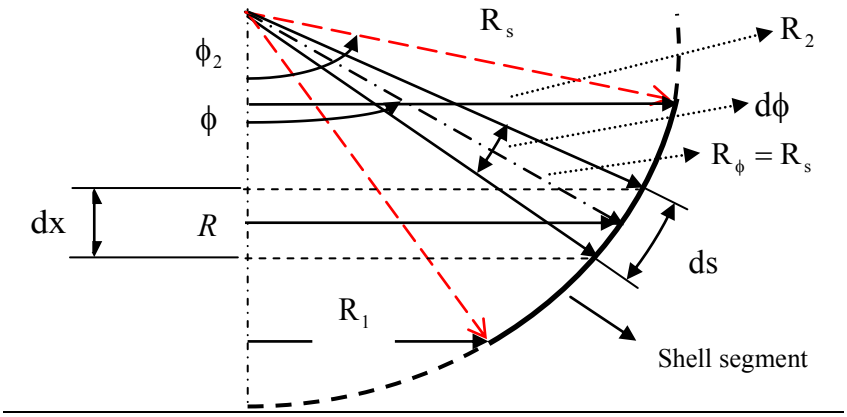

Figure 3.3 Spherical shell of revolution geometry

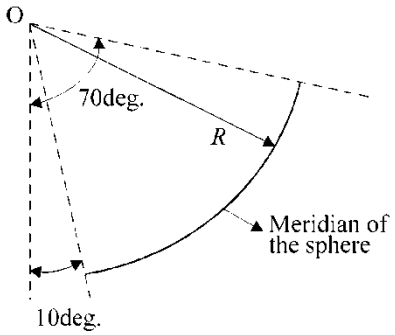

Figure 3.4. Geometry of the spherical shell studied

For spherical shells of revolution or any general shell of revolution, the variation of the winding angle with respect to meridional coordinate ϕ should be obtained. Therefore, first a relationship between $\frac{d\alpha}{d\phi}$ and $\frac{d\alpha}{dx}$ has to be derived where $\frac{d\alpha}{d\phi}$ can be obtained employing chain rule for $\frac{d\alpha}{dx}$.

In this case Eq. (3.8) simplifies to

$$\frac{d\alpha}{d\phi} = \frac{fst - \cot\phi \sin\alpha}{\cos\alpha} \tag{3.17}$$

where ϕ is the meridional coordinate shown in Figure2.1. A detailed derivation of Eq. (3.17) is presented in Appendix B.

It should be noted that Eq. (3.17) cannot be explicitly integrated because ϕ and α variables cannot be separated. For a truncated spherical shell of revolution, to determine the winding angle at a meridional location ϕ Eq. (3.17) has to be integrated from a known winding angle α_1 at one edge of the shell (ϕ_1) to any meridional location (ϕ). It should be noted that during the numerical integration of Eq. (2.57) in shell segments, for a conical shell of revolution the winding angle can be directly calculated from Eq. (3.15) at each integration step. However, for a spherical shell of revolution calculation of the winding angle at a meridional location necessitates another numerical integration of Eq. (3.17) at each integration step during the numerical integration of Eq. (2.57) in shell segments. Therefore, computational cost increases substantially. For the spherical shell of revolution, to overcome the computational cost of determining the winding angle at any meridional location the winding angles at the centers of each shell segment are calculated in the beginning, and they are taken as constant for the whole shell segment during the numerical integration of Eq. (2.57). Thus, numerical integration of Eq. (3.17) at each integration step during the numerical integration of Eq. (2.57) is eliminated. It should be noted that as long as sufficient number of shell segments is used during the numerical integration of Eq. (2.57), assigning constant winding angle, which is

calculated at the center of the shell segment, to the whole segment brings about no accuracy lost in determining the natural frequencies.

3.3 THICKNESS VARIATION

In filament winding operation, any unit length of the fiber at any location on the surface of the shell of revolution brings with itself the same amount of matrix, and the number of fibers in a cross-section is always constant. Therefore, the amount of material in a circumferential slice of the shell of revolution, with unit fiber length at a fiber orientation angle of α, should remain constant. Thus, it follows that the thickness of a general filament wound shell of revolution, at any axial location, can be calculated from Eq. (3.18) [6, 18, 43].

$$t = t_1 \frac{R_1 \cos\alpha_1}{R \cos\alpha} \tag{3.18}$$

where t represents the thickness of a single ply at the axial location where the radius is R, and t_1 represents the thickness of a single ply at one edge of the shell of revolution where the radius is R_1.

3.4 APPLICABILITY OF THE WINDING LAWS

In case of geodesic or semi-geodesic winding of shells of revolution Eqs. (3.8) and (3.18), which give the variation of the winding angle and thickness along the shell of revolution, are valid if winding angle α is less than 90^o. For pure circumferential winding fiber orientation angle is 90^o, therefore Eqs.(3.8) and (3.18) do not apply, and thickness remains constant since any unit length of the fiber brings with itself the same amount of matrix. Equation (3.18) shows that the thickness of the shell of revolution increases substantially when the fiber orientation angle approaches 90^o. Practically the increase in the thickness of the shell of revolution is caused by fiber concentration on a relatively small area due to the repetitive rotation of the fiber around the circumference.

For the geodesic winding it is clear from Eq. (3.10) that if the winding starts at the small radius edge of the shell of revolution, as long as the initial winding angle is less than 90^o, then the winding angle will decrease along the meridian and it will always be less than 90^o. However, if the winding starts at the large radius edge, then the winding angle will increase along the meridian of the shell, and depending on the initial winding angle and the ratio of the radii (R_1/R), the winding angle may reach 90^o somewhere along the axis of the shell of revolution.

For the semi-geodesic winding depending on the shell geometry, initial winding angle and available friction the winding angle may increase along the shell axis even though the winding starts at the small radius edge; the increase of the winding angle along the shell axis is demonstrated for a truncated conical shell in Section 5.1.

3.5 INTEGRATION OF SEMI-GEODESIC WINDING LAWS TO THE NUMERICAL INTEGRATION BASED COMPUTER CODE

The computer code developed to determine the natural frequencies and the variation of all the fundamental shell variables of laminated anisotropic shells of revolution employs the geodesic winding angle calculation for the fibers. Introduction of the friction to the winding process allows the use of semi-geodesic fiber paths. For conical shells of revolution Eq. (3.15) describes the semi-geodesic winding angle as a function of initial winding angle, geometry of the shell and the slippage tendency. Thus, for conical shell geodesic winding angle formula Eq. (3.10) is replaced by semi-geodesic angle formula derived (Eq. (3.15)). The analytical solution obtained for the conical shell decreases the computational costs and allows calculating and employing winding angle at every meridional step of DIVPAG solver. However, the convenience of analytical solution is not applicable for a spherical shell of revolution. For a spherical shell of revolution, winding angle at every meridional coordinate should be calculated by integrating Eq. (3.17) from a known winding angle α_1 to any meridional location. As mentioned before in section 3.4, integration of Eq. (3.17) to determine the winding angle at meridional locations of each DIVPAG step increases the computational costs drastically. Although, computer code for this approach is generated, to overcome the high computational cost the winding angles at the centers of each shell segment are calculated in the beginning of the code and assigned to the whole segment respectively as constant values for each segment. It should be stated that this approach might bring some accuracy loss for small number of shell segments; however as long as sufficient number of shell segments is selected, this approach leads to the same results as the first approach. Results comparing two methods will be presented in the next sections of this thesis in detail.

CHAPTER 4

VERIFICATION AND COMPARISON WITH FINITE ELEMENT SOLUTION

Present study employs the multisegment numerical integration technique in order to determine natural frequencies and the transformed displacements and stress resultants. Most of the data on the vibration analysis of composite shells of revolution can be found on shells of revolution with constant radii of curvature such as cylindrical shells of revolution which have constant thickness and winding angle. For composite shells of revolution with variable radii of curvature the variation of thickness and winding angle has not been taken into consideration in the literature except for the work of Korjakin et.al [42]. Korjakin analyzed the damped vibrations of conical shells of revolution by incorporating the thickness and winding angle change due to geodesic winding.

Validation of this multisegment numerical integration method for composite shells of revolution with constant thickness and winding angle has been previously given by Yavuzbalkan [44] and Kayran and Yavuzbalkan [57]. However, for semi-geodesic winding it has not been possible to find data to compare against. Therefore, due to limited references on the topic, a comparison study is conducted using a commercial finite element solver NASTRAN v2007.0, and the results of multisegment numerical integration and finite element method are compared.

For comparison purposes, analysis of an anisotropic shell is performed for a conical shell geometry which is clamped at small radius end and fixed at large end. The shell studied has the material and geometric properties as given below. Material directions are presented in Figure 4.1.

- Modulus in the fibre direction: E_1 =213.74GPa, Modulus transverse to fibre: E_2 =18.62 GPa
- Shear moduli: $G_{12} = G_{13} = 5.171$ GPa, $G_{23} = 4.137$ GPa, Poisson's ratio: ν_{12} =0.28
- Mass density: ρ =2051.88 kg m^{-3}
- Shell small radius, $R_{\min}$= 57 cm, Shell large radius, $R_{\max}$ = 60 cm

- Stacking sequence for starting winding angle of 30^o is $[30^o/-30^o/30^o/-30^o]_S$ at the small radius end.
- Preset slippage tendency, *fst* = 0.2

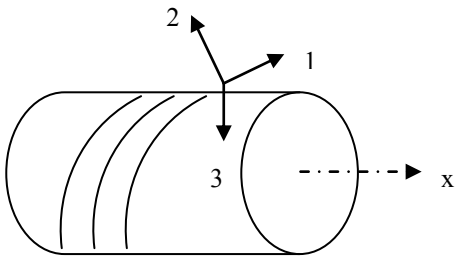

Figure 4.1 Direction definitions

Comparison of natural frequencies in Chapter 4 and 5 was made based on the non-dimensional frequency parameter given in Eq. (4.1);

$$\Omega = \omega h \sqrt{\rho / E_1} \tag{4.1}$$

The comparison study has been performed for the conical shell by using 50 segments along axial direction. In order to confirm mesh density used in the finite element model (FEM), case studies with different mesh sizes on the conical model were carried out. Influence of mesh density is presented in Appendix C. The results presented in Appendix C show that division of the shell structure into 50 segments in the meridional direction is a highly acceptable compromise between output quality and the computation time.

A continuous solution comparison is avoided as in case of inexistent analytical solution (e.g. spherical shell); continuous solution is not cost-effective and not employed. In addition, the use of high number of axial elements necessitates large number of elements in the circumferential direction and this increases the computational cost of the finite element solution.

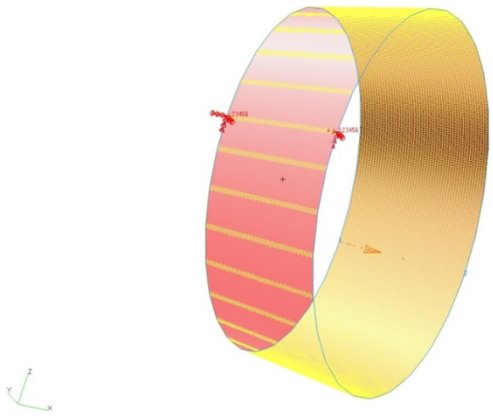

Figure 4.2 Meshed finite element model of the conical shell geometry

In order to realize FEA model shown in Figure 4.2, conical geometry is meshed in PATRAN 2005 r2 and elements corresponding to same segment on axial location are assigned with the same winding angle and thickness using the values calculated externally. The winding angle and thickness assignments to the elements in the circumferential slice at a particular axial location have been made manually without writing an external subroutine to automate the process. Automatic assignment of the winding angle and layer thicknesses to the elements still needs to be worked on as a future work.

In case of the conical shell studied in this section, using the available analytical solution, the winding angle and thickness values at the axial midpoint of each segment is calculated and assigned as constant to the corresponding elements. However, in order to extend the present study to shells of revolutions other than conical geometry, a numerical solution is necessary to define winding angles and thicknesses. As solution of Eq. (2.88) is possible analytically for conical shell geometry, it is used for the purpose of defining the most accurate numerical approach. Different integration possibilities considered can be stated as following (see Figure 4.3 and 4.4 for a graphical representation);

1. Integration from the beginning of the shell to the midpoint of the segment
2. Integration from the midpoint of the segment before to the midpoint of the current segment
3. Integration from the beginning of the shell to the end of segment and assigning the average of beginning and end winding angle of segment to the midpoint value of the segment
4. Integration from the end of segment to the beginning of next segment and assigning the average value to the midpoint of the segment.

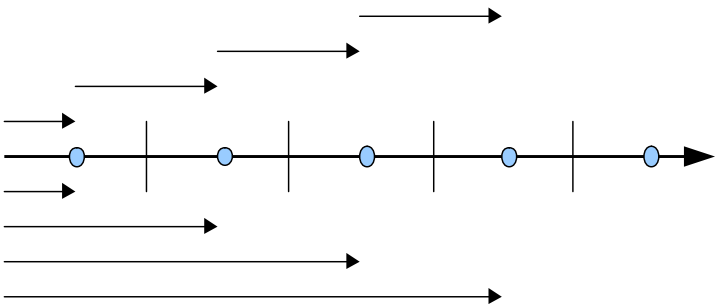

Figure 4.3 Graphical representation for the numerical integration options 1 and 2. Directly solve for the midpoint value and assign this value to the segment.

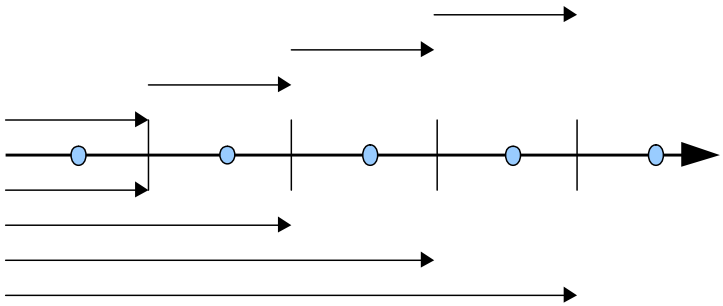

Figure 4.4 Graphical representation for the numerical integration options 3 and 4. Use the average of the beginning and end of each segment for the relevant segment.

In case of integrating from the beginning of the shell for each segment, as the number of segment increases, the integration step increases as well. To compensate this deterioration of solution resolution, in the solver the numerical integration step is related proportionally to the number of segment. Eq. (4.2) shows the step size adaptation used which is calculating the step size (H) considering the current axial location (R) and segment number ($L_{SEGMENT}$). In Eq. (4.2), the multiplier "50" in the denominator is selected as a result of trade-off analysis between computation cost and solution accuracy.

$$H = \frac{(R - R_i)}{50 \cdot L_{SEGMENT}} \tag{4.2}$$

4th order Runge-Kutta (RK4) solution is adapted to the current differential problem and Eq. (2.93) is integrated numerically. Table 4.1 shows the winding angles, in radians, calculated using different methods for a conical shell which is wound starting with 30^o from the small end and slippage tendency is 0.2. Although all four approaches gave good results as, compared to analytical solution as presented in Table 4.1, the best accuracy considering all axial location is obtained by employing the integration method 1. As a result of this analysis, method 1 is used for all numerical integration solutions throughout this research.

Table 4.1 Comparison of different numerical integration approaches with analytical solution for a 500 segment conical shell. (fst=0.2, α_1=30^o)

Winding angle [radians]					
Segment #	***Method 1***	***Method 2***	***Method 3***	***Method 4***	***Analytical***
1	0.52354999	0.52354999	0.523549926	0.523549926	0.52354999
100	0.517100598	0.517087631	0.517100472	0.517087633	0.517100598
200	0.510754125	0.510728473	0.510754002	0.510754002	0.510754002
300	0.504569613	0.504531737	0.504569614	0.50453174	0.504569735
400	0.498540844	0.498491072	0.498540845	0.498490955	0.498540963
500	0.492661586	0.492600003	0.492661588	0.492600063	0.492661703

Once the method for numerical integration method is decided, it is necessary to determine the accuracy of the RK4 method compared to the analytical solution. Table 4.2 shows the comparison of the normalized frequencies calculated using analytical and numerical method of calculation procedure of winding angle for the conical shell which is geometrically described above. The initial winding angle is taken as 45^o, preset slippage tendency is 0.2 and shell is divided into 50 segments in the axial direction for multisegment solution. Calculations are performed for two different boundary conditions clamped-free (CFS) and clamped-clamped (CCS). The small radius edge is taken as clamped and large radius edge is taken as free and clamped, respectively. As it can be seen from Table 4.2 percent errors in case of numerical integration based calculation of the winding angle is very small and does not cause any problems to be used in case needed (e.g. spherical shell analysis).

Table 4.2 Comparison of normalized frequencies calculated using analytical and numerical calculation procedure of the winding angle. (50 segments, fst=0.2, α_1=45^o)

	Analitical Solution		RK4 Solution		% ERROR	
n	***CFS***	***CCS***	***CFS***	***CCS***	***CFS***	***CCS***
0	0.888541	0.989288	0.888538	0.989281	0.000338	0.000708
1	0.815486	1.012917	0.815484	1.012909	0.000245	0.000790
2	0.646735	1.060461	0.646734	1.060453	0.000155	0.000754
3	0.474222	1.097605	0.474223	1.097597	0.000211	0.000729
4	0.341413	1.135936	0.341415	1.135928	0.000586	0.000704
5	0.251200	1.124479	0.251201	1.124477	0.000398	0.000178
6	0.194719	0.979998	0.194720	0.979999	0.000514	0.000102
7	0.163799	0.841352	0.163799	0.841354	0.000000	0.000238
8	0.152973	0.723383	0.152973	0.723386	0.000000	0.000415
9	0.157610	0.629213	0.157609	0.629216	0.000634	0.000477
11	0.195922	0.512601	0.195920	0.512602	0.001021	0.000195
13	0.256012	0.483099	0.256009	0.483097	0.001172	0.000414
15	0.330097	0.518269	0.330093	0.518266	0.001212	0.000579

Figure 4.5 shows the mode shapes and natural frequencies for circumferential wave numbers ranging from n=0 to n=5. Given plots are the outputs calculated by NASTRAN v2007.0 solver and represented in PATRAN 2005 r2. In Figure 4.5 half of the total number of nodal points gives the circumferential wave number. Thus, in the comparison of the results of the finite element solution with the results of multi-segment numerical integration solution the wave number is taken as the main parameter in identifying the right mode used in comparing the natural frequencies.

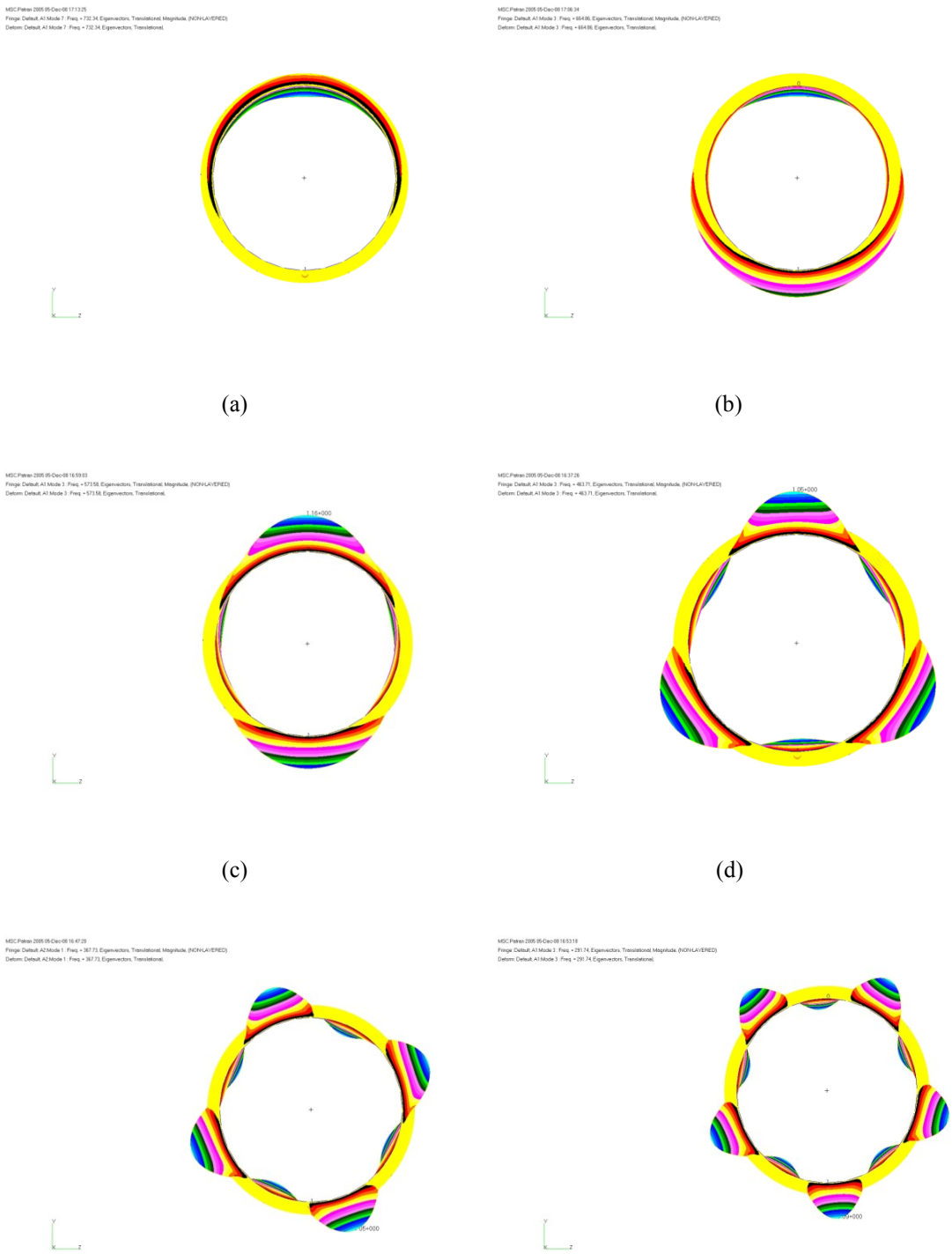

(a) (b)

(c) (d)

(e) (f)

Figure 4.5 Finite Element Model output results for ***(a)*** n=0, ***(b)*** n=1, ***(c)*** n=2, ***(d)*** n=3, ***(e)*** n=4, ***(f)*** n=5

Table 4.3 gives a comparison between natural frequencies determined by employing analytical and numerical calculation of winding angle and thickness at each axial location. To overcome the computational cost of determining the winding angle at any meridional location the winding angles at the centers of each shell segment are calculated in the beginning, and they are taken as constant for the whole shell segment. As mentioned before, analytical results presented in Table 4.3 represents the natural frequencies obtained using continuous (at each DIVPAG step) calculation of winding angle along the axial coordinates. On the other hand, numerical determination of the winding angle employs RK4 from the beginning of the shell to midpoint of each segment for 50 segments. Similarly, FEM assumes constant winding angle and thicknesses for each segment, where midpoint winding angles and thicknesses are calculated analytically externally.

The results show that most of the non-dimensional frequency parameters agree very well up to the fourth digit for the numerical and analytical determination of the winding angle. Finite element solution has a maximum 3% of deviation from the solution determined by the multisegment numerical integration method modified for semi-geodesic fiber paths. Based on the comparison of the natural frequencies determined by the use of multi-segment numerical integration method and the finite element method it can be concluded that maximum 3% difference is an acceptable difference and the verification is complete.

Table 4.3 Comparison of natural frequencies calculated using numerical integration method and finite element method.

Analytical Calculation of Winding Angle – Natural Frequency Output			
n	***f [rad/s]***	***Ω***	
0	4526.20	0.8510	
1	4302.04	0.8088	
2	3689.88	0.6937	
3	2988.18	0.5618	
4	2365.08	0.4446	
5	1868.82	0.3513	
Numerical Calculation of Winding Angle – Natural Frequency Output (50 Segment)			
n	***f [rad/s]***	***Ω***	
0	4526.21	0.8510	
1	4302.05	0.8088	
2	3689.88	0.6937	
3	2988.19	0.5618	
4	2365.09	0.4446	
5	1868.83	0.3514	
FEM Output (50 segment)			
n	***f [rad/s]***	***Ω***	***Difference %***
0	4601.43	0.8651	1.63
1	4177.44	0.7854	-2.98
2	3603.91	0.6776	-2.39
3	2913.58	0.5478	-2.56
4	2310.52	0.4344	-2.36
5	1833.06	0.3446	-1.95

One should note that the verification study presented in this chapter is not conducted in order to define the accuracy of the multi-segment numerical integration solution technique. multi-segment numerical integration solution method is a semi-analytical solution, only assumptions are the assumptions of Reissner-Naghdi linear shell theory and the power of this technique in the determination of free vibration characteristics for shells of revolution manufactured using geodesic path is very well proven by the previous studies [55, 57].

However, for a shell of revolution wound using semi-geodesic path, there is no reference in the literature to compare the results obtained by multi-segment solution method. In this case, finite element analysis is just a reference study to check the proper application of the multi-segment numerical integration solution technique.

CHAPTER 5

NUMERICAL RESULTS AND DISCUSSION

5.1 FILAMENT WOUND TRUNCATED CONICAL SHELLS OF REVOLUTION.

5.1.1 Effect of semi-geodesic winding on the winding angle, thickness, stiffness coefficients and natural frequencies

Undamped free vibration characteristics of filament wound conical shells of revolution, with varying fiber orientation angle and thickness, is first studied for a truncated conical shell which has a small end radius of 0.53m, large end radius of 0.6 m and cone angle β of 10^o.

The shell studied is assumed to be manufactured from high modulus graphite epoxy with the following properties:

Modulus in the fiber direction: E_1=213.74GPa, Modulus transverse to fiber: E_2 =18.62 GPa, Poisson's ratio: ν_{12} =0.28, Shear moduli: $G_{12} = G_{13} = 5.171\,\text{GPa}$, $G_{23} = 4.137\,\text{GPa}$, Mass density: ρ =2051.88 kg m^{-3}, eight ply shell with symmetric layout $[\theta/-\theta/\theta/-\theta]_S$ and with equal ply thickness of 0.24 mm at the starting edge of the winding which is the small radius edge. The material properties are selected in accordance with Kayran and Yavuzbalkan [57] for comparison purposes.

For a filament wound truncated conical shell for which the winding starts from the small radius end, the effect of semi-geodesic winding on winding angle and thickness along meridional direction is shown in Figures 5.1 and 5.2. It should be noted that the thickness variation of the shell presented in Figure 5.2 is normalized with respect to the initial thickness at the small radius end. In order to investigate the effect of semi-geodesic winding for the whole range of possible starting winding angles, initial winding angles for the presented analysis are selected as 15^o, 30^o, 45^o, 60^o and 75^o. In Figure 5.1 variation of winding angle is given in units of degree considering the ease of commenting on the applicability of winding and magnitude effect of the preset

slippage tendency. As mentioned in section 3.4, applied method is only valid if the winding angle α is less than 90°. Equation (3.18) shows that the thickness of the shell of revolution increases substantially when the fiber orientation angle approaches 90°. Practically the increase in the thickness of the shell of revolution is caused by fiber concentration on a relatively small area due to the repetitive rotation of the fiber around the circumference. This effect can be seen on graphs (e) on both Figures 5.1 and 5.2 where the initial winding angle is 75° and preset slippage tendency is 0.3. It is observed that in given case the winding angle increases along meridional direction and at about 40% of the shell ending angle reaches to 90° and due to the repetitive rotation of the fiber, thickness of the shell increases indefinitely.

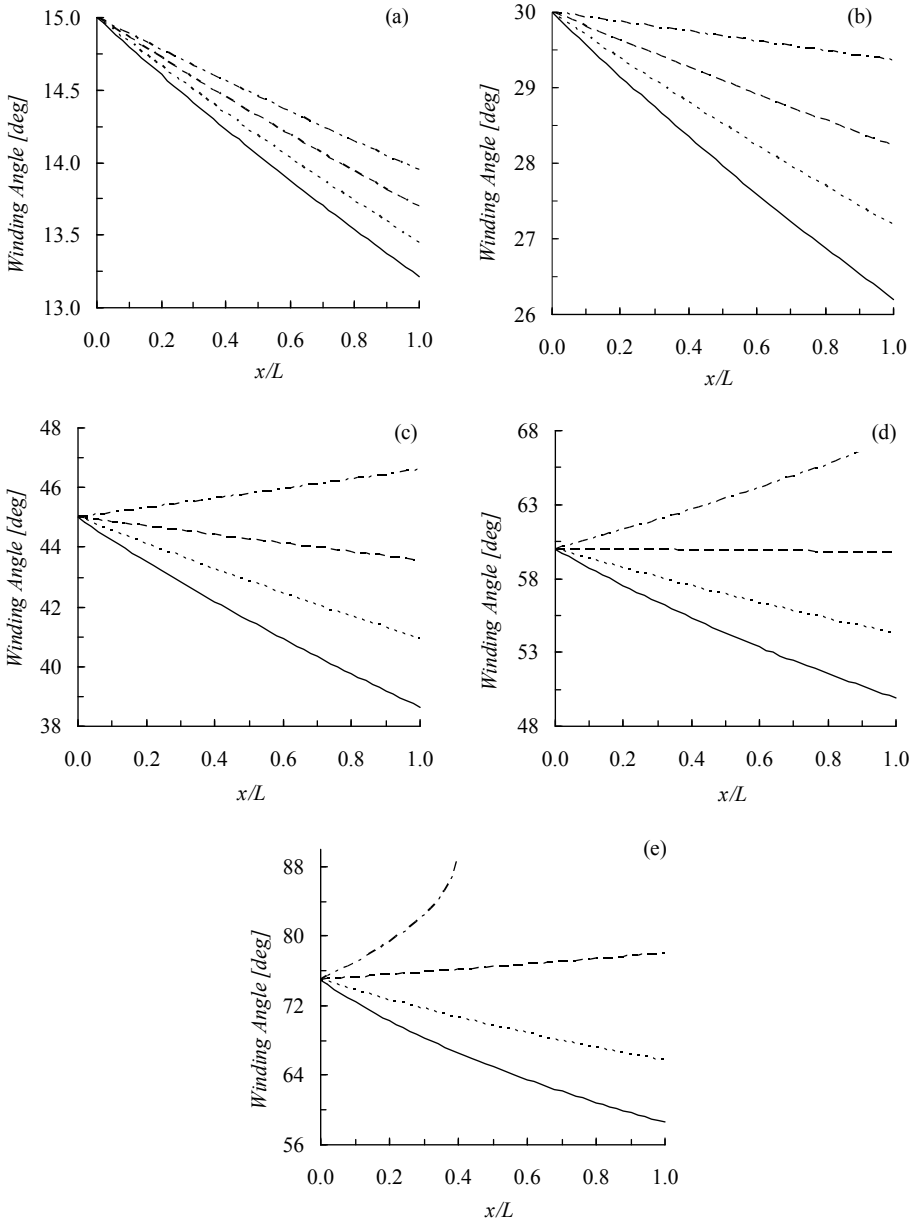

Figure 5.1 Variation of the winding angle along the meridional coordinate. ***(a)*** α_1=15°; ***(b)*** α_1=30°; ***(c)*** α_1=45°, ***(d)*** α_1=60°; ***(e)*** α_1=75°

———: geodesic; - - - - -: fst=0.1; — — —: fst=0.2 ; — · — · —: fst=0.3

It should also be noted that for semi-geodesic winding depending on the shell geometry, initial winding angle and available slippage tendency the winding angle may increase along the shell axis even though the winding starts at the small radius edge. From Figure 5.1 it can be seen that the winding angle is higher when the preset slippage tendency is higher, and even though the winding starts at the small radius edge, if the preset slippage tendency is above a certain value the winding angle increases along the meridian of the shell of revolution. Figure 5.2 also shows that the thickness of the filament wound shell of revolution with a higher preset slippage tendency is higher compared to the thickness attained with a lower preset slippage tendency during the filament winding process. It should also be noted that depending on the slippage tendency, initial winding angle and the geometry of the shell of revolution, thickness may increase or decrease along the meridian. For instance, for the initial winding angle of 60^o thickness increases along the meridian for the preset slippage tendency of 0.3. For geodesic winding and semi-geodesic winding with slippage tendencies of 0.1 and 0.2, thickness decreases along the meridian. Calculations also showed that when the initial winding angle is decreased, the relative differences among the winding angles and thicknesses, which are attained with the use of different preset slippage tendencies during the winding process, also decrease.

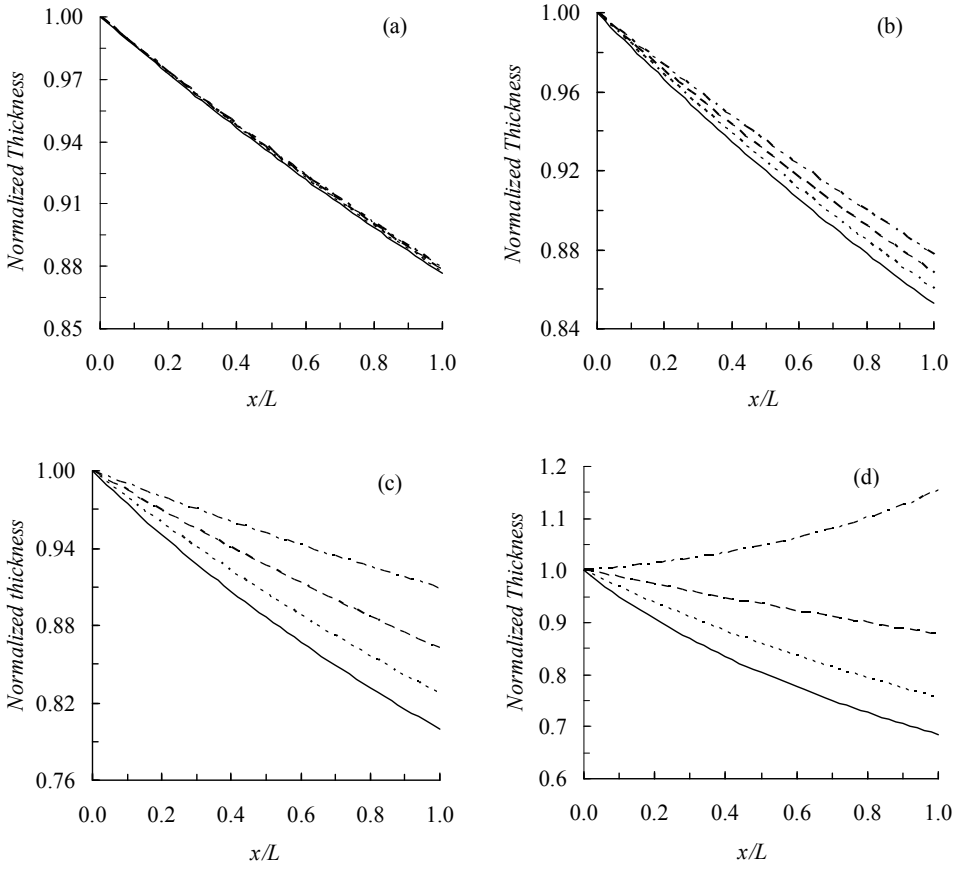

Figure 5.2 Variation of the thickness along the meridional coordinate. ***(a)*** α_1=15^o; ***(b)***α_1=30^o; ***(c)*** α_1=45^o, ***(d)*** α_1=60^o; ***(e)*** α_1=75^o

———: geodesic; - - - - - : fst=0.1; — — — : fst=0.2 ; — · — · — : fst=0.3

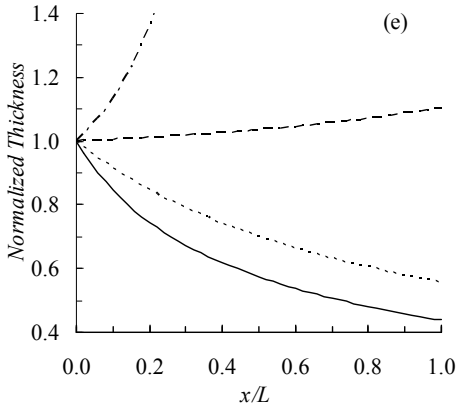

Figure 5.2 (continued) Variation of the thickness along the meridional coordinate.
(a) α_1=15°; ***(b)***α_1=30°; ***(c)*** α_1=45°, ***(d)*** α_1=60°; ***(e)*** α_1=75°

———: geodesic; - - - - - : fst=0.1; — — — : fst=0.2 ; — · — · — : fst=0.3

By employing different preset slippage tendencies the effect of semi geodesic winding on the natural frequencies is investigated for the initial winding angles in the range of 15°-75° at the small radius edge. Figures 5.3-5.7 show the variation of the normalized major stiffness coefficients for different preset slippage tendencies and for the initial winding angles of 15°, 30°, 45°, 60° and 75° respectively. In Figures 5.3-5.7 extensional stiffness coefficients (A_{11}, A_{22} and A_{66}) are normalized with respect to the value of A_{11}, bending stiffness coefficients D_{11}, D_{22} and D_{66} are normalized with respect to the value of D_{11} and bending stiffness coefficients D_{16} and D_{26} are normalized with respect to the value of D_{16} at the small radius edge of the conical shell.

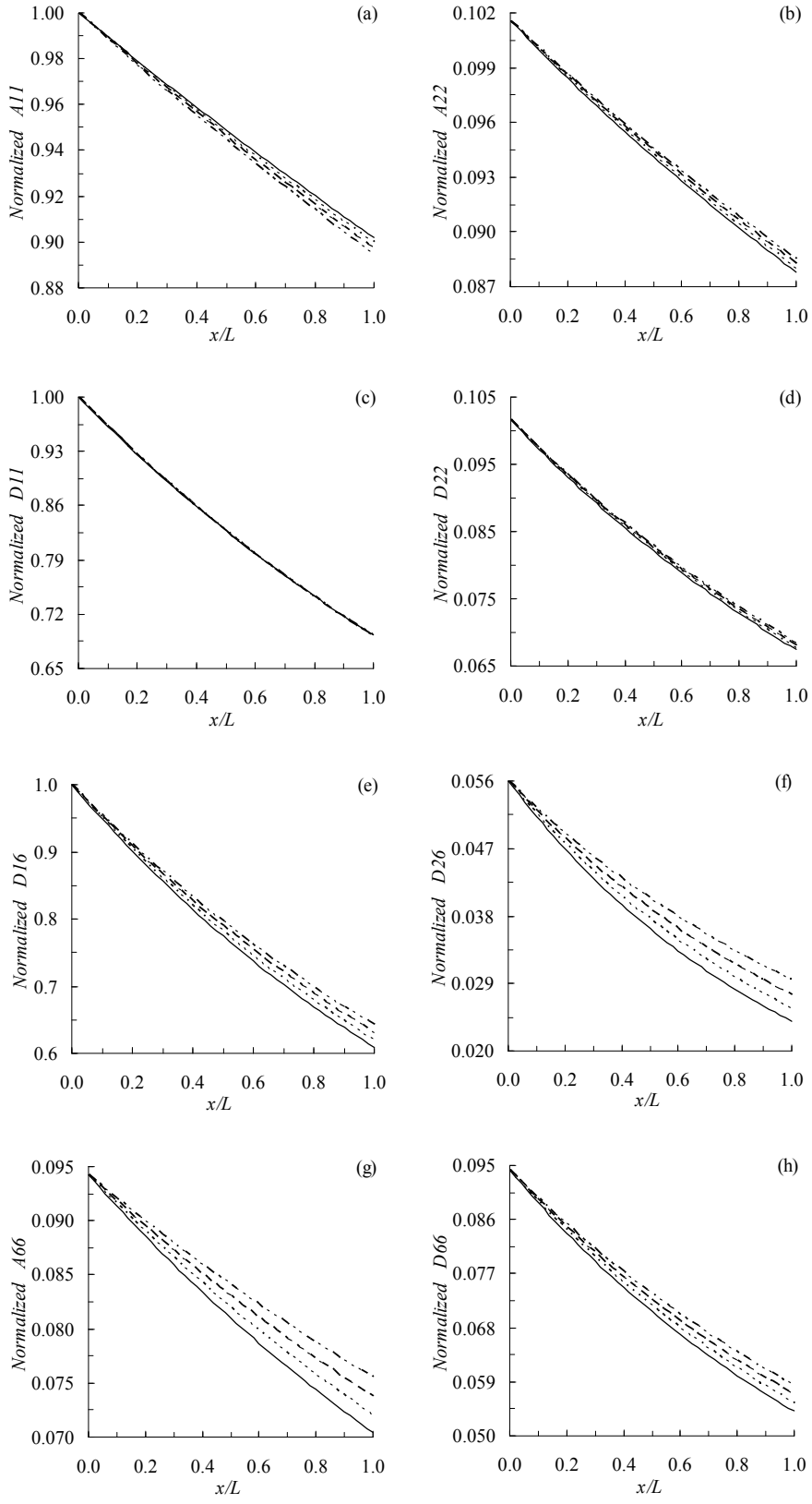

Figure 5.3 Variation of stiffness coefficients along the meridional coordinate for α_1=15^o

———: geodesic; - - - - - : fst=0.1; — — — : fst=0.2 ; — · — · — : fst=0.3

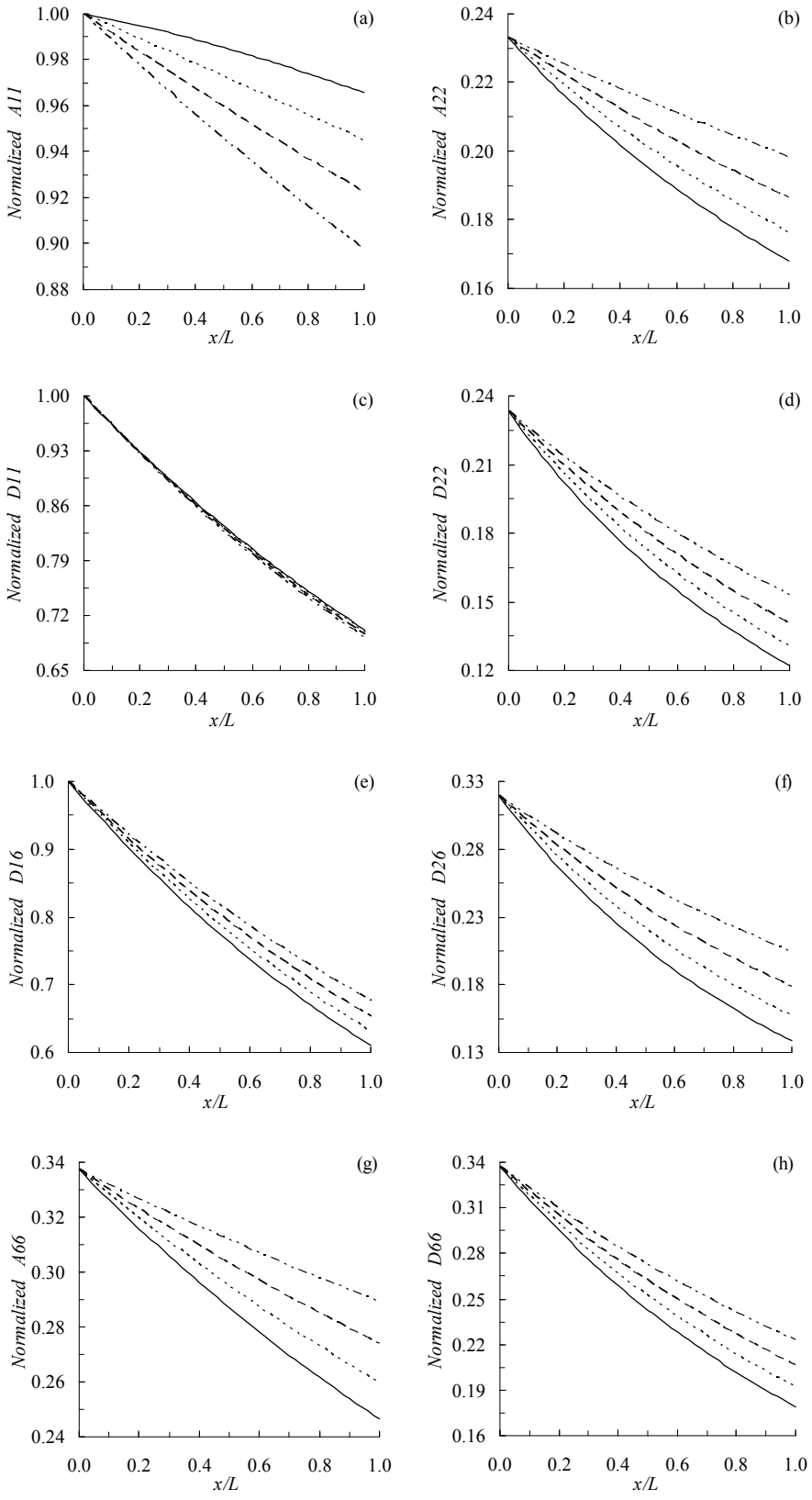

Figure 5.4 Variation of stiffness coefficients along the meridional coordinate for α_1=30^o

———: geodesic; - - - - - : fst=0.1; — — — : fst=0.2 ; — · — · — : fst=0.3

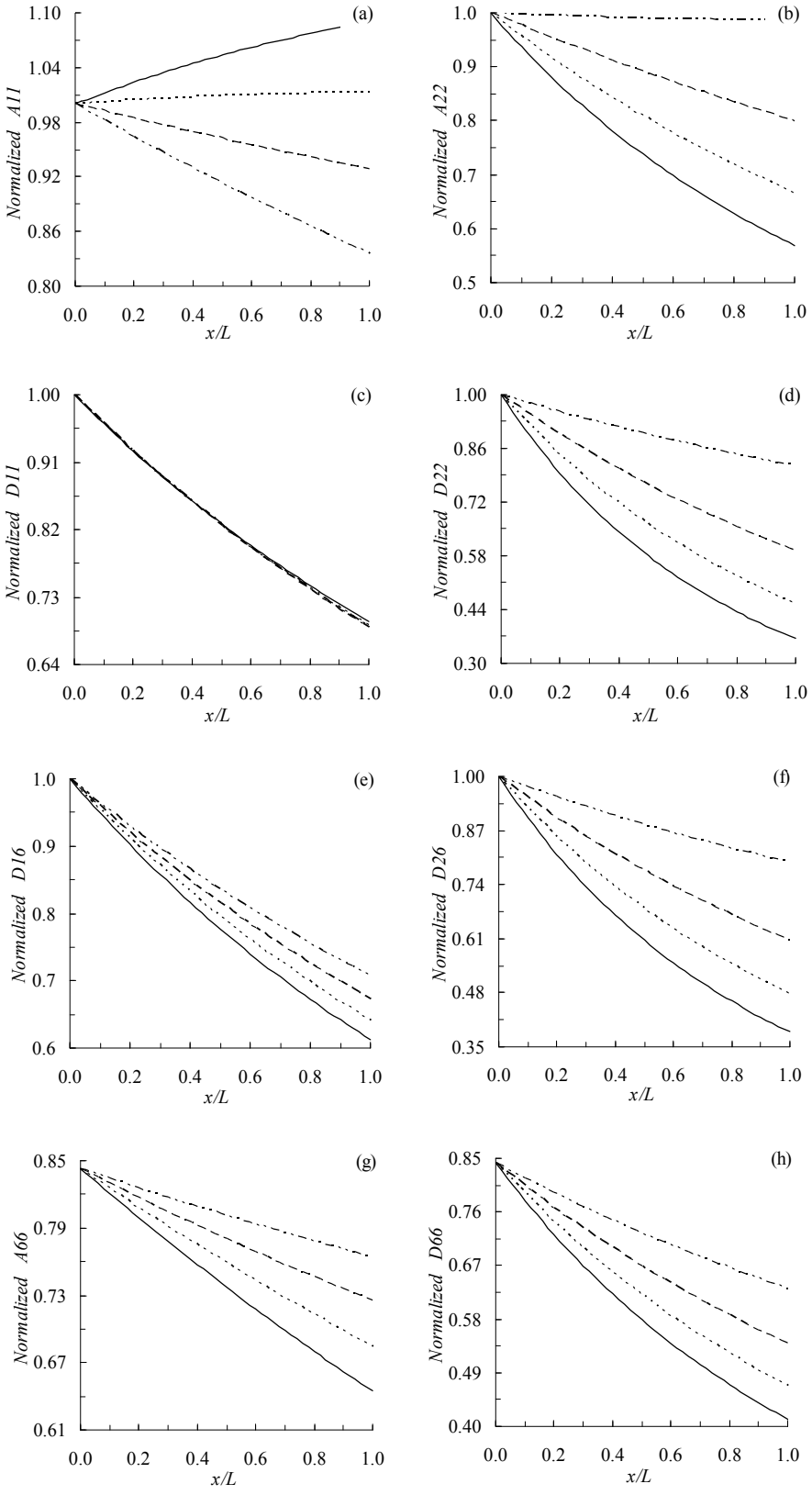

Figure 5.5 Variation of stiffness coefficients along the meridional coordinate for α_1=45^o

———: geodesic; - - - - - : fst=0.1; — — — : fst=0.2 ; — · — · — : fst=0.3

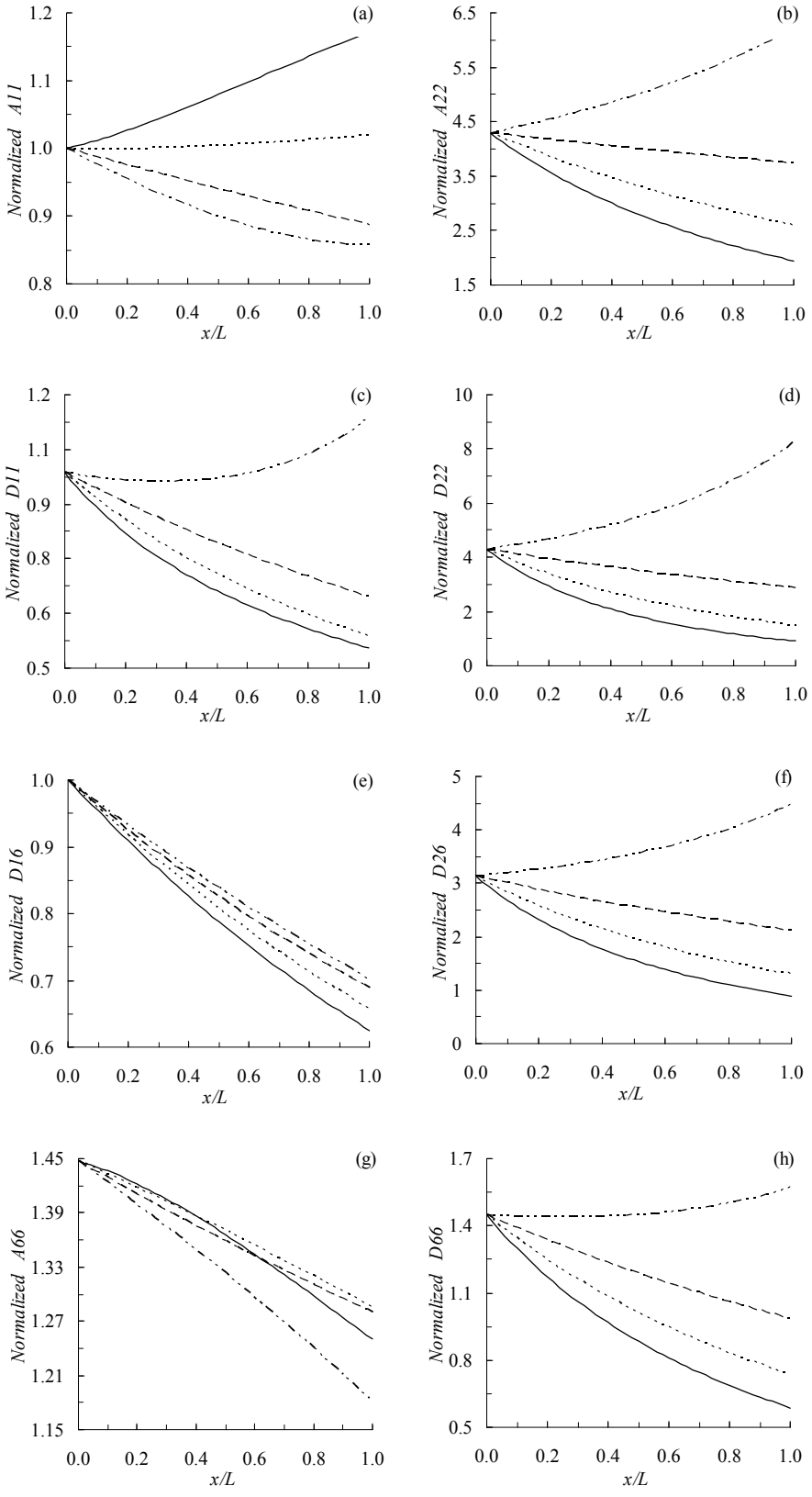

Figure 5.6 Variation of stiffness coefficients along the meridional coordinate for α_1=60^o

———: geodesic; - - - - - -: fst=0.1; — — —: fst=0.2 ; — · — · —: fst=0.3

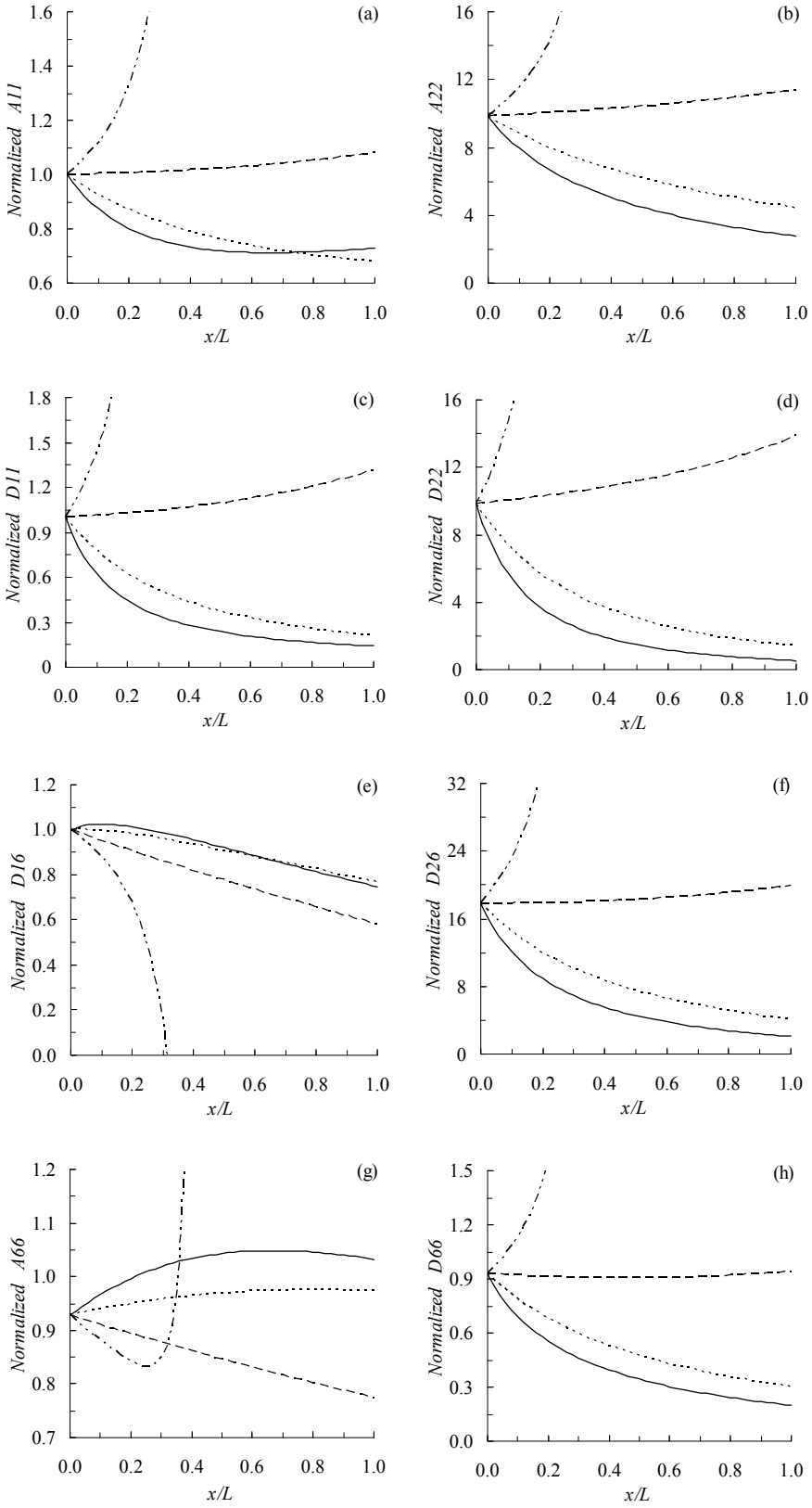

Figure 5.7 Variation of stiffness coefficients along the meridional coordinate for α_1=75^o

———: geodesic; - - - - - : fst=0.1; — — — : fst=0.2 ; — · — · — : fst=0.3

Note that for a given initial winding angle and thickness, stiffness coefficients calculated at the small radius edge of the shell will also be the same for different preset slippage tendencies. Therefore, the stiffness coefficients are normalized with respect to the value of the stiffness coefficients at the small raidus edge where the winding angle is assumed to start.

Although, it is difficult to draw a general conclusion on the effect of semi-geodesic winding on stiffness coefficients, some observations on the behavior of the stiffness terms for different preset slippage tendencies and initial winding angles can be stated in this section. Figures 5.3-5.7 shows that during the filament winding operation, application of higher preset slippage tendency results in higher bending stiffness coefficients, however depending on the initial winding angle, the extensional stiffness coefficient may be higher for low preset slippage tendency. This effect for bending stiffness terms may be explained by the layer thickness variation. Since bending stiffness is proportional to the third power of the thickness, higher thickness attained by higher preset slippage tendency causes bending stiffness coefficients to be higher.

When the initial winding angle decreases, relative differences between the extensional and bending stiffness coefficients of the shells manufactured with different preset slippage tendency also decrease. Although, the shear stiffness coefficient A_{66} satisfies this statement for low starting angles, for high starting angles high preset slippage tendency has a decreasing effect on the shear stiffness coefficient A_{66}. On the other hand, for the initial winding angles of 15^o, 30^o, 45^o, 60^o higher preset slippage tendency results in lower extensional stiffness coefficient in the meridional direction A_{11}. The decrease of the extensional stiffness in the meridional direction with the increase in the preset slippage tendency is due to the higher winding angle attained during the winding for the high preset slippage tendency case. Figures 5.3-5.7 also show that if the preset slippage tendency is below a certain value, bending stiffness coefficients D_{11} and D_{22} decrease along the span of the shell. In general it was observed that for the initial winding angles in the range of 15^o-75^o, higher preset slippage tendency resulted in higher extensional and bending stiffness in the circumferential direction. For the particular symmetrical shell wall layout with even number of layers, the only non-vanishing coupling stiffness coeffcients are D_{16} and D_{26}, and existence of coupling terms makes the shell more flexible and this has a lowering effect on the natural frequencies.

Analyzing the meridional variation effect of the initial winding angle and the slippage tendency on the stiffness terms, one may conclude that for relatively low initial winding angles such as 15^o, the preset slippage tendency has negligible effect on stiffness coefficients. Both extensional and bending stiffness coefficients decrease in the meridional direction for 15^o and 30^o starting angles. For the initial winding angles of 45^o and 60^o, meridional extensional stiffness coefficient A_{11} decreases in meridional direction for the preset slippage tendency 0.2 and 0.3 and increases for geodesic winding and for the preset slippage tendency 0.1. Stiffness coefficients A_{22},

D_{11}, D_{22}, D_{66}, D_{12} and D_{26} decrease in meridional direction for the starting winding angles 45^o and 60^o except when preset slippage tendency is set to 0.3 for the 60^o starting winding angle. In that case, all the listed stiffness coefficients increase in meridional direction. D_{16}, bending-twisting coupling stiffness coefficient always decreases in the meridional direction and the effect of slippage tendency and initial winding angle is small for the investigated conical shell configuration.

Finally, for the 75^o initial winding angle case all the stiffness coefficients start to increase without bound at a certain meridional location. This increase is due to the fact that at that meridional location the orientation of the fibers becomes almost circumferential which means that the winding angle approaches to 90^o. From Eq. (3.18) it can be seen that the thickness of the shell of revolution increases substantially when the fiber orientation angle approaches 90^o. Practically the increase in the thickness of the shell of revolution is caused by fiber concentration on a relatively small area due to the repetitive rotation of the fiber around the circumference.

For the conical shell of revolution, Figures 5.8 and 5.9 give the variation of the non-dimensional fundamental natural frequency calculated by Eq.(4.1) with respect to circumferential wave number, for three different initial winding angles (α_1), four different preset slippage tendency (including geodesic), and two edge conditions.

The following abbreviations are used for the legends in Figures 5.8 - 5.10 and Tables 5.1 - 5.2:

CFS: Clamped at the small radius edge, free at the large radius edge, winding starts at the small radius edge

CCS: Clamped at the small radius edge, clamped at the large radius edge, winding starts at the small radius edge

Note that in Figures 5.8 and 5.9, non-dimensional fundamental natural frequencies which are calculated for the initial winding angles of 30^o, 45^o, and 60^o are presented. For small initial winding angles, the effect of preset slippage tendency on the fundamental natural frequencies is negligible. The low effect of preset slippage tendency on the natural frequencies for small initial winding angles is due to the small effect of the preset slippage tendency on the variation of the winding angle and the thickness. One can argue that even for 30^o initial winding angle results shown in Figure 5.8(a) clearly shows that the effect of semi-geodesic winding is not significant. For large initial winding angles, the effect of slippage tendency is seen to be more effective on the natural frequencies.

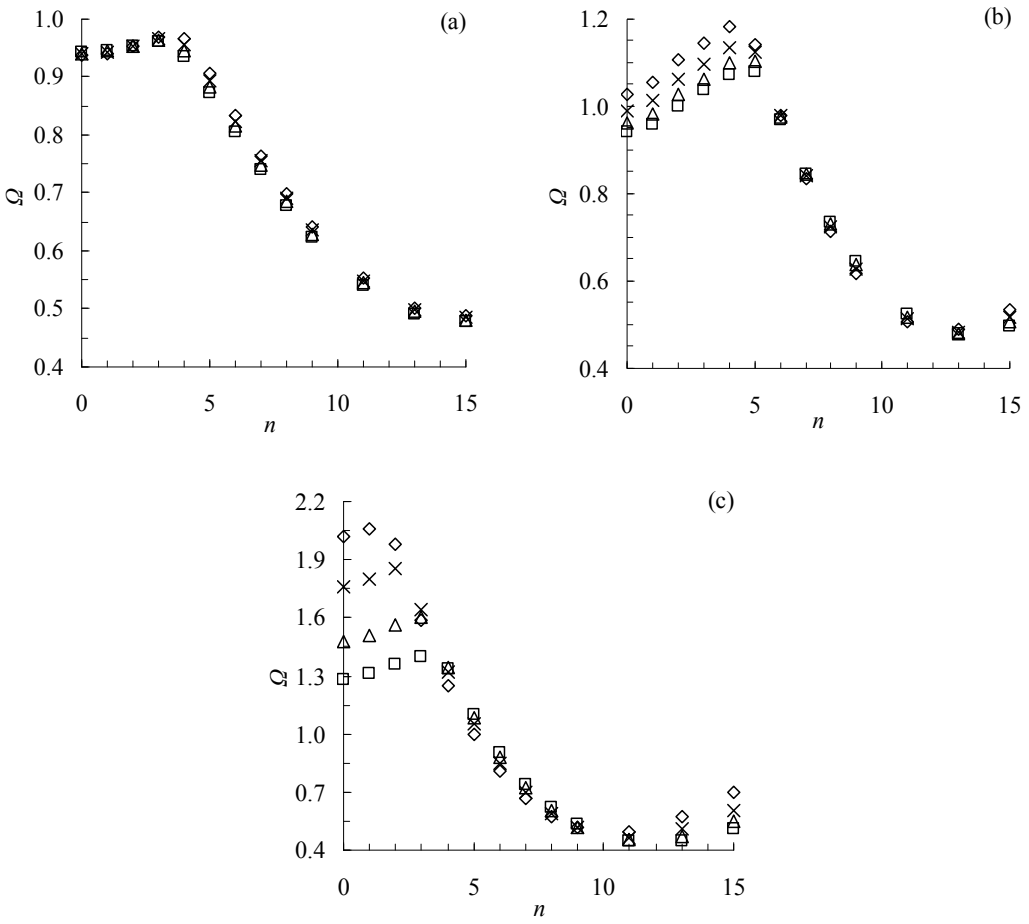

Figure 5.8 Natural frequency versus n, CCS; ***(a)*** α_1=30^o, ***(b)*** α_1=45^o, ***(c)*** α_1=60^o

□: geodesic; Δ: fst=0.1 ; x: fst=0.2 ; ◊: fst=0.3

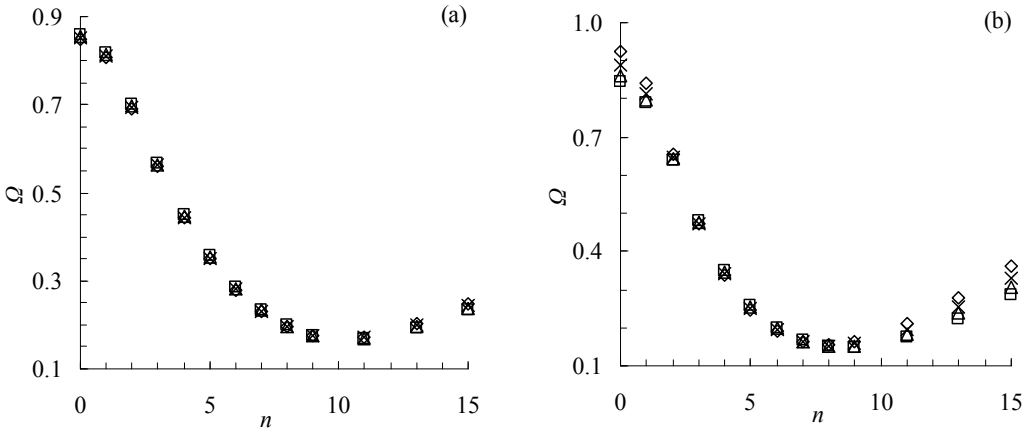

Figure 5.9 Natural frequency versus n, CFS; ***(a)*** α_1=30^o, ***(b)*** α_1=45^o, ***(c)*** α_1=60^o

□: geodesic; Δ: fst=0.1 ; x: fst=0.2 ; ◊: fst=0.3

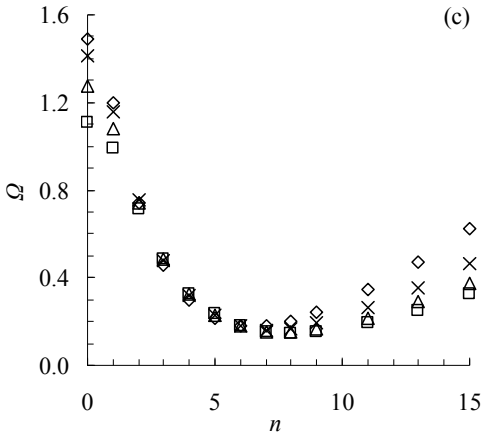

Figure 5.9 (continued) Natural frequency versus n, CFS; ***(a)*** α_1=30°, ***(b)*** α_1=45°, ***(c)*** α_1=60°
□: geodesic; Δ: fst=0.1 ; x: fst=0.2 ; ◊: fst=0.3

Figures 5.8 and 5.9 show that at high circumferential wave numbers when the preset slippage tendency is increased, natural frequencies of conical shells, with clamped-free and clamped-clamped edge conditions, also increase. This behavior is mainly attributed to the dominance of bending strain energy contribution to the total strain energy at high circumferential wave numbers [58]. At high circumferential wave numbers, circumferential slices of the shell essentially behave like a beam under circumferential bending. For a particular circumferential wave number, the number of nodes is twice the circumferential wave number and this implies that at high circumferential wave numbers there are many nodal points around the circumference which implies that the shell mainly undergoes circumferential bending. Therefore, at high circumferential wave numbers the bending stiffness coefficient in the circumferential direction (D_{22}) predominantly governs the magnitude of the natural frequency. From Figures 5.8 and 5.9, it can be seen that the circumferential bending stiffness coefficient D_{22} of the conical shell with higher preset slippage tendency is higher than the circumferential bending stiffness coefficient, of the shell with lower preset slippage tendency, over the whole span of the shell. However, the thickness of the shell with a higher preset slippage tendency is also higher and higher inertia tends to lower the frequency (Figure 5.2). Therefore, the bending stiffness coefficient D_{22} shows its effect on the natural frequency only at high circumferential wave numbers.

At low circumferential wave numbers, compared to the bending strain energy, the extensional strain energy is more dominant in its contribution to the total strain energy [58]. Therefore, extensional stiffness coefficients are expected to play a dominant role on the natural frequencies. However, for the initial winding angle of 60°, Figure 5.6 shows that except for the extensional stiffness coefficient in the meridional direction, higher preset slippage tendency causes A_{22}, D_{11} and D_{22} to be higher compared to the corresponding stiffness coefficients of the shell manufactured with lower preset slippage tendency. Although the thickness of the shell with higher preset slippage tendency is higher, Figures 5.8 and 5.9 show that similar to the situation for

the high circumferential wave numbers, the net effect of stiffness and inertia cause the natural frequencies to increase with the increase in preset slippage tendency.

Figure 5.10 shows the variation of the natural frequencies with the initial winding angle for different preset slippage tendency for a shell which is clamped at the small radius edge and free at the large radius end. Figure 5.10 shows that if the initial winding angle is further increased above 60^o, that natural frequencies start to decrease for low circumferential wave numbers such as n=1-3. This behavior can be attributed to the fact that when the initial winding angle is further increased, the increase in the thickness becomes very high and the increase in the inertia due to the thickness increase becomes the dominant factor and natural frequencies decrease. At low circumferential wave numbers extensional strain energy is the dominant part of total strain energy, therefore above a certain thickness value the inertia increase starts to dominate. The decrease in the natural frequencies is more pronounced with the increase in the preset slippage tendency. This effect is valid up to the wave number at which the bending strain energy becomes more important than the extensional strain energy and D_{22} starts to dominate. As it was discussed before, at high circumferential wave numbers the bending stiffness coefficient in the circumferential direction is very dominant on the natural frequencies especially when the preset slippage tendency is high. However, for low preset slippage tendency when the initial winding angle is further increased it is seen that the natural frequencies of the higher circumferential modes drop. This drop is mainly attributed to the decrease in the shell thickness when the initial winding angle is increased. For instance, Figures 5.2 (d) and 5.2(e) show that the thickness of the shell with the initial winding angle 75^o is considerably smaller than the thickness of the shell with the initial winding angle of 60^o. Since the circumferential bending stiffness coefficient is proportional to the third power of the thickness, although the winding angle over the span of the shell is higher for the 75^o initial winding angle case compared to the 60^o initial winding angle case, the circumferential bending stiffness coefficient of the shell with the initial winding angle of 75^o should be smaller than the circumferential bending stiffness coefficient of the shell with the initial winding angle of 60^o over a longer span of the shell. For the 75^o and 60^o initial winding angle cases the comparison of the circumferential bending stiffness coefficient D_{22} is given in Figure 5.11. In this figure the stiffness coefficients are normalized with respect to the meridional bending stiffness coefficient D_{11} of the conical shell which has an initial winding angle of 60^o. From Figure 5.11 it can be clearly seen that D_{22} of the conical shell with the 60^o initial winding angle is higher than the D_{22} of the conical shell with the 75^o initial winding angle over a longer span of the shell of revolution for both geodesic winding and semi-geodesic winding with fst=0.1. Figure 5.10 also shows that at high circumferential wave numbers and at high initial winding angles, the drop of natural frequencies of conical shells manufactured with lower preset slippage tendency, such as geodesic winding, is higher than the drop seen in the frequencies of conical shells manufactured with higher preset slippage tendency, such as fst=0.1. The reason for this difference can be best explained by examining Figure 5.11. For the 60^o and 75^o initial winding

angle cases, the difference in the circumferential bending stiffness D_{22} for the geodesic winding case is higher than the corresponding difference for the semi-geodesic winding case with fst=0.1. Therefore, at high circumferential wave numbers and in the high initial winding angle range, if the preset slippage tendency is low the drop of natural frequency is higher compared to the drop for higher preset slippage tendency, as the initial winding angle is increased. Thus, at high circumferential wave numbers when the initial winding angle is further increased, the drop of the natural frequencies of the shells with low preset slippage tendency is another indication that at high circumferential wave numbers circumferential bending stiffness coefficient D_{22} is the dominant term affecting the natural frequencies.

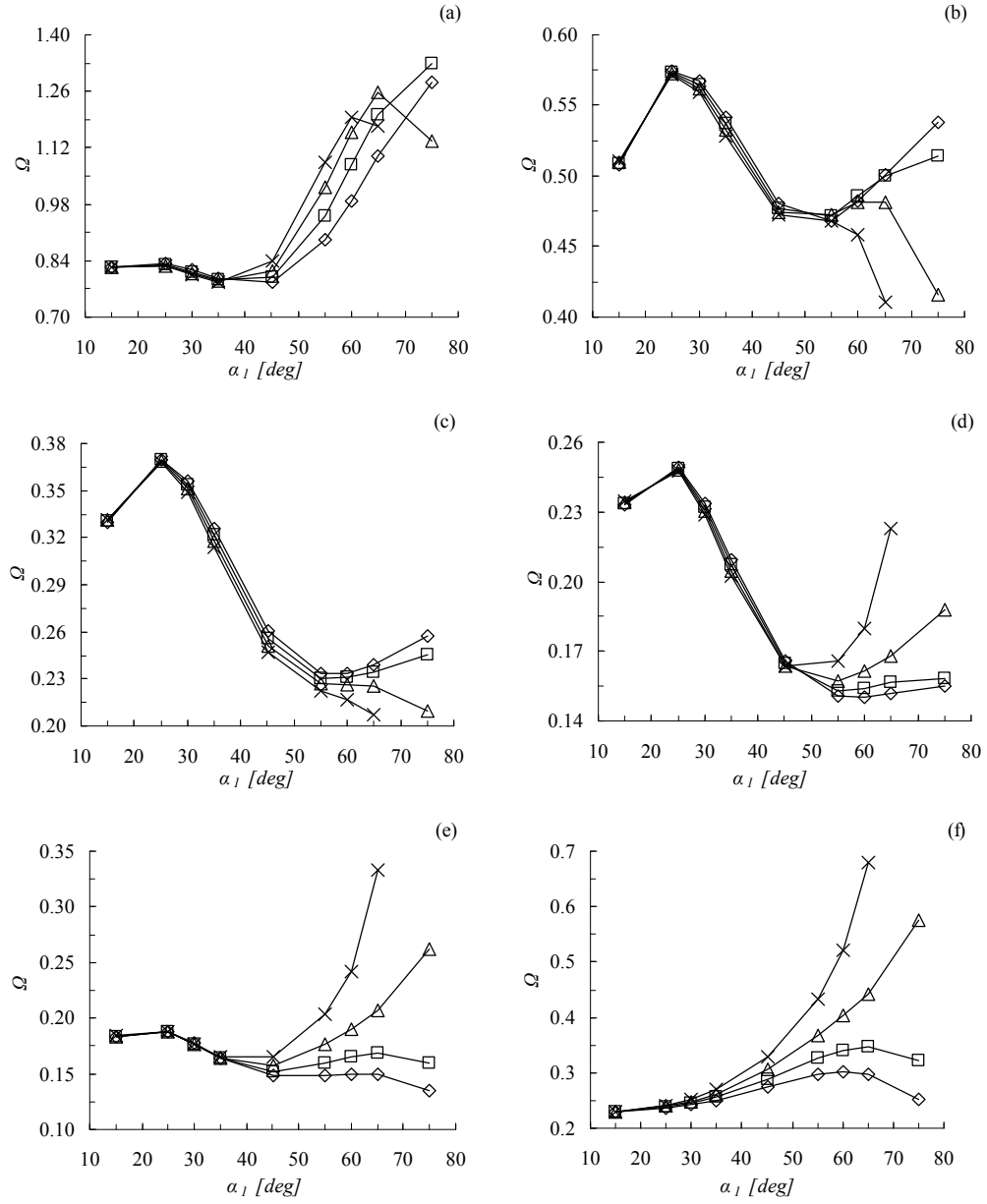

Figure 5.10 Variation of fundamental natural frequency with initial winding angle, CFS; ***(a)*** n=1, ***(b)*** n=3, ***(c)*** n=5, ***(d)*** n=7, ***(e)*** n=9, ***(f)*** n=13, ***(g)*** n=15

◊: geodesic; □: fst=0.1 ; Δ: fst=0.2 ; x: fst=0.3

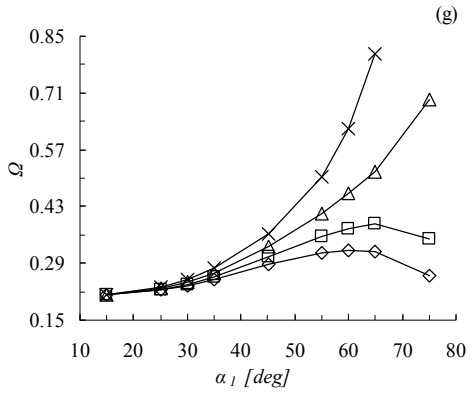

Figure 5.10 (continued) Variation of fundamental natural frequency with initial winding angle, CFS; ***(a)*** n=1, ***(b)*** n=3, ***(c)*** n=5, ***(d)*** n=7, ***(e)*** n=9, ***(f)*** n=13, ***(g)*** n=15

◊: geodesic; □: fst=0.1 ; Δ: fst=0.2 ; x: fst=0.3

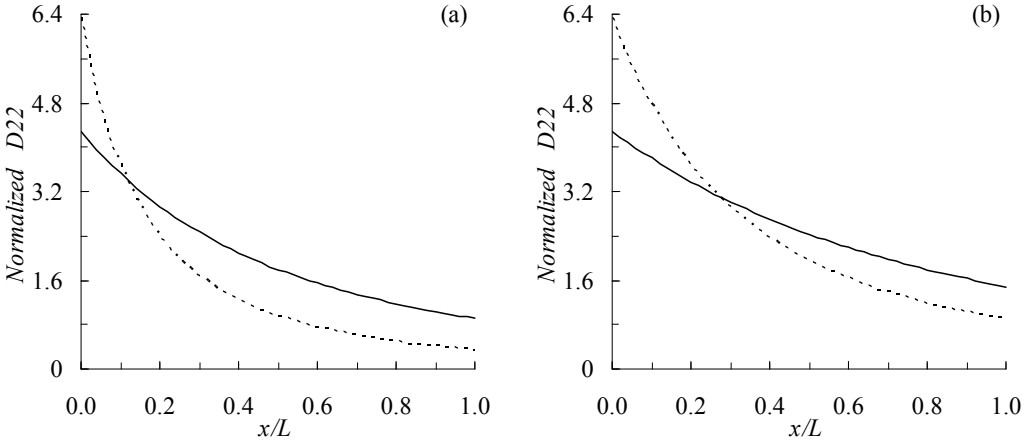

Figure 5.11 Meridional variation of circumferential bending stiffness coefficient D_{22} for ***(a)***geodesic winding; ***(b)*** fst=0.1

———: 60°; - - - - -: 75°

For the three different initial winding angles (α_1=30°, 45°, 60°) Tables 5.1 and 5.2 summarize the fundamental non-dimensional frequencies (Eq. (4.1)) for the clamped-free and clamped-clamped edge conditions, respectively. It can be seen that when the initial winding angle is decreased the effect of preset slippage tendency reduces, and for the low and high circumferential wave numbers natural frequencies of shells manufactured by different preset slippage tendency, during the filament winding process, approach each other. It should be noted that when the initial winding angle is decreased the circumferential bending stiffness (D_{22}) also decreases, therefore at high circumferential wave numbers the effect of circumferential bending stiffness on the natural frequencies also reduces. This observation also confirms that at high circumferential wave numbers bending stiffness coefficient in the circumferential direction is the main parameter affecting the natural frequency. On the other hand, at low circumferential wave numbers when the initial winding angle is decreased, extensional stiffness coefficient in the

meridional direction (A_{11}) also starts to be effective on the natural frequency. From Tables 5.1 and 5.2 it can be seen that especially for low circumferential wave numbers and for low initial winding angle such as 30^o, natural frequencies of conical shells with lower preset slippage tendency are slightly higher than the frequencies of shells with higher preset slippage tendency. It should be noted that for low initial winding angles such as 30^o the thickness of the shell manufactured with low preset slippage tendency is smaller than the thickness of the shell manufactured with higher preset slippage tendency. Figure 5.2(b) shows this clearly. Therefore, the effect of lower inertia due to lower thickness on the frequencies should not be overlooked.

Table 5.1 Fundamental non-dimensional frequencies corresponding to different wave numbers for CFS

	$\alpha_1=30^o$				$\alpha_1=45^o$				$\alpha_1=60^o$			
	fst				***fst***				***fst***			
n	***0***	***0.1***	***0.2***	***0.3***	***0***	***0.1***	***0.2***	***0.3***	***0***	***0.1***	***0.2***	***0.3***
0	0.860	0.856	0.851	0.847	0.844	0.861	0.889	0.924	1.108	1.273	1.411	1.492
1	0.816	0.813	0.809	0.806	0.788	0.798	0.815	0.840	0.988	1.078	1.158	1.197
2	0.700	0.697	0.694	0.691	0.641	0.642	0.647	0.655	0.716	0.742	0.758	0.743
3	0.567	0.565	0.562	0.559	0.480	0.477	0.474	0.473	0.482	0.485	0.481	0.458
5	0.356	0.354	0.352	0.349	0.260	0.256	0.251	0.247	0.233	0.231	0.226	0.217
7	0.234	0.232	0.231	0.229	0.166	0.165	0.164	0.164	0.150	0.154	0.162	0.180
9	0.177	0.177	0.177	0.176	0.148	0.152	0.158	0.165	0.150	0.165	0.191	0.242
11	0.169	0.170	0.171	0.173	0.175	0.184	0.196	0.211	0.191	0.218	0.261	0.344
13	0.192	0.195	0.198	0.202	0.224	0.238	0.256	0.279	0.251	0.290	0.353	0.471
15	0.235	0.239	0.244	0.249	0.286	0.306	0.330	0.361	0.323	0.376	0.461	0.622

Table 5.2 Fundamental non-dimensional frequencies corresponding to different wave numbers for CCS

	$\alpha_1=30^o$				$\alpha_1=45^o$				$\alpha_1=60^o$			
	fst				***fst***				***fst***			
n	***0***	***0.1***	***0.2***	***0.3***	***0***	***0.1***	***0.2***	***0.3***	***0***	***0.1***	***0.2***	***0.3***
0	0.944	0.941	0.939	0.937	0.942	0.961	0.989	1.029	1.284	1.479	1.758	2.022
1	0.946	0.945	0.943	0.941	0.960	0.982	1.013	1.056	1.309	1.509	1.800	2.060
2	0.954	0.954	0.953	0.953	1.001	1.026	1.060	1.107	1.356	1.560	1.855	1.983
3	0.961	0.964	0.966	0.969	1.038	1.063	1.098	1.143	1.398	1.601	1.642	1.585
5	0.874	0.884	0.895	0.906	1.081	1.103	1.124	1.141	1.103	1.085	1.052	0.997
7	0.739	0.747	0.756	0.765	0.846	0.845	0.841	0.834	0.739	0.719	0.695	0.667
9	0.624	0.630	0.636	0.642	0.645	0.638	0.629	0.619	0.531	0.521	0.515	0.515
11	0.540	0.544	0.548	0.553	0.523	0.518	0.513	0.508	0.445	0.451	0.466	0.497
13	0.491	0.495	0.498	0.502	0.478	0.480	0.483	0.489	0.449	0.472	0.508	0.570
15	0.478	0.482	0.486	0.489	0.495	0.505	0.518	0.535	0.507	0.547	0.605	0.696

It should be noted that except for the high circumferential wave number side, without a closed form solution for the natural frequencies, parametric effect of the stiffness coefficients, thickness, circumferential wave number and the boundary conditions cannot be explicitly identified. Therefore, one cannot always draw an effect-result type of conclusion like the situation on the high circumferential wave number side where the bending stiffness coefficient in the circumferential direction (D_{22}) stands out as the main parameter governing the natural frequency.

5.1.2 Effect of cone angle on the variation of the winding angle, thickness and natural frequencies

In order to investigate the effect of cone angle on the variation of winding angle, thickness and natural frequencies of a filament wound conical shell of revolution, results for conical shell of revolution with two different cone angles are compared. In the analyses cone angles are taken as 10^o and 20^o. As it can be seen in Figure 3.2, when the cone angle is changed, different cone geometries are possible depending on the design considerations. For this study, small end radius, R_{min} and slant length, SL , are selected as constant and axial length of the shell as well as large end radius, R_{max}, are allowed to change with the varying cone angle, β.

Being consistent with the geometry analyzed in Chapter 5, small end radius is selected as 0.53 m, and slant length is fixed to 0.40311 m. Using the given small end radius and slant length, for cone angle of 20^o, large end radius, R_{max} is calculated as 0.66787 m.

Results for the two conical shells with different cone angles are presented below. The variation of the winding angle, thickness along the shell axis and the free vibration characteristics of the two conical shells of revolution are compared for two different preset slippage tendencies. As mentioned, different geometries with the same cone angle can be created, and this analysis can be extended to those geometries if required as long as the slant length is defined by the design.

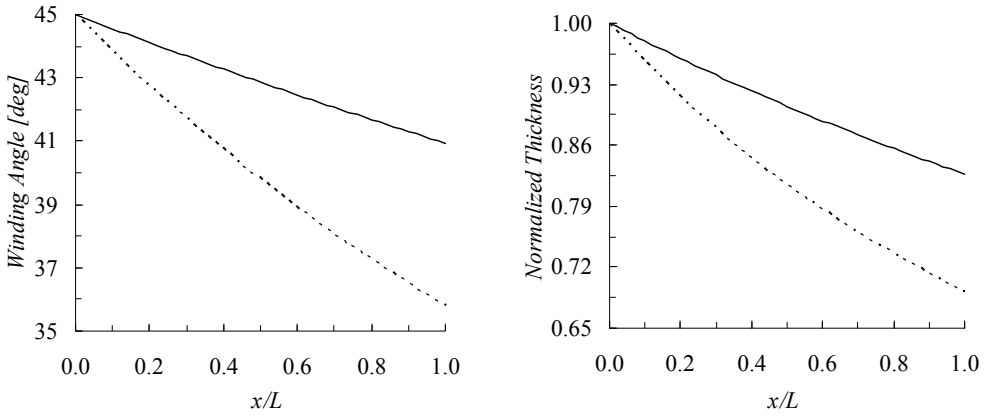

Figure 5.12 Variation of the winding angle and thickness along meridional direction for two different cone angles using fst=0.1

———: β=10°; - - - - -: β=20°

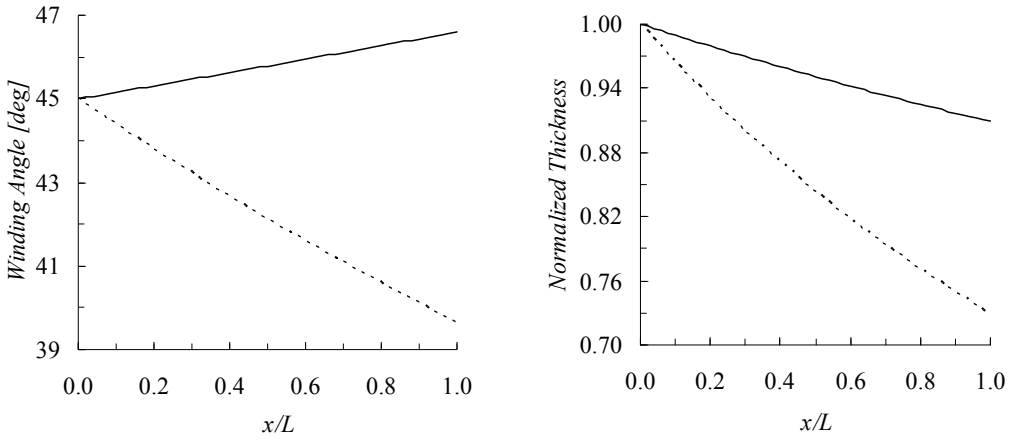

Figure 5.13 Variation of the winding angle and thickness along meridional direction for two different cone angles using fst=0.3

———: β=10°; - - - - - : β=20°

Figures 5.12 and 5.13 show the variation of winding angle and thickness along the meridional direction for two different truncated conical shells of revolution having cone angles, β=10° and 20°, and for two preset slippage tendency, fst=0.1 and 0.3 respectively. Both shells are assumed to be wound with starting winding angle, α_1=45° at the small radius edge. From Figures 5.12 and 5.13 it can be seen that when the cone angle is increased the winding angle and thickness decreases compared to the low cone angle case for both preset slippage tendencies analyzed. It is also seen that for the same cone angle when the preset slippage tendency is increased the winding angle and the thickness becomes higher over the span of the shell compared to the low preset slippage tendency.

Figure 5.14 shows the variation of the natural frequencies of the conical shells with the circumferential wave number for two different boundary conditions, two different cone angles and for two different preset slippage tendency. Figure 5.14-(a) gives the natural frequencies of the conical shell which is clamped at both ends. On the other hand, Figure 5.14-(b) gives the natural frequencies of the conical shell which is clamped at the small radius end and free at the large radius end. The natural frequencies are also presented in tabular form in Table 5.3 for both edge conditions.

As mentioned in section 5.1, without a closed form solution for the natural frequencies, parametric effect of different terms cannot be explicitly identified. However, for the two conical shells, with two different cone angles, analyzed it is observed that when the cone angle is increased the natural frequencies drop for almost all circumferential vibration modes. This drop in the natural frequencies is mainly attributed to the combined effect of the variation of the winding angle and thickness. At high circumferential wave numbers the dominant stiffness coefficient affecting the natural frequency is the bending stiffness coefficient in the circumferential direction

D_{22}. When the cone angle is increased, the winding angle and thickness decrease. The decrease of the winding angle and thickness due to an increase in the cone angle accounts for drop in the bending stiffness coefficient in the circumferential direction D_{22}. It should be noted that although the reduction in the thickness has an increasing effect on the natural frequencies, the increase of the circumferential length of the cone in a way compensates the effect of thickness reduction. Therefore, the decrease of the circumferential bending stiffness D_{22} due to the increase of the cone angle accounts for the drop of the natural frequency at high circumferential wave numbers.

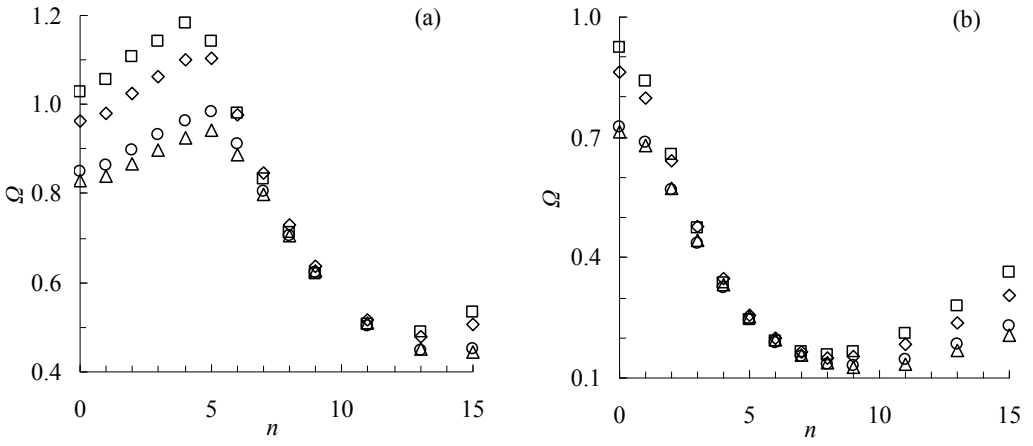

Figure 5.14 Variation of the fundamental non-dimensional frequencies for two different cone angles for ***(a)*** CCS, ***(b)*** CFS

◊: β=10°, fst=0.1; □: β=10°, fst=0.3; Δ: β=20°, fst=0.1; o: β=20°, fst=0.3

At low circumferential wave numbers it is expected that the extensional stiffness coefficients to be dominant on the natural frequencies. When the cone angle is increased the decrease of the winding angle has an augmenting effect on the stiffness coefficients in the meridional direction (stiffness coefficients with subscript 11) whereas the decrease of the winding angle has a lowering effect on the stiffness coefficients in the circumferential direction. Therefore, without a closed form solution for the natural frequencies, it is not possible to infer a general conclusion on the effect of the stiffness coefficients on the natural frequencies. However, it can be concluded that the combined effect of the change of the winding angle and the thickness due to an increase in the cone angle accounts for a drop in the natural frequencies, and the drop of the natural frequencies is mainly attributed to the decrease of the thickness when the cone angle is increased.

After analyzing Figure 5.14 another remark can be made on the effect of the semi-geodesic winding. From Figure 5.14, it is seen that the effect of preset slippage tendency is more pronounced for lower cone angles. This result is seen because of the effect of cone angle on the winding angle and the thickness variation as explained above. Since the winding angle and the thickness along the meridional axis is affected less from the preset slippage tendency as the cone

angle increases, the differences in the natural frequencies of the shells wound by applying two different preset slippage tendency is less for the higher cone angle case. This conclusion can be extracted from a careful examination of Figures 5.12 and 5.13.

Table 5.3 Fundamental non-dimensional frequencies for two different cone angles and preset slippage tendencies

	β=10^O, *fst*=0.1		β=10^O, *fst*=0.3		β=20^O, *fst*=0.1		β=20^O, *fst*=0.3	
n	***CFS***	***CCS***	***CFS***	***CCS***	***CFS***	***CCS***	***CFS***	***CCS***
0	0.861	0.961	0.924	1.029	0.713	0.828	0.727	0.851
1	0.798	0.982	0.840	1.056	0.678	0.840	0.686	0.865
2	0.642	1.026	0.655	1.107	0.571	0.867	0.570	0.898
3	0.477	1.063	0.473	1.143	0.444	0.898	0.437	0.932
4	0.346	1.100	0.337	1.184	0.334	0.925	0.325	0.963
5	0.256	1.103	0.247	1.141	0.252	0.941	0.244	0.983
6	0.198	0.976	0.192	0.980	0.195	0.888	0.189	0.913
7	0.165	0.845	0.164	0.834	0.158	0.797	0.154	0.806
8	0.151	0.731	0.157	0.713	0.137	0.707	0.136	0.707
9	0.152	0.638	0.165	0.619	0.127	0.628	0.130	0.622
11	0.184	0.518	0.211	0.508	0.136	0.510	0.146	0.502
13	0.238	0.480	0.279	0.489	0.167	0.450	0.183	0.449
15	0.306	0.505	0.361	0.535	0.208	0.443	0.231	0.453

5.1.3 Effect of semi geodesic winding on the mode shapes

The effect of semi-geodesic winding on the mode shapes of the conical shell which is clamped at both edges is given in Figures 5.15 - 5.17. For the particular solution, circumferential wave number is taken as one (n=1) and three different initial winding angle 30^o, 45^o, 60^o are investigated. For this configuration and the initial winding angles and the preset slippage tendencies used, the dominant fundamental vibration mode was identified as the lateral displacement (w^0). The dominant displacement mode is decided after the normalization process of the fundamental shell variables. The normalization of the displacement mode shapes is made with respect to the largest fundamental variable that is determined along the axis of the shell of revolution during the solution of the fundamental shell variables. Thus, the displacement component which has a value of unity somewhere along the axis of the shell of revolution is the dominant mode at that frequency. Figures 5.15 - 5.17 present the normalized cosine and sine parts of the lateral, meridional and circumferential displacements given by Eq. (2.42) and (2.43). It should be noted that in this particular example, independent from the initial winding angle and preset slippage tendency, cosine part of the lateral displacement mode dominates the mode shape since the sine part is much smaller. The actual variation of the lateral displacement over the whole conical shell can be constructed by utilizing the cosine and sine parts of the lateral displacement in Eq.(2.40) for n=1.

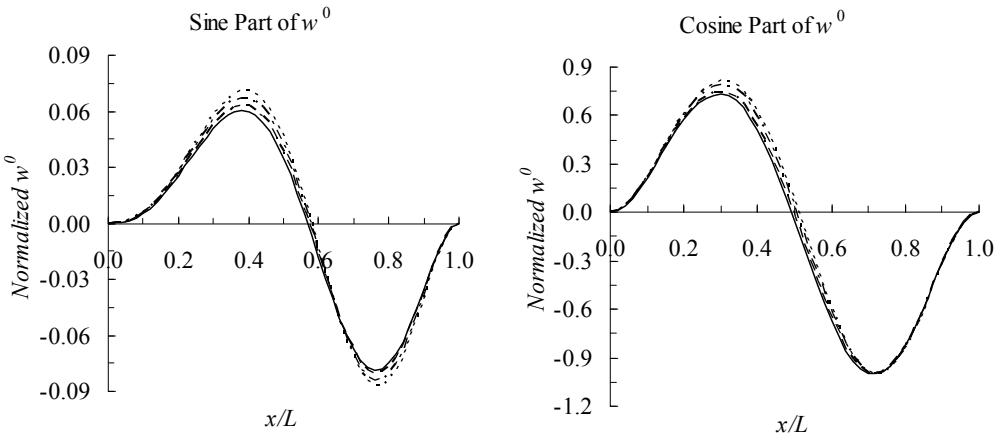

(a)

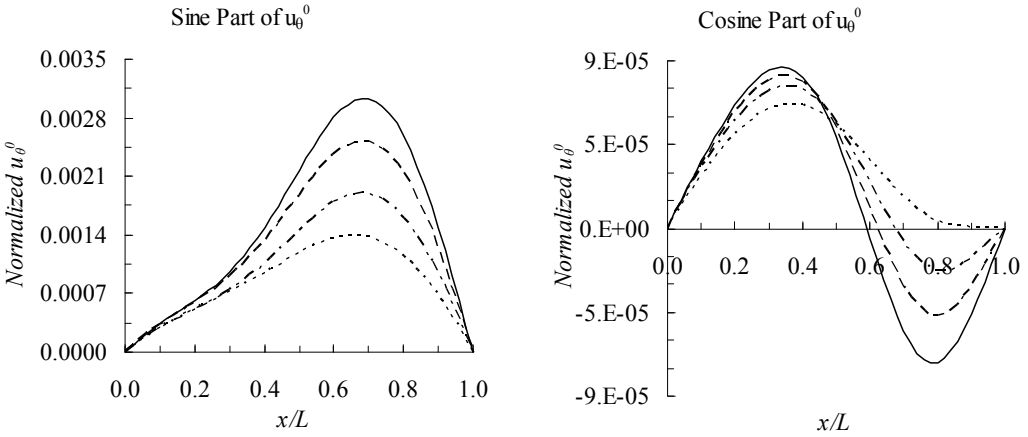

(b)

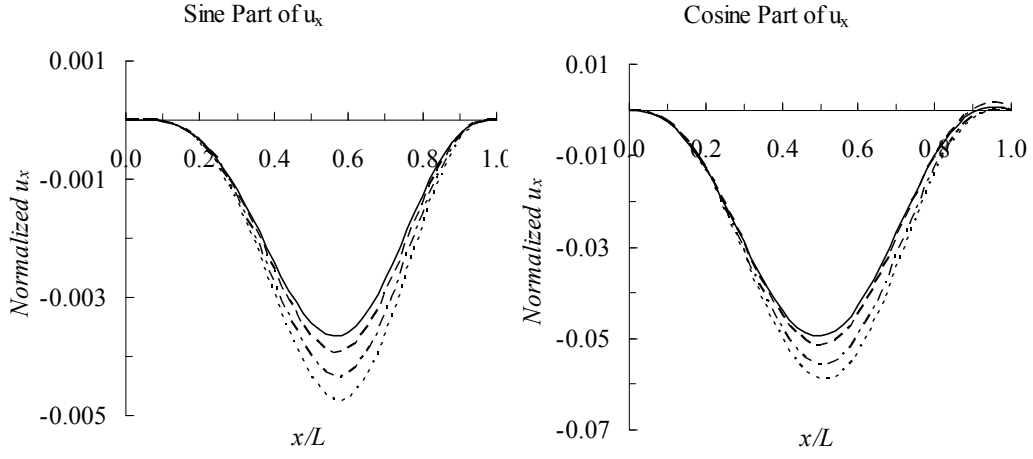

(c)

Figure 5.15 ***(a)*** Lateral, ***(b)*** circumferential, ***(c)*** meridional displacement mode shapes for the conical shell of revolution; α_1=30°

———: geodesic; — — — : fst=0.1; — · — · —: fst=0.2 ; - - - - - : fst=0.3

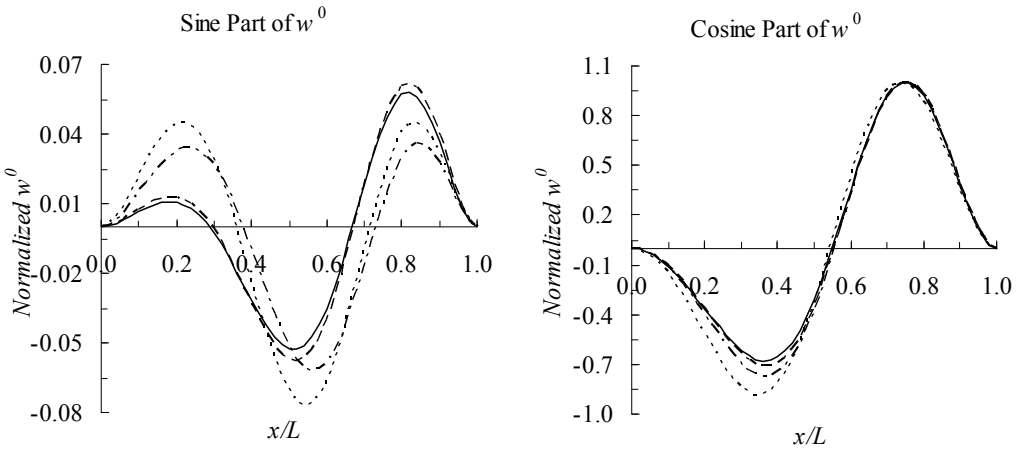

(a)

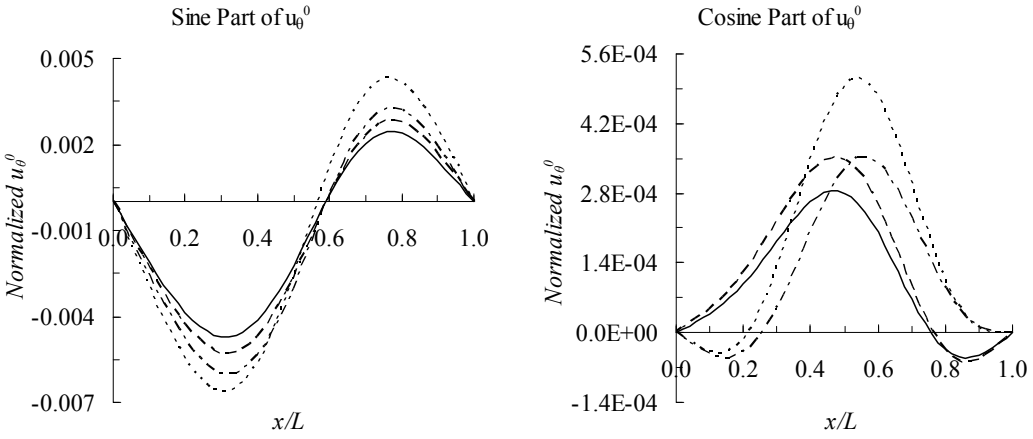

(b)

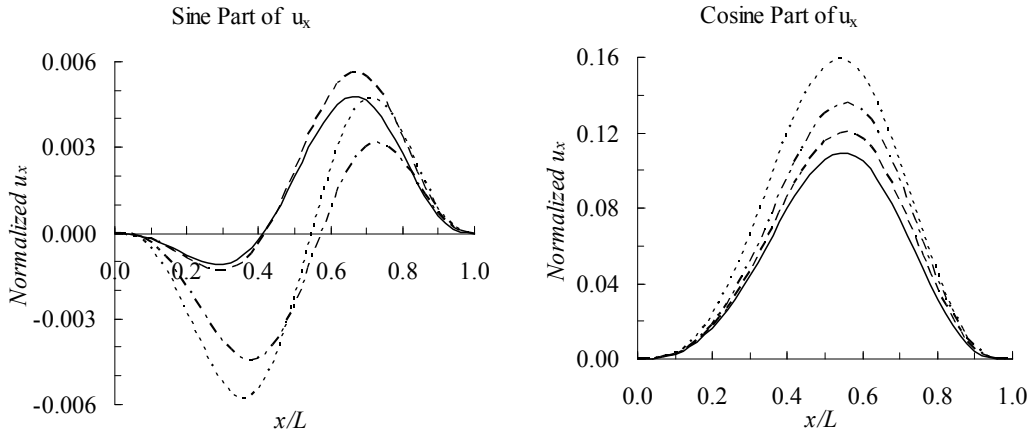

(c)

Figure 5.16 ***(a)*** Lateral, ***(b)*** circumferential, ***(c)*** meridional displacement mode shapes for the conical shell of revolution α_1=45°

———: geodesic; — — — : fst=0.1; — · — · —: fst=0.2 ; - - - - - : fst=0.3

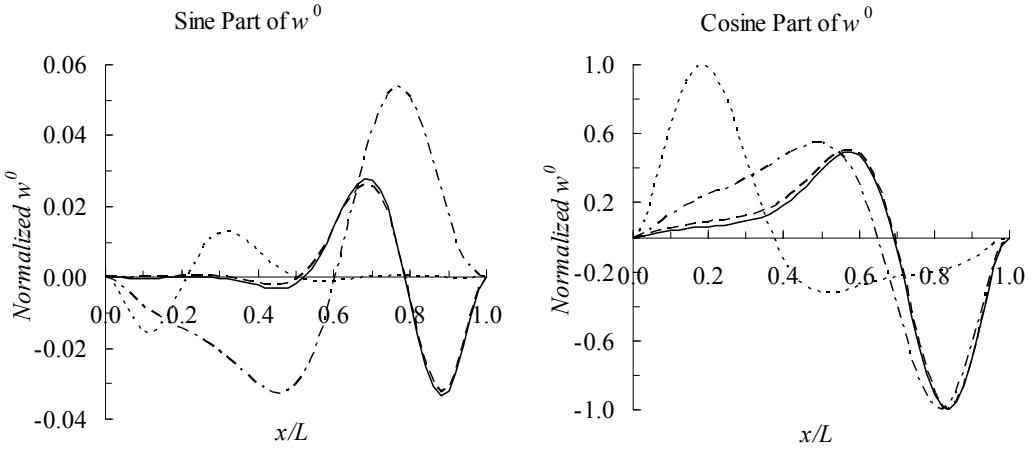

(a)

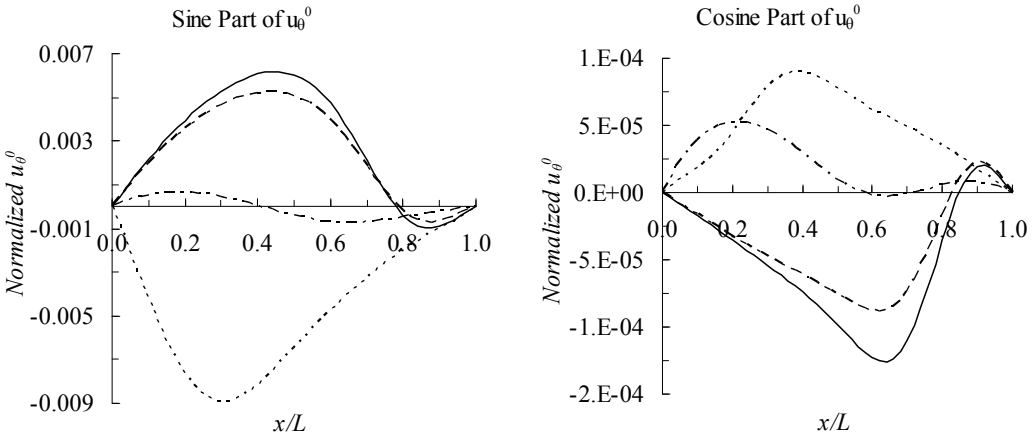

(b)

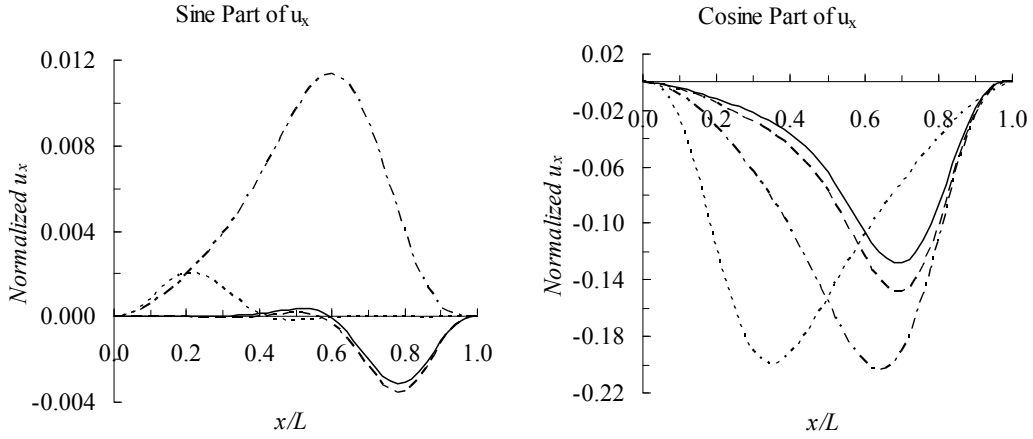

(c)

Figure 5.17 ***(a)*** Lateral, ***(b)*** circumferential, ***(c)*** meridional displacement mode shapes for the conical shell of revolution α_1=60°

——— : geodesic; — — — : fst=0.1; — · — · — : fst=0.2 ; - - - - - : fst=0.3

For the present investigation, increasing the initial winding angle introduces a noticeable effect of the preset slippage tendency. Almost inexistent shift in lateral mode shape for the 30^o initial winding angle becomes a critical design consideration for using larger starting winding angles and for using different values of preset slippage tendencies. For the 60^o initial winding angle, Figure 5.17 shows that for low preset slippage tendency the lateral displacement mode shapes are almost identical as shown by the geodesic winding case and semi-geodesic winding case with the preset slippage tendency of 0.1. When the preset slippage tendency is increased, it is observed that the peak displacement point shifts towards the small radius edge. From Figure 5.17 it can be seen that for the semi-geodesic winding case with the preset slippage tendency of 0.3, the shift of the peak displacement point towards the small radius edge is approximately 60 percent of the span of the shell.

For the initial winding angle of 60^o and for the case with the preset slippage tendency of 0.3, Figures 5.2 and 5.6 show that the thickness and meridional bending stiffness coefficient D_{11} increase towards the larger radius edge of the conical shell. Therefore, the shift of peak lateral displacement location towards the small radius edge is mainly attributed to the increased thickness and stiffness of the shell towards the larger radius edge for the case with the preset slippage tendency of 0.3. The increased bending stiffness of shell near the larger radius edge cause the peak displacement location to shift towards the small radius edge for the high preset slippage tendency case.

Similar to the 60^o initial winding angle case, Figure 5.16 shows the shift of peak lateral displacement location of the dominant mode shape (cosine part of lateral displacement) towards the small radius edge for the initial winding angle of 45^o. However, this shift is much smaller compared to the shift of peak lateral displacement shift for the 60^o initial winding angle case presented in Figure 5.17. At high initial winding angles the effect of preset slippage tendency is more pronounced on the stiffness coefficients. The shift of the peak lateral displacement point is towards the small radius edge becomes significant at high initial winding angles and at high preset slippage tendency.

From Figure 5.15, it can be seen that for the 30^o initial winding angle case the effect of preset slippage tendency is almost negligible. For the particular shell of revolution studied, it is seen that especially when the initial winding angle is high, the preset slippage tendency can be a significant design parameter affecting the mode shapes of the filament wound shells of revolution.

For the 60^o initial winding case it is also observed that when the preset slippage tendency is increased the nodal point of the lateral displacement also shifts towards the small radius edge. For the preset slippage tendency of 0.3 the shift of the nodal point towards the small radius edge is also significant. Figure 5.17(a) shows that the shift in the nodal point towards the small radius edge is approximately 30% of the span of the shell compared to the geodesic winding case. With

this case study, it is shown that the semi-geodesic winding may have a significant effect on the mode shapes depending on the preset slippage tendency used during the filament winding process.

5.2 FILAMENT WOUND TRUNCATED SPHERICAL SHELLS OF REVOLUTION

5.2.1 Effect of semi-geodesic winding on the winding angle, thickness, stiffness coefficients and natural frequencies

By implementing the semi-analytical method of solution, a sample study is also performed for the effect of the semi-geodesic winding on the natural frequencies of truncated filament wound spherical shells. The truncated sphere is assumed to have a radius of 1 m, and overall thickness of 5.76 mm at the small radius edge. The shell is clamped at the narrow end corresponding to a meridian angle of $\phi = 10^o$. The outer edge of the spherical shell, corresponding to a meridian angle of $\phi = 70^o$, is clamped, and let free (Figure 2.1), resulting in analysis for two different boundary conditions. Each ply is assumed to be composed of high modulus graphite epoxy, with the same material properties used in the conical shell example, and each ply has a thickness of 0.24 mm at the narrow end. Shell wall is composed of 24 layers with alternating winding angles $[\,\theta/-\theta/\theta/-\theta/\theta/-\theta/\theta/-\theta/\theta/-\theta/\theta/-\theta\,]_S$.

The analyses are performed for the spherical shell which is wound by starting the winding at the narrow end. In order to investigate the effect of semi-geodesic winding on stiffness coefficients and vibration characteristics, initial winding angles of 25^o, 45^o, and 65^o are selected. Figure 5.18 gives the variation of the winding angle with respect to the normalized meridian of the spherical shell for different preset slippage tendencies. Similar to the truncated conical shell analyzed in section 5.1, variation of the winding angle is presented in Figure 5.18 where the winding angle has the units of degrees, and the thickness variation along the meridional direction is given in Figure 5.19 where the thickness is normalized with respect to the initial thickness at the narrow end corresponding to a meridian angle of $\phi = 10^o$.

It should be noted that the variation of the winding angle is obtained by numerically integrating Eq.(3.17) from a known winding angle at the starting edge of the winding to any general meridional location.

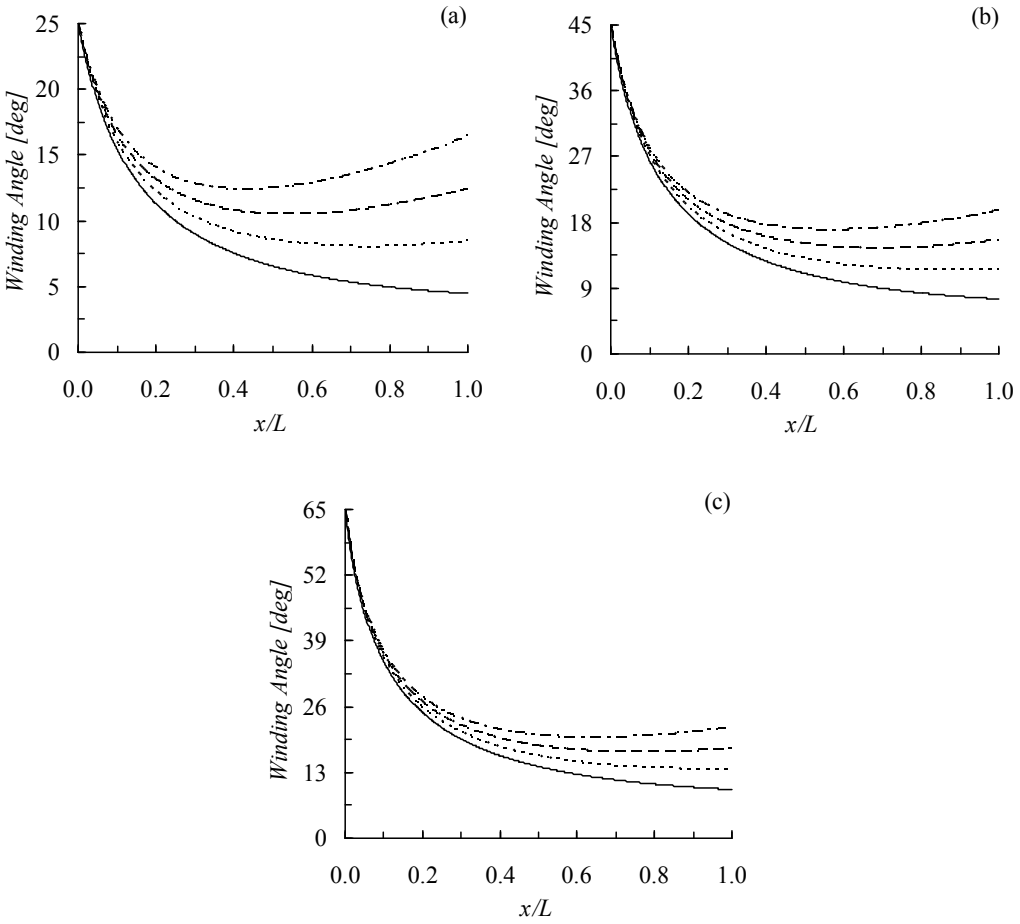

Figure 5.18 Variaton of the winding angle along the meridian of the shell for initial winding angle of ***(a)*** 25°; ***(b)*** 45°; ***(c)*** 65°

———: geodesic; - - - - -: fst=0.1; — — —: fst=0.2 ; — · — · —: fst=0.3

For the particular spherical shell geometry it is seen that the winding angles for the cases with different preset slippage tendencies show sharp drops near the small radius edge and as the outer edge is approached winding angles level out. Similar to the behavior for the conical shell, winding angle is higher when the preset slippage tendency is higher, and if the preset slippage tendency is above a certain value winding angle starts to increase towards the outer edge after an initial drop near the small radius edge where the winding starts. However, for the spherical shell studied, winding angle never exceeds the initial winding angle unlike the situation for the conical shell with the preset slippage tendency of 0.3 (Figure 5.1 (c), (d), (e)). It is noticed that when the initial winding angle is decreased, the rate of drop of the winding angle near the small radius edge also decreases, and for the high preset slippage tendency case the winding angle starts to increase earlier along the meridian of the shell. It should be noted that for the conical shell analyzed in the previous section, if the initial winding angle is small, the effect of preset slippage tendency on the winding angle is also small and when the initial winding angle is increased, the effect of preset slippage tendency on the winding angle becomes significant (Figure 5.1). However for the

spherical shell investigated such a conclusion cannot be inferred from the results given in Figure 5.18.

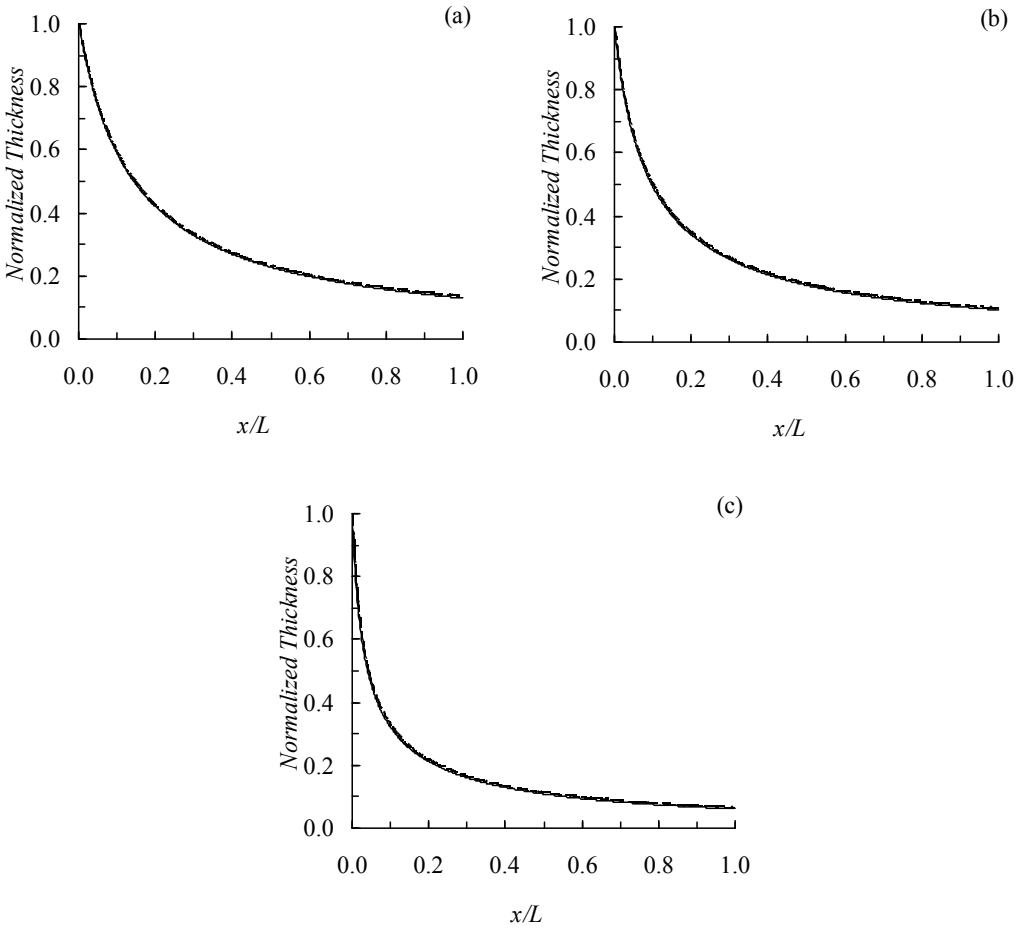

Figure 5.19 Variation of the normalized thickness along the meridian of the shell for initial winding angle of ***(a)*** 25°; ***(b)*** 45°; ***(c)*** 65°

———: geodesic; - - - - - : fst=0.1; — — — : fst=0.2 ; — · — · — : fst=0.3

Figure 5.19 shows that when the initial winding angle is increased the decrease in the thickness near the narrow end of the shell becomes steeper and the shell, which has a lower initial winding angle, is thicker. Figure 5.19 shows that for the three different initial winding angles the effect of preset slippage tendency on the thickness variation is very small such that in Figure 5.19 the thickness variation curves corresponding to different preset slippage tendency cannot be distinguished from each other. When the numerical values in Figure. 5.19 are examined, it is observed that higher preset slippage tendency causes slight increases in the thickness over the whole span of the spherical shell of revolution.

Figure 5.20 shows the variation of the normalized thickness of the spherical shell for three different initial winding angles and for the preset slippage tendency of 0.2. It is seen that for the same preset slippage tendency when the initial winding angle is increased the decrease in the thickness near the narrow end of the shell becomes steeper and the shell, which has a lower initial

winding angle, is thicker. For other preset slippage tendency cases similar thickness variations are calculated and it is observed that higher preset slippage tendency causes slight increases in the thickness over the whole span of the spherical shell of revolution.

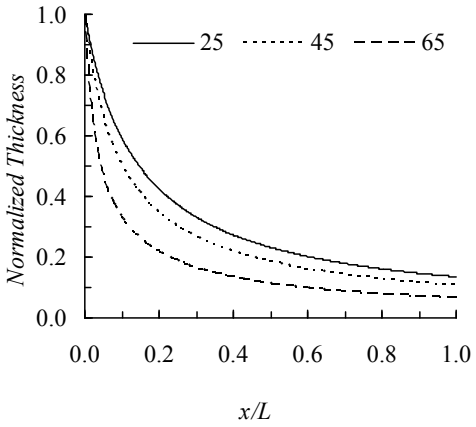

Figure 5.20 Variation of the normalized thickness along the meridian of the shell for fst=0.2 and different initial winding angles

Figures 5.21 - 5.23 give the variation of the normalized extensional stiffness coefficients (A_{ij}) and normalized bending stiffness coefficients (D_{ij}) with respect to the normalized meridian of the truncated spherical shell. The variation of stiffness coefficients are plotted for three different initial winding angle 25^o, 45^o and 65^o. Normalization is employed in a similar manner to the conical shell stiffness analysis; extensional stiffness coefficients (A_{11}, A_{22} and A_{66}) are normalized with respect to the value of A_{11}, bending stiffness coefficients D_{11}, D_{22} and D_{66} are normalized with respect to the value of D_{11} and bending stiffness coefficients D_{16} and D_{26} are normalized with respect to the value of D_{16} at the small radius edge of the conical shell. Note that all stiffness coefficient terms are represented in a logarithmic scale because of the steep variations, except for the extensional stiffness coefficient in the meridional direction, A_{11} term which does not vary as steep as other stiffness terms.

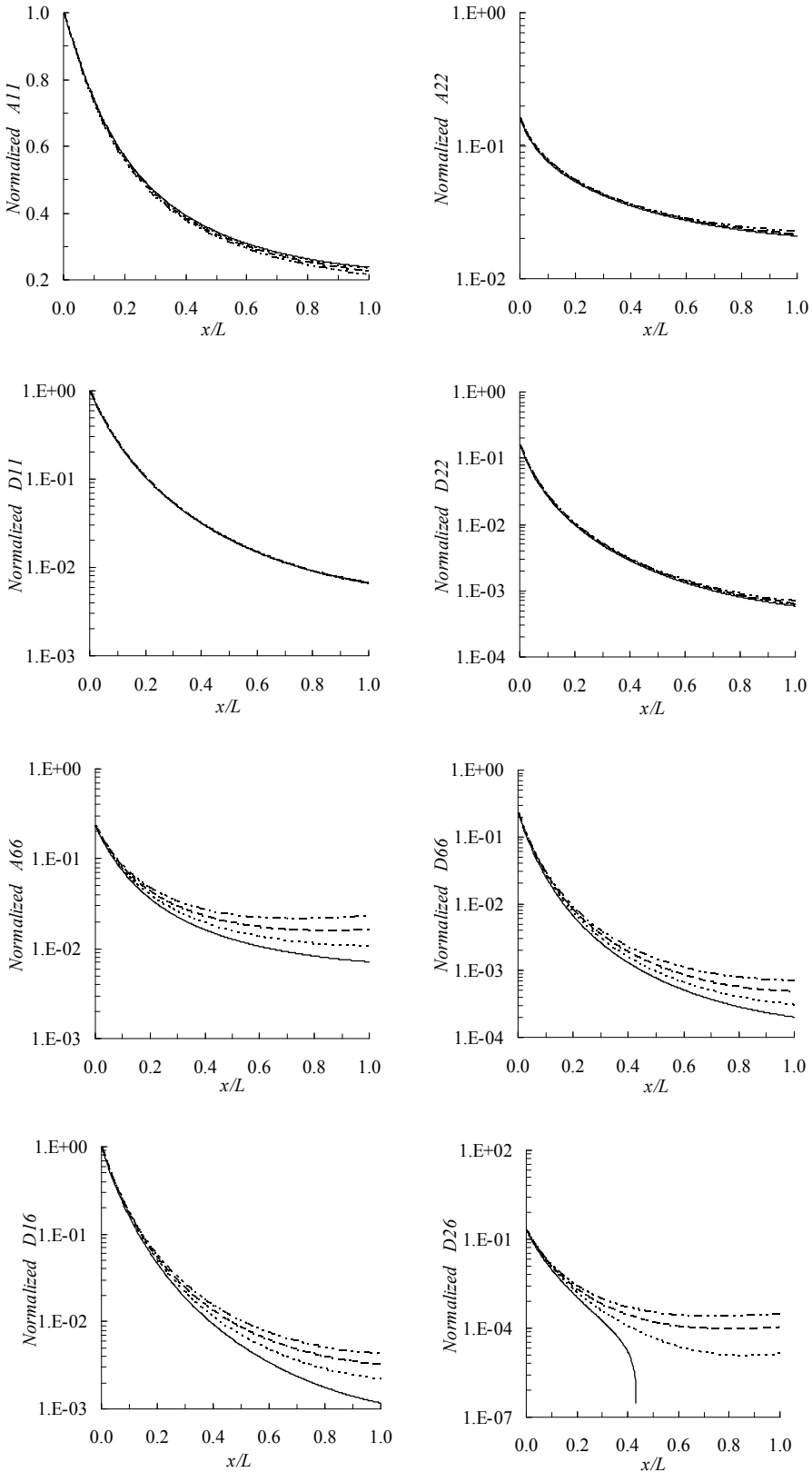

Figure 5.21 Stiffness coefficients along normalized meridian of the spherical shell for α_1=25^o

———: geodesic; - - - - - -: fst=0.1; — — —: fst=0.2 ; — · — · —: fst=0.3

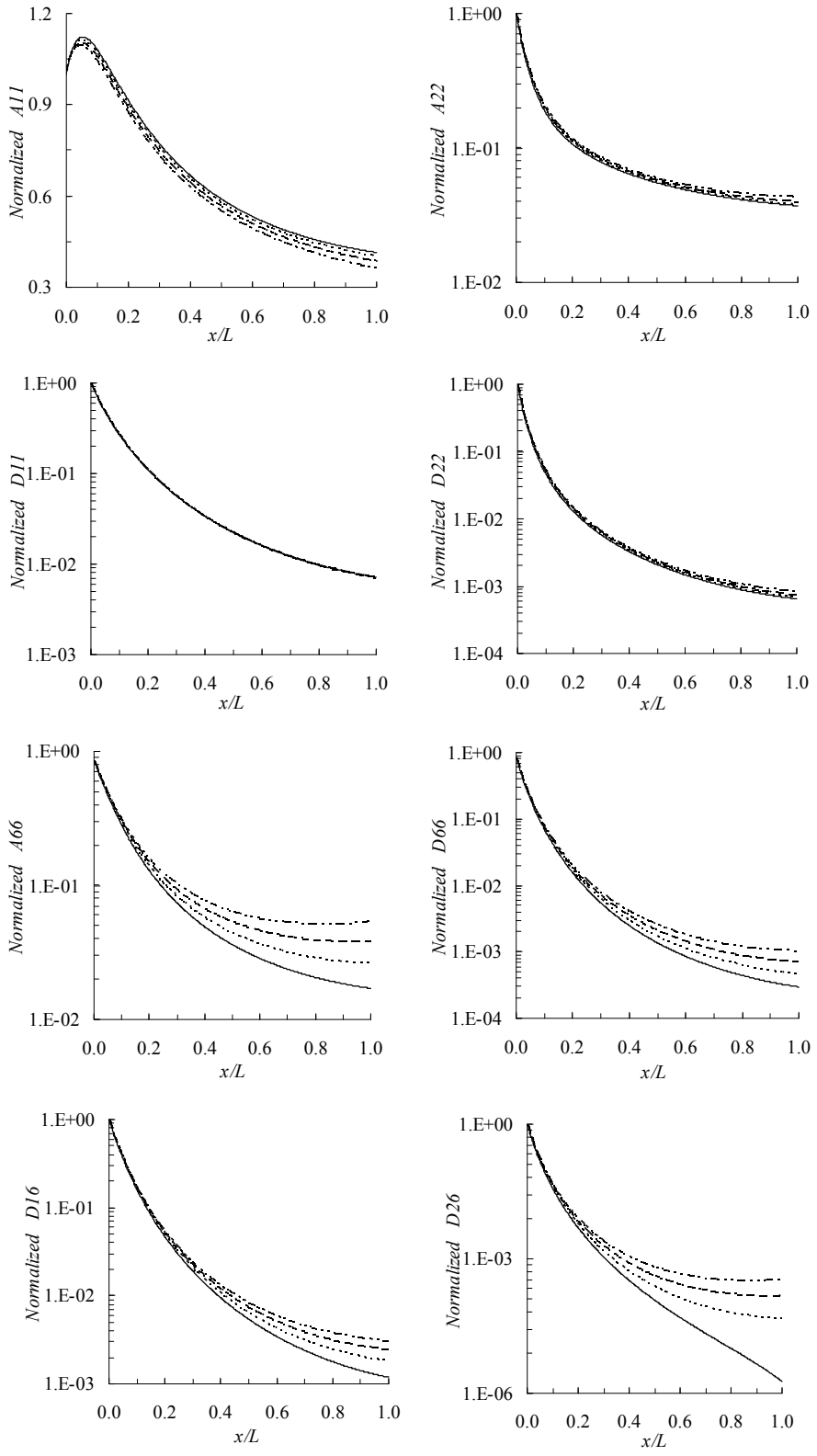

Figure 5.22 Stiffness coefficients along normalized meridian of the spherical shell for α_1=45^o

———: geodesic; - - - - - : fst=0.1; — — — : fst=0.2 ; — · — · — : fst=0.3

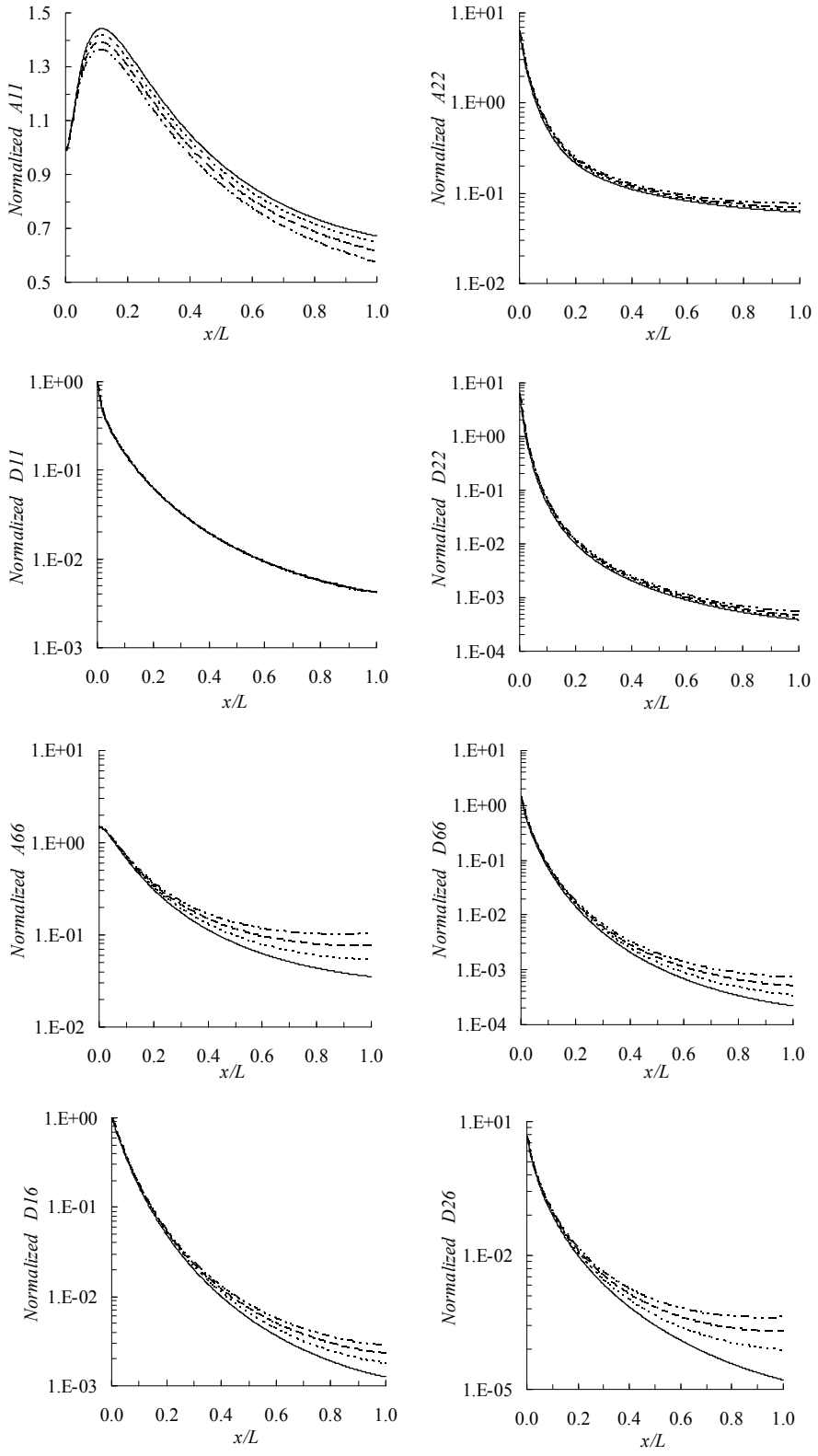

Figure 5.23 Stiffness coefficients along normalized meridian of the spherical shell for α_1=65^o

———: geodesic; - - - - - : fst=0.1; — — — : fst=0.2 ; — · — · — : fst=0.3

Figures 5.21-5.23 show that, similar to the conical shells of revolution, winding operation by applying higher preset slippage tendency results in higher bending stiffness coefficient, but extensional stiffness coefficient might be higher or lower. Unlike conical shells, the effect of initial winding angle on the relative differences between the stiffness coefficients of the shells manufactured applying different preset slippage tendency is less significant for a spherical shell of revolution. The less significant effect of the preset slippage tendency used in the manufacturing of the spherical shells of revolution on the stiffness coefficients, compared to the corresponding effect for conical shells, can be explained considering the variation of the winding angle and thickness of the spherical shell of revolutions, as shown in Figures 5.18 and 5.19. From Figure 5.18 it can be seen that especially for high initial winding angles the effect of preset slippage tendency on the variation of the winding angles is less pronounced in the spherical shell of revolution compared to the conical shells of revolution. More importantly, Figure 5.19 shows that the effect of the preset slippage tendency on the thickness variation is very small for initial winding angles 25^o, 45^o and 65^o. Therefore, the effect of thickness on the relative differences between the stiffness coefficients of the spherical shells, which are manufactured with different preset slippage tendencies, is also very small. Therefore, the main reason for the lower effect of the preset slippage tendency on the stiffness coefficients is mainly attributed to the fact that the differences between the thicknesses of the spherical shells of revolution, which are wound with different preset slippage tendencies, are very small.

For the geodesic winding and 25^o initial winding angle case, the bending-twisting coupling coefficient D_{26} is seen to decrease sharply beyond the 40% span location, as seen in Figure 21. This sharp decrease is due to the fact that for the geodesic winding case, the winding angle decreases along the shell axis continuously such that below the 7^o winding angle D_{26} becomes negative. Therefore, in the logarithmic the complete curve for D_{26} is not shown.

In general it was observed that, for the initial winding angle in the range of 25^o-65^o studied, higher preset slippage tendency resulted in higher extensional and bending stiffness in the circumferential direction. Generally, all stiffness coefficients are steeply decreasing along the meridional direction for all initial winding angles. However, for the extensional stiffness coefficient in the meridional direction, A_{11}, the preset slippage tendency has a lowering effect on the stiffness and for the initial winding angles of 45^o and 65^o A_{11} slightly increases close to the small radius end.

For the clamped-free and clamped-clamped truncated spherical shell of revolution natural frequencies are calculated by the numerical integration based solution technique described. Figures 5.24 and 5.25 give the variation of the non-dimensional fundamental frequency (Eq. (4.1)), corresponding to non-axisymmetric vibration modes, with respect to the circumferential wave number for the initial winding angles of 25^o, 45^o, 65^o and for different preset slippage tendencies. For the particular spherical shell geometry it is seen that unlike the situation

for the conical shell of revolution, at low circumferential wave numbers the effect of preset slippage tendency on the natural frequencies is not much and the natural frequencies of shells manufactured by different preset slippage tendencies are very close to each other. At higher circumferential wave numbers when the preset slippage tendency is increased, similar to the behaviour observed in conical shells, natural frequencies of the spherical shell increase. The increase in the natural frequencies with the increase in the preset slippage tendency is again attributed to the higher circumferential bending stiffness coefficient (D_{22}) of the spherical shell manufactured with higher preset slippage tendency. From Figure 5.18 it can be seen that the winding angle of the shell manufactured with higher preset slippage tendency is higher than the winding angle of the shell manufactured with lower preset slippage tendency over the whole span of the shell. In addition, higher preset slippage tendency causes slight increases in the thickness over the whole span of spherical shell of revolution. Therefore, the combined effect of higher winding angle and slightly higher thickness over span of the shell results in higher circumferential bending stiffness. It should be noted that although the thickness of the spherical shell with higher preset slippage tendency is higher, the increase of the natural frequencies with the circumferential wave number indicates that at high circumferential wave numbers the circumferential bending stiffness becomes more effective on the natural frequencies compared to the effect of inertia. Similar to the conclusion drawn for the conical shell example, for the spherical shell on the high circumferential wave number side bending stiffness coefficient in the circumferential direction (D_{22}) also stands out as the main parameter governing the natural frequency, and higher preset slippage tendency results in higher fundamental natural frequencies. However, on the low circumferential wave number side one can not single out a parameter which is dominant on the natural frequencies.

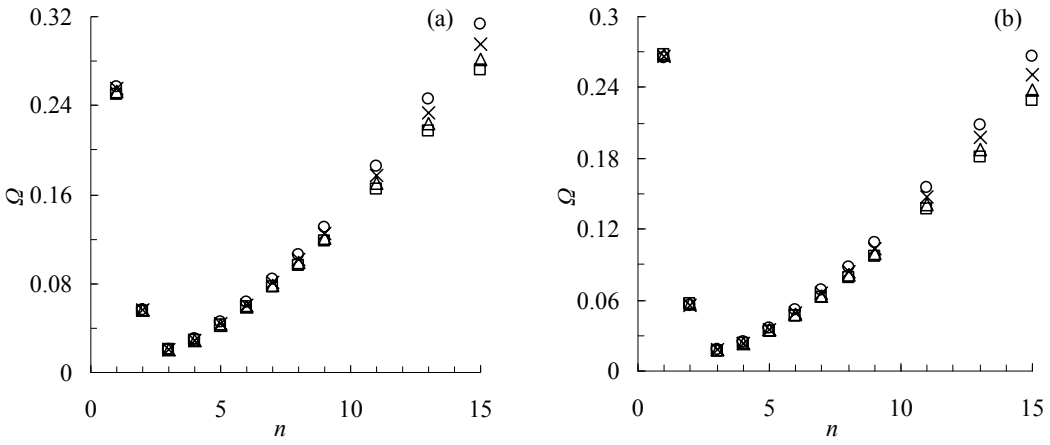

Figure 5.24 Natural Frequency versus n; CFS; Spherical Shell ***(a)*** α_1=25°;
(b)α_1=45°; ***(c)*** α_1=65°
□: geodesic; Δ: fst=0.1 ; x: fst=0.2 ; o: fst=0.3

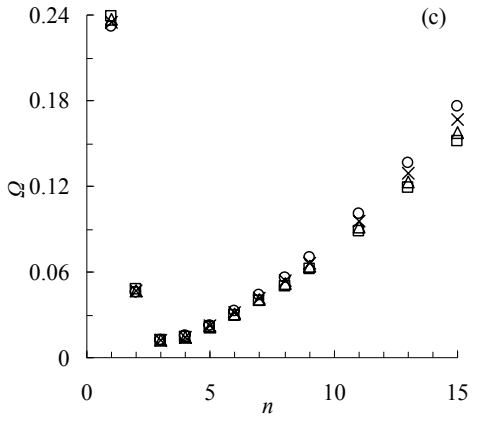

Figure 5.24 (continued) Natural Frequency versus n; CFS; Spherical Shell
(a)α_1=25°; ***(b)*** α_1=45°; ***(c)*** α_1=65°
□: geodesic; Δ: fst=0.1 ; x: fst=0.2 ; o: fst=0.3

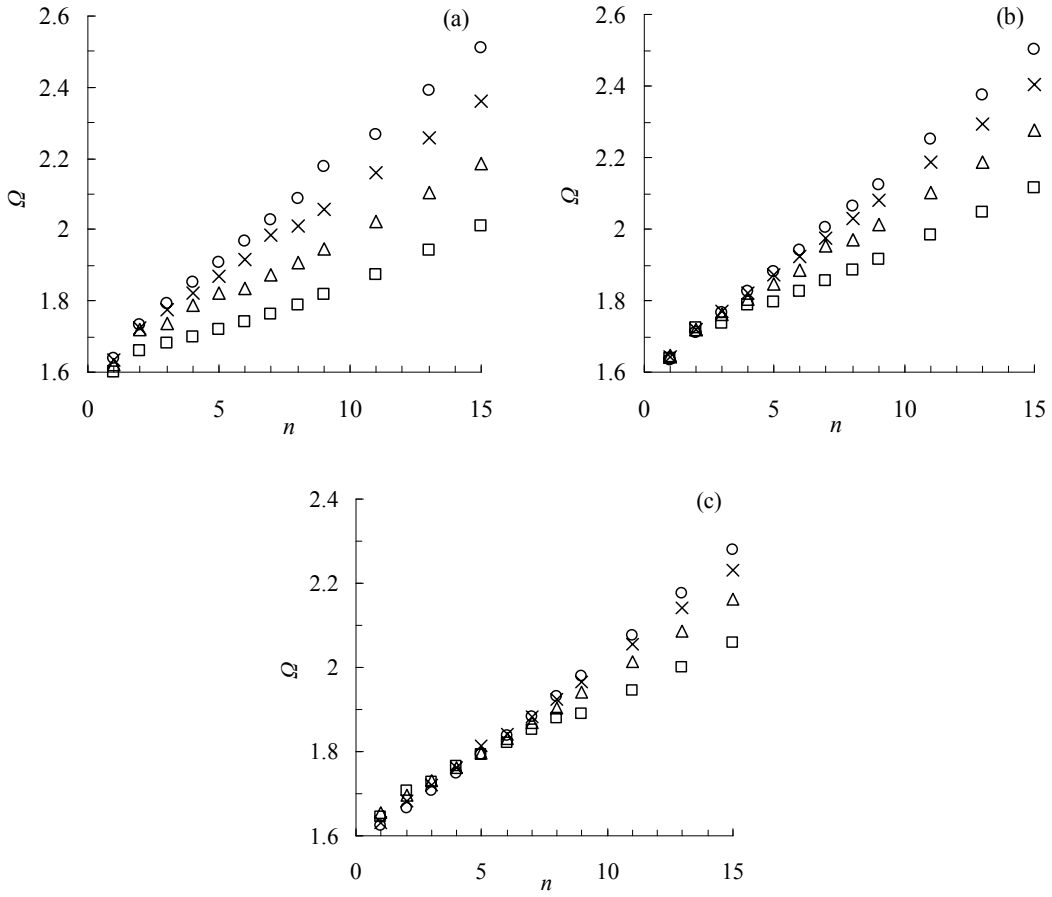

Figure 5.25 Natural Frequency versus n; CCS; Spherical Shell ***(a)*** α_1=25°;
(b) α_1=45°; ***(c)*** α_1=65°
□: geodesic; Δ: fst=0.1 ; x: fst=0.2 ; o: fst=0.3

Tables 5.4 and 5.5 give the natural frequencies of the spherical shell of revolution for two different boundary conditions. Table 5.4 gives the natural frequencies for the clamped-free shell, and Table 5.5 gives the natural frequencies for the clamped-clamped shell. It is noted that at high circumferential wave numbers when the initial winding angle is increased the differences between the natural frequencies for different preset slippage tendency cases become less compared to the cases when the initial winding angle is low. Although high preset slippage tendency still accounts for higher natural frequencies due to the higher circumferential bending stiffness attained by higher preset slippage tendency, the differences between the natural frequencies of the spherical shells wound by different preset slippage tendency is less for the high initial winding case compared to the low initial winding case. However, for the conical shell studied when the initial winding angle is increased the differences between the natural frequencies of conical shells wound by applying different preset slippage tendency also increase (Figures 5.8 and 5.9). This behaviour is just opposite of the behaviour observed in spherical shell of revolution. The main reason for this may be attributed to the fact that for the spherical shell of revolution, when the winding angle is increased frequencies decrease whereas for the conical shell studied natural frequencies increase when the initial winding angle is increased. Therefore, when the initial winding angle is increased the differences between the natural frequencies of spherical shells wound by applying different preset slippage tendencies may become less compared to the differences between the natural frequencies of the spherical shell of revolution which has a low initial winding angle.

It is noticed that when the initial winding angle is increased thickness becomes less compared to the thickness attained when the initial winding angle is low and the effect of thickness on the circumferential bending stiffness D_{22} becomes more dominant than the winding angle. Therefore, for the same preset slippage tendency, when the winding angle is increased the circumferential bending stiffness drops. Since at high circumferential wave numbers the circumferential bending stiffness is the most effective parameter on the natural frequency, natural frequencies also decrease when the initial winding angle is increased. As a matter of fact for the spherical shell of revolution studied, except for some low circumferential wave numbers, for the same preset slippage tendency the natural frequencies are seen to decrease with the increase in the initial winding angle for almost all circumferential vibration modes.

Table 5.4 Fundamental non-dimensional frequencies corresponding to different wave numbers for CFS

	$\alpha_1=25^o$				$\alpha_1=45^o$				$\alpha_1=65^o$			
	fst				***fst***				***fst***			
n	***0***	***0.1***	***0.2***	***0.3***	***0***	***0.1***	***0.2***	***0.3***	***0***	***0.1***	***0.2***	***0.3***
0	0.769	0.763	0.756	0.748	0.695	0.687	0.677	0.667	0.610	0.601	0.592	0.582
1	0.250	0.253	0.256	0.257	0.268	0.268	0.267	0.265	0.239	0.237	0.234	0.231
2	0.055	0.056	0.056	0.056	0.057	0.056	0.056	0.056	0.047	0.047	0.047	0.046
3	0.020	0.021	0.021	0.021	0.017	0.018	0.018	0.018	0.012	0.012	0.012	0.012
5	0.042	0.043	0.044	0.045	0.034	0.034	0.035	0.036	0.021	0.021	0.022	0.023
7	0.077	0.078	0.080	0.083	0.062	0.064	0.066	0.069	0.039	0.040	0.042	0.043
9	0.118	0.121	0.125	0.131	0.097	0.100	0.104	0.109	0.062	0.064	0.066	0.070
11	0.165	0.170	0.177	0.185	0.137	0.141	0.148	0.156	0.089	0.092	0.096	0.101
13	0.216	0.224	0.234	0.246	0.181	0.188	0.197	0.209	0.119	0.123	0.129	0.137
15	0.271	0.282	0.296	0.313	0.228	0.238	0.251	0.267	0.151	0.158	0.166	0.176

Table 5.5 Fundamental non-dimensional frequencies corresponding to different wave numbers for CCS

	$\alpha_1=25^o$				$\alpha_1=45^o$				$\alpha_1=65^o$			
	fst				***fst***				***fst***			
n	***0***	***0.1***	***0.2***	***0.3***	***0***	***0.1***	***0.2***	***0.3***	***0***	***0.1***	***0.2***	***0.3***
0	1.559	1.549	1.535	1.516	1.523	1.507	1.487	1.462	1.480	1.460	1.436	1.407
1	1.601	1.621	1.634	1.638	1.639	1.645	1.644	1.635	1.644	1.656	1.632	1.626
2	1.660	1.718	1.725	1.734	1.722	1.718	1.719	1.710	1.705	1.695	1.684	1.666
3	1.682	1.737	1.774	1.793	1.737	1.762	1.770	1.767	1.727	1.730	1.722	1.707
5	1.719	1.824	1.867	1.908	1.795	1.845	1.872	1.883	1.793	1.798	1.812	1.793
7	1.763	1.872	1.987	2.026	1.855	1.954	1.976	2.003	1.850	1.868	1.882	1.884
9	1.816	1.945	2.059	2.177	1.916	2.014	2.082	2.125	1.888	1.940	1.967	1.979
11	1.875	2.022	2.158	2.267	1.981	2.100	2.188	2.251	1.945	2.013	2.054	2.077
13	1.940	2.102	2.258	2.389	2.048	2.187	2.296	2.376	2.001	2.087	2.142	2.177
15	2.009	2.185	2.359	2.511	2.117	2.275	2.403	2.503	2.060	2.161	2.231	2.279

Figures 5.26 and 5.27 show the variation of the fundamental natural frequency of the spherical shell of revolution with respect to the initial winding angle for different circumferential wave numbers, preset slippage tendencies and for two different edge conditions. For the spherical shell which is clamped at the narrow end and free at the outer edge, Figure 5.26 gives the variation of the non-dimensional natural frequency with respect the initial winding angle for different circumferential wave numbers. Depending on the particular circumferential vibration mode, the natural frequencies either decrease continuously or start to decrease beyond a certain

initial winding angle. It can be seen from Figure 5.26 that for high circumferential wave numbers natural frequency monotonically decrease and the highest frequency occurs at low initial winding angles. On the other hand, for low circumferential wave numbers natural frequencies corresponding to spherical shells wound with different slippage tendencies initially increase and then start to decrease, so they have a peak value in the initial winding angle range 5^{o}-75^{o}.

Based on the variation of the natural frequency with the initial winding angle, it can also be inferred that when the initial winding angle is increased, the effect of the stiffness coefficients become more dominant on the natural frequencies compared to the effect of the inertia. The decrease of the thickness of the shell wall along the shell axis implies that the translatory and rotary inertia also decrease, and the decrease in the inertia terms would tend to increase the natural frequencies. Since the natural frequencies decrease at high initial winding angles, this implies that the stiffness coefficients become more effective on the natural frequencies compared to the effect of inertia.

Figure 5.26 clearly displays that except for some low circumferential wave numbers such as n=1, natural frequencies of the spherical shell of revolution manufactured with higher preset slippage tendency during the winding process has higher natural frequencies. Slightly higher thickness of shells wound with higher preset slippage tendency is considered to be the main reason for higher frequencies.

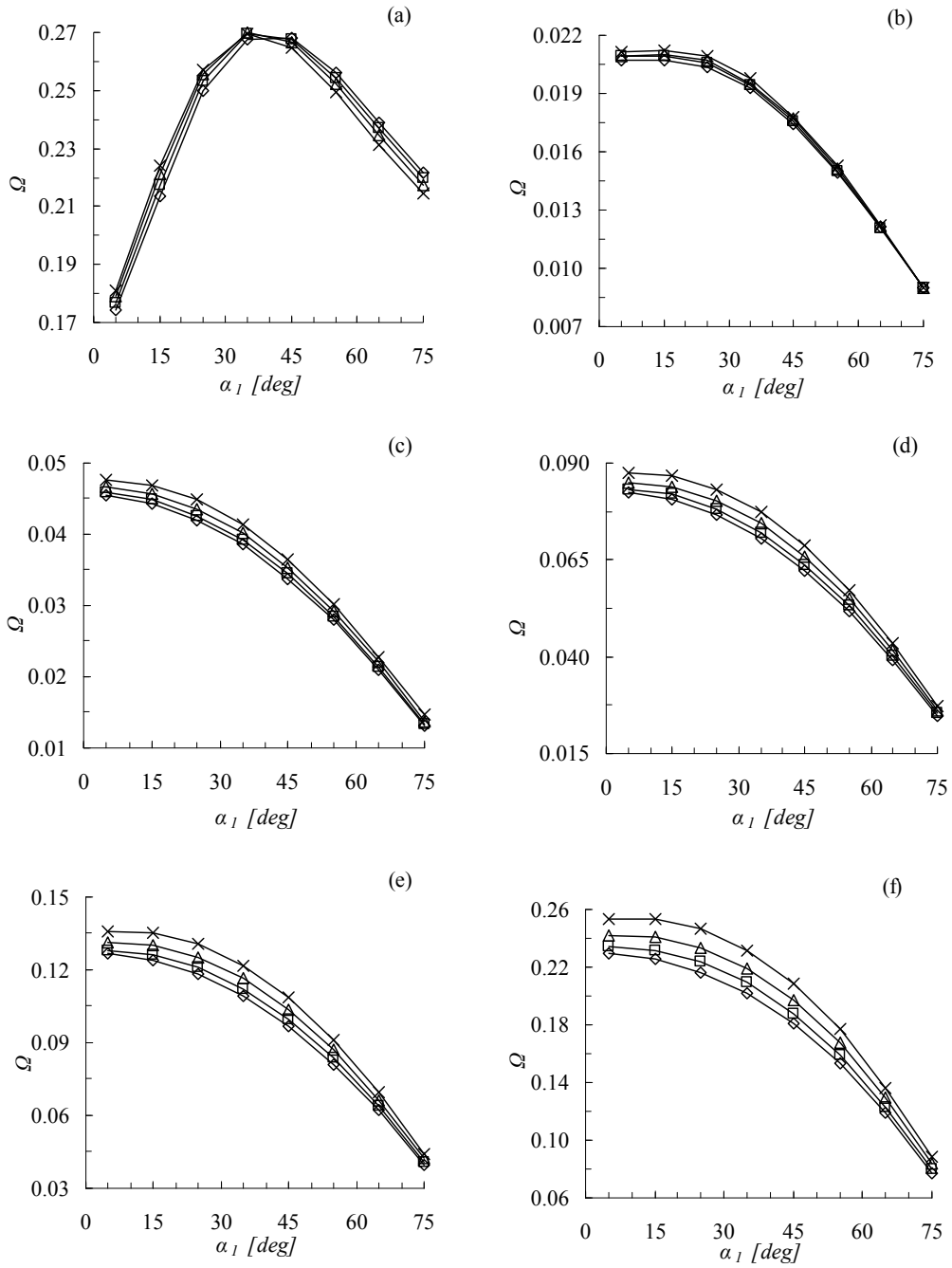

Figure 5.26 Variation of the natural frequency with initial winding angle: CFS;
(a) n=1, ***(b)*** n=3, ***(c)*** n=5, ***(d)*** n=7, ***(e)*** n=9, ***(f)*** n=13, ***(g)*** n=15

◊: geodesic; □: fst=0.1 ; Δ: fst=0.2 ; x: fst=0.3

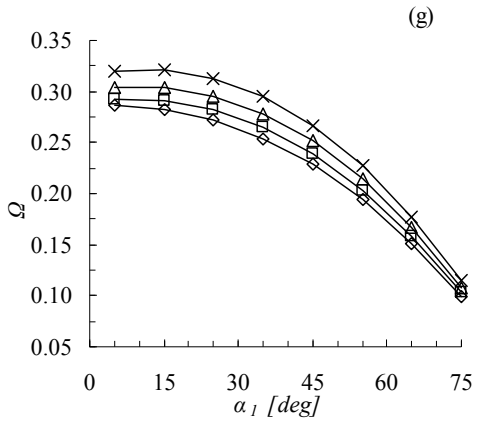

Figure 5.26 (continued) Variation of the natural frequency with initial winding angle: CFS; ***(a)*** n=1, ***(b)*** n=3, ***(c)*** n=5, ***(d)*** n=7, ***(e)*** n=9, ***(f)*** n=13, ***(g)*** n=15

◊: geodesic; □: fst=0.1 ; Δ: fst=0.2 ; x: fst=0.3

Figure 5.27 gives the variation of the non-dimensional frequency with respect to the initial winding angle for the filament wound spherical shell which is clamped at both edges. Similar to the clamped-free case, eventually at high initial winding angles, the natural frequencies start to decrease due to the significant decrease of the stiffness coefficients caused by thinning of the shell wall along the shell axis (Figure 5.19). However, for the clamped clamped case, in the low initial winding angle range (for angles less than 30^o-35^o) an increase of the natural frequencies with the initial winding angle is seen for most circumferential wave numbers. This behaviour is an indication that the combined effect of stiffness coefficients and the variable inertia on the natural frequencies changes when the outer edge is clamped. Comparison of Figures 5.26 and 5.27 also reveal that for the clamped-clamped spherical shell the effect of the preset slippage tendency on the natural frequencies is more significant compared to the effect of preset slippage tendency on the natural frequencies of the clamped-free spherical shell of revolution. Such a conclusion could have also been drawn from the examination of Tables 5.4 and 5.5. It can be seen that at high circumferential wave numbers regardless of the boundary condition and the initial winding angle, application of higher preset slippage tendency during the winding process results in higher natural frequencies. For the axisymmetric vibration mode low preset slippage tendency is seen to cause higher natural frequencies for both edge conditions and for almost all initial winding angles. In general for certain low circumferential wave numbers, such as n=1,2 for the clamped-clamped case, for low initial winding angles natural frequencies are higher if the preset slippage tendency is high and for high initial winding angles the natural frequencies are lower if the preset slippage tendency is high. This conclusion is more obvious for the clamped-clamped spherical shell of revolution.

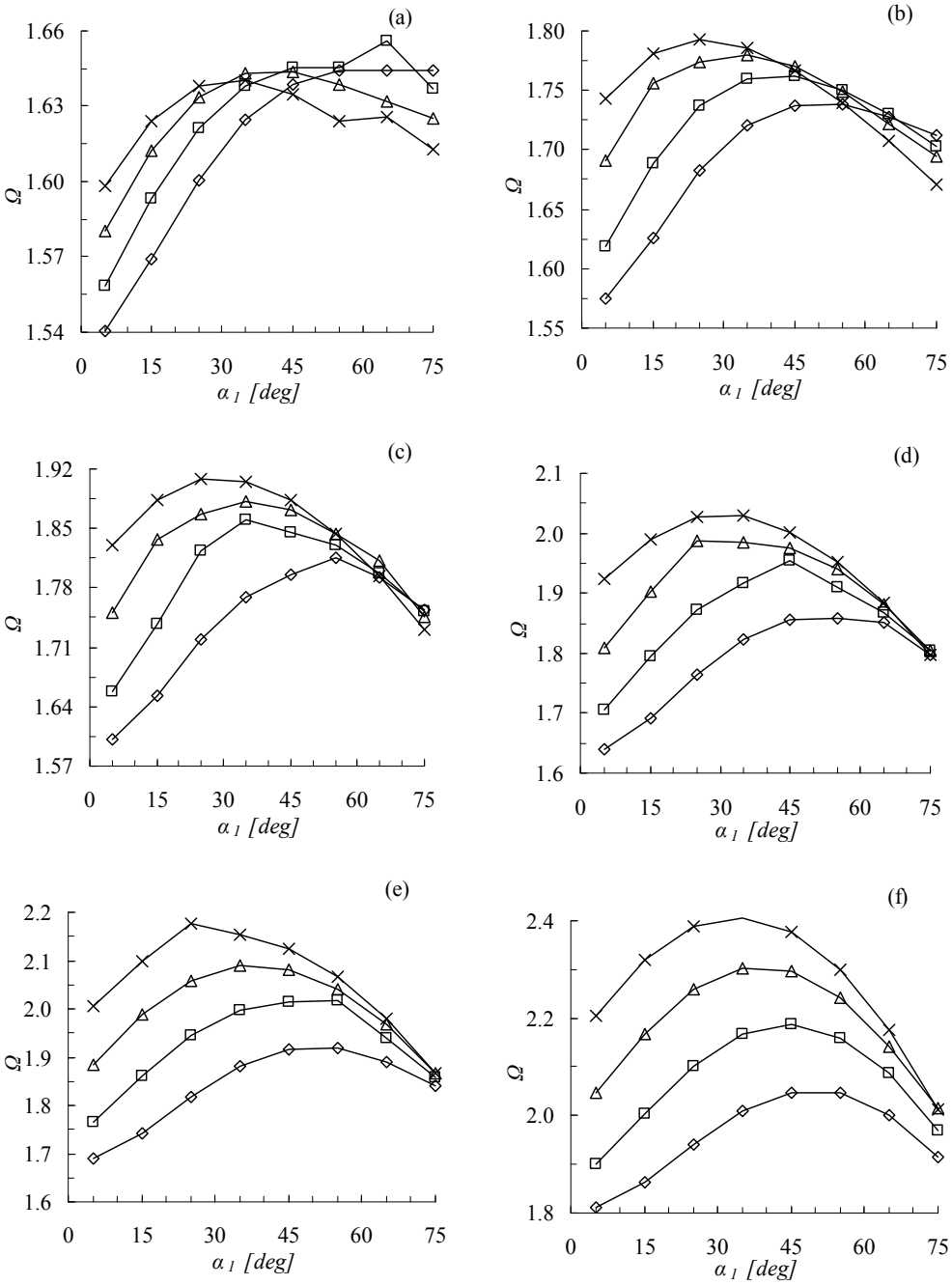

Figure 5.27 Variation of natural frequency with initial winding angle: CCS;
(a) n=1, ***(b)*** n=3, ***(c)*** n=5, ***(d)*** n=7, ***(e)*** n=9, ***(f)*** n=13, ***(g)*** n=15

◊: geodesic; □: fst=0.1 ; Δ: fst=0.2 ; x: fst=0.3

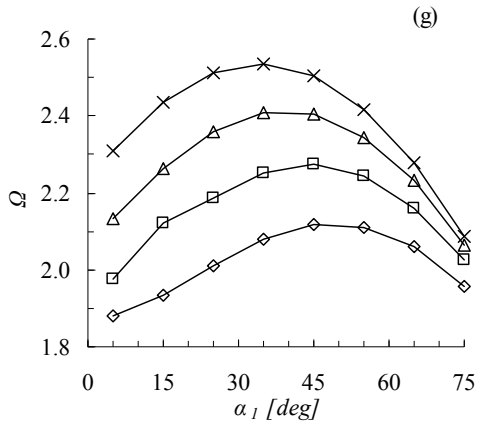

Figure 5.27 (continued) Variation of natural frequency with initial winding angle: CCS; ***(a)*** n=1, ***(b)*** n=3, ***(c)*** n=5, ***(d)*** n=7, ***(e)*** n=9, ***(f)*** n=13, ***(g)*** n=15

◊: geodesic; □: fst=0.1 ; Δ: fst=0.2 ; x: fst=0.3

The study of the variation of the natural frequencies with the initial winding angle and different preset slippage tendencies shows that the slippage tendency applied during the winding process can be an important parameter in altering the dynamic characteristics of shells of revolution. Therefore, it is recommended that the slippage tendency effect during the so-called semi-geodesic winding process be exploited in the best way in any design problem related to the filament wound composite shells of revolution. This study intends to stress the significant effect of the preset slippage tendency applied during the winding process on the dynamic characteristics, or in particular natural frequencies and modes shapes of filament wound shells of revolution.

5.2.2 Effect of semi geodesic winding on the mode shapes

The effect of semi-geodesic winding on the mode shapes of the spherical shell of revolution which is clamped at both edges is given in Figures 5.28-5.30. For the particular solution, circumferential wave number is taken as one (n=1) and the fundamental mode shapes corresponding to lateral displacement (w^0), circumferential displacement ($u_\theta{}^0$) and meridional displacement ($u_\varphi{}^0$) are obtained for three different initial winding angles 25°, 45°, 65° and different preset slippage tendencies. It should be noted that for the spherical shell configuration, initial winding angles and preset slippage tendencies, the dominant fundamental vibration mode was identified as the lateral displacement (w^0) similar to the conical shell studied.

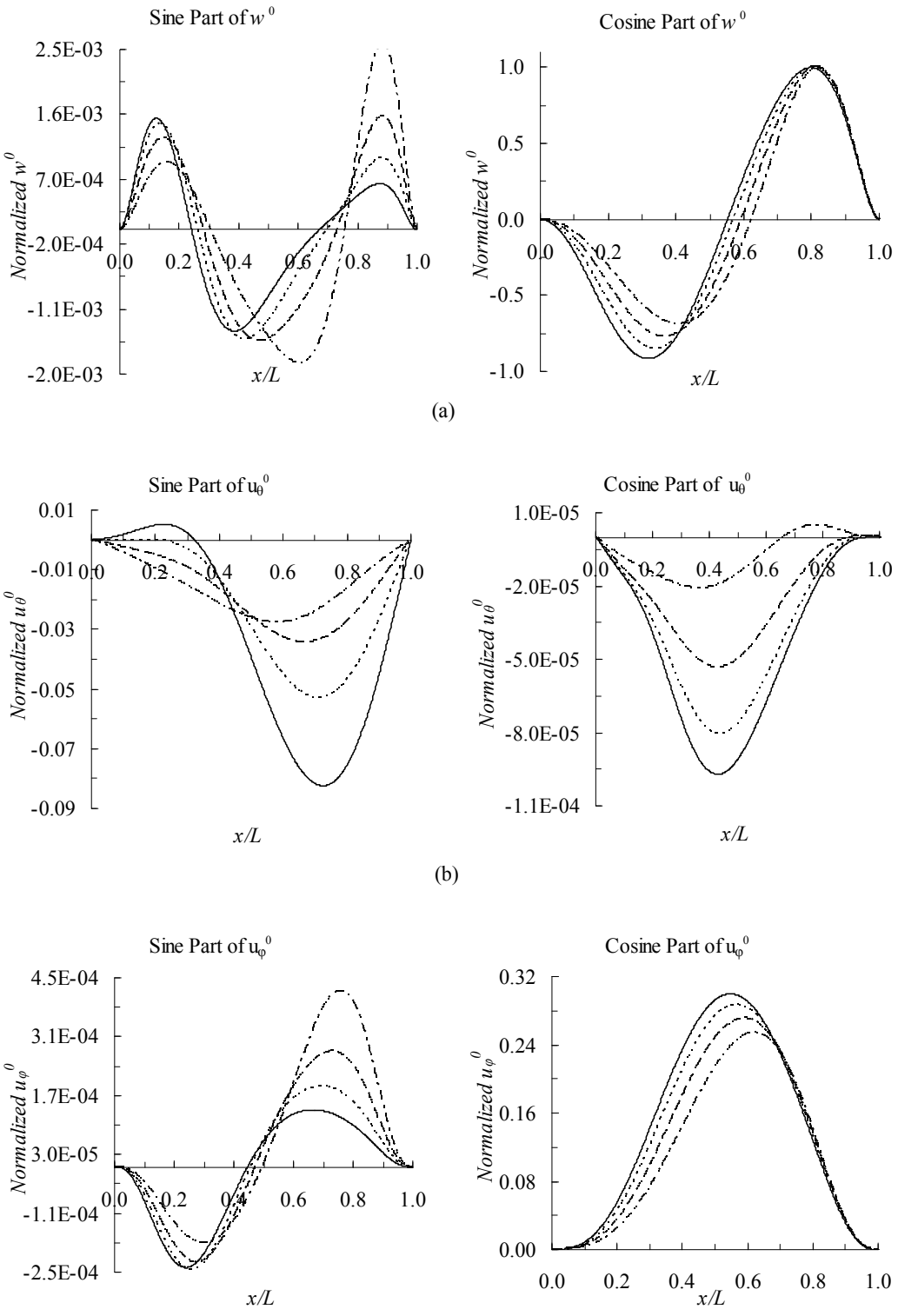

Figure 5.28 ***(a)*** Lateral, ***(b)*** circumferential, ***(c)*** meridional displacement mode shapes for spherical shell of revolution; α_1=25°

———: geodesic; — — — : fst=0.1; — · — · —: fst=0.2 ; - - - - - : fst=0.3

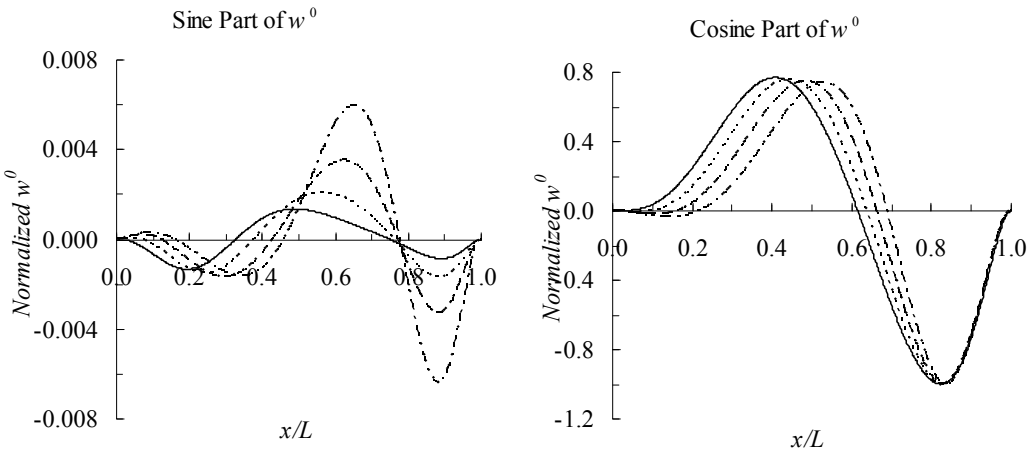

(a)

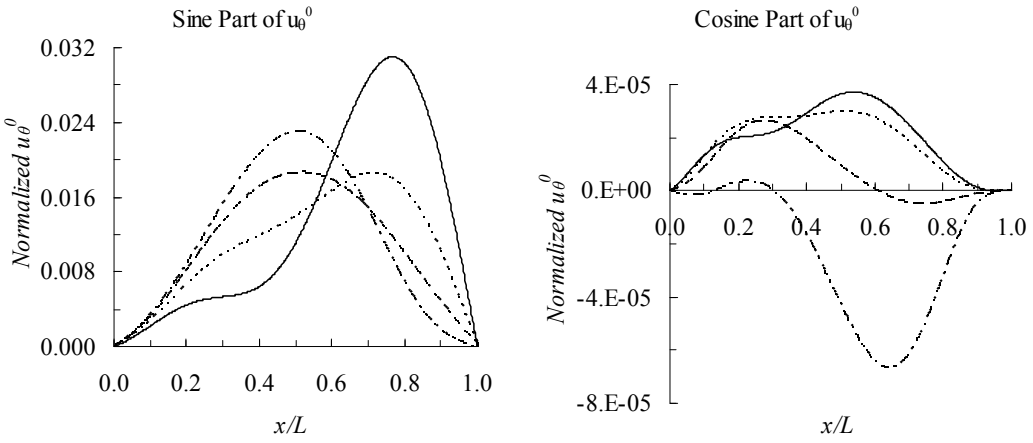

(b)

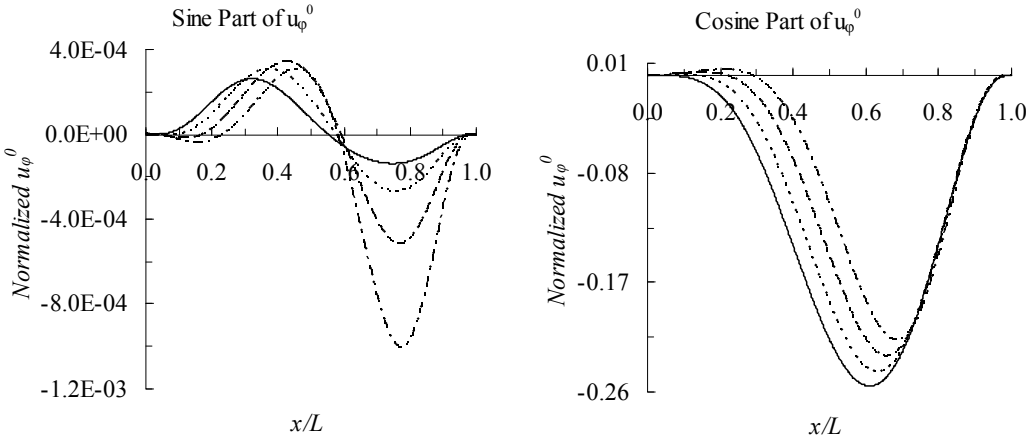

(c)

Figure 5.29 ***(a)*** Lateral, ***(b)*** circumferential, ***(c)*** meridional displacement mode shapes for spherical shell of revolution; α_1=45°

———: geodesic; — — — : fst=0.1; —·—·—: fst=0.2 ; - - - - - : fst=0.3

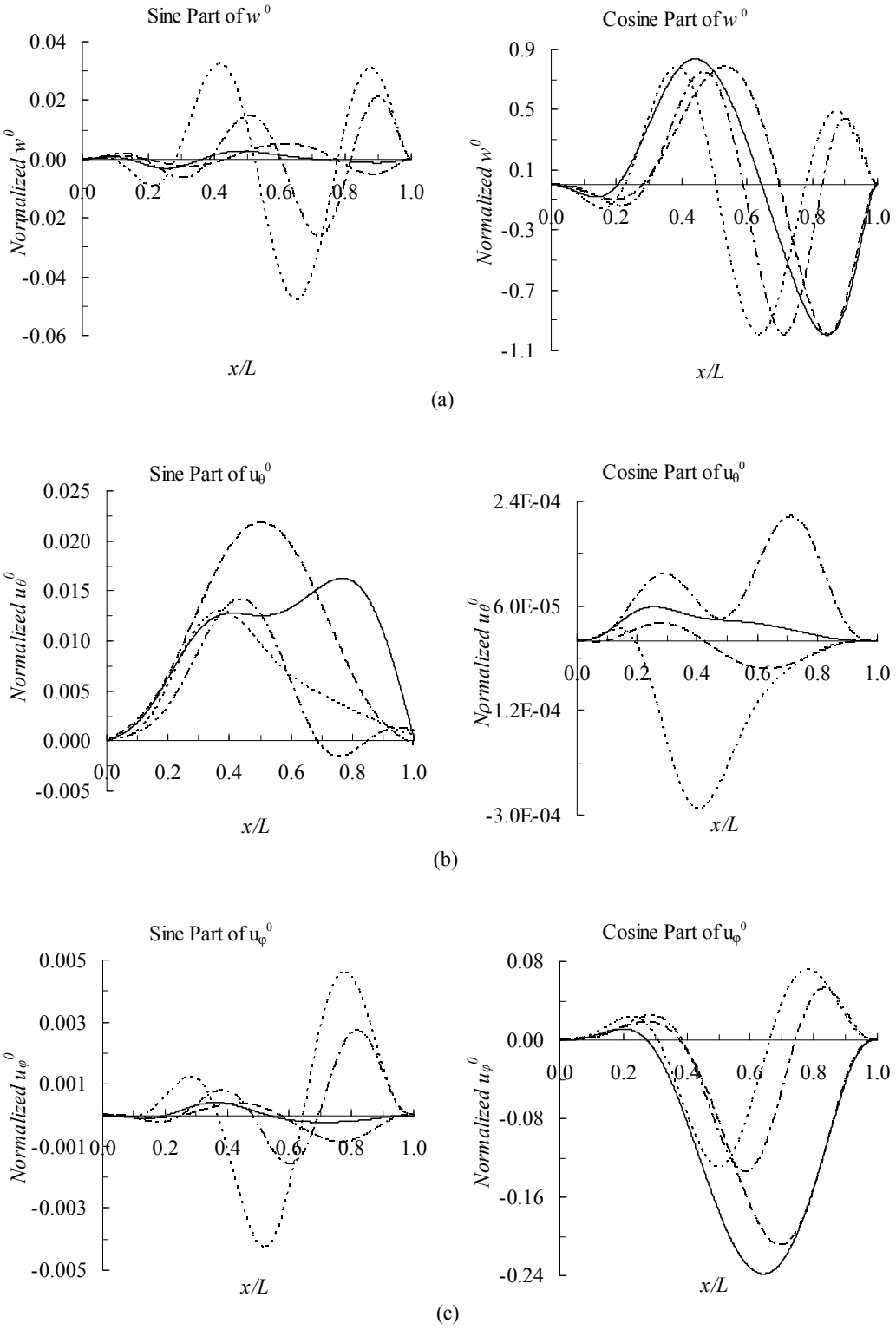

Figure 5.30 ***(a)*** Lateral, ***(b)*** circumferential, ***(c)*** meridional displacement mode shapes for spherical shell of revolution; α_1=65°

———: geodesic; — — — : fst=0.1; — · — · —: fst=0.2 ; - - - - - : fst=0.3

Examination of the mode shapes of the spherical shell of revolution reveals that similar to the conical shell example studied, the initial winding angle and the preset slippage tendency applied has a noticeable influence on the mode shapes. However, for the spherical shell configuration investigated, preset slippage tendency is also seen to be more effective when the initial winding angle is small, compared to the conical shell of revolution studied.

For the spherical shell of revolution the increase in the preset slippage tendency results in slight decreases in the bending stiffness in the meridional direction (D_{11}). Figures 5.21-5.23 show this, but since the stiffness values are very close to each other it is not easy to distinguish the curves from each other. Contrary to the conical shell example studied, the effect of slippage tendency on the mode shapes does not lead to a general conclusion which is valid for all initial winding angles and preset slippage tendencies. The main reason of this is the bending stiffness coefficients which are not varying noticeably with the changing slippage tendencies unlike conical shell bending stiffness terms which were increasing considerably with the increasing preset slippage tendency. This slight change in bending stiffness terms for a spherical shell might cause the thickness (inertia) and other stiffness terms to be more influential. However, it is difficult to comment on the effect of each term on the mode shape variation.

Figures 5.28-5.30 also show that the peaks of the displacements show up near the larger radius edge of the sphere for the different initial winding angle and preset slippage tendency cases studied. The main reason for this is that for the spherical shell of revolution studied the thickness and the stiffness coefficients decrease towards the large radius edge and therefore the peaks shift towards the large radius edge.

As for the conical shell it is seen that the preset slippage tendency can significantly affect the modes shapes of the spherical shell of revolution by altering the peak displacement locations and relative magnitudes. It can also be stated that for the spherical shell of revolution, introduction of slippage tendency is more influential also for small initial winding angle cases as opposed to the conical shells.

This influence of the slippage tendency on the natural frequencies and mode shapes of filament wound shells of revolution makes the preset slippage tendency, to be applied during the winding process, an important design parameter such that the designer will have one more parameter to control towards altering the dynamic characteristics of the shell of revolution during the design process.

CHAPTER 6

CONCLUSION AND FUTURE WORK

In the present study, multi-segment numerical integration technique is extended to the solution of the free vibration problem of composite shells of revolution which are wound along the semi-geodesic fiber paths counting on the preset slippage tendency used during the winding process. Winding laws which are applicable to general shells of revolution are specialized for conical and spherical shells of revolution and the continuous variation of the winding angle and the thickness due to different preset slippage tendency, which is applied during the winding process, is incorporated into the semi-analytical solution method.

Chapter 2 presented the governing equations and method of solution to the derived governing equations for the free vibration analysis for anisotropic laminated composite shells of revolution. The governing equations for the free vibration analysis are initially obtained in terms of fundamental shell variables, and they are reduced to a system of first order ordinary differential equations by the application of finite exponential Fourier Transform, resulting in a two point boundary value problem including 20 homogeneous linear first order ordinary differential equations which are written in matrix form in terms of a coefficient matrix *K*. The elements of the coefficient matrix *K* includes geometric and material properties of the shell of revolution, and for any linear shell theory and shell of revolution type a similar coefficient matrix can be derived. The resulting two point boundary value problem was reduced to a series of initial value problems. The multisegment numerical integration method was carried out via dividing the shell into segments so as to obtain series of convergent initial value problems which could be solved by any numerical integration routine available. Natural frequencies within a given range were calculated by the Frequency Trial Method employed by Kayran and Yavuzbalkan [57] which locates the probable natural frequencies by checking the slope change of the determinant of the characteristic matrix C_M. Once a natural frequency is found, the variation of the fundamental shell variables along the shell axis could be determined using the recursive relations obtained during the construction of the eigenvalue problem

Filament winding laws are reviewed in Chapter 3 to introduce the variation of the winding angle and the thickness of filament wound shells of revolution along the meridian due to the semi-geodesic winding. The geometry and winding patterns are the basic parameters governing the manufacturing of a filament wound shell of revolution. In this section the applicability of semi-geodesic fiber path, relying on the preset slippage tendency used during the manufacturing, is investigated. Specifically, the effect of preset slippage tendency on the variation of winding angle and the thickness along the meridian of the filament wound shells of revolution is studied. The expressions which gives the variation of winding angle along the longitudinal direction of shell are derived for a conical and spherical shell. Winding agle and thickness are the two important parameters which govern the stiffness coefficients. Sample calculations showed that in general, the use of higher preset slippage tendency in the winding process results in higher winding angle and thickness along the whole meridian of the shell of revolution. In this section, integration of semi-geodesic winding laws to the numerical integration based solution method for the dynamic analysis of filament wound shells of revolution is also described. The main conclusion of the combination of Chapters 2 and 3 is that as long as continuous variation, along the meridian of the shell of revolution, of the elements of the coefficient matrix K of the fundamental system of equations governing the free vibration of shells of revolution, is coded accordingly arbitrary meridional variation of the shell properties can be handled very accurately by the numerical integration based solution method. Therefore, once the effect of the semi-geodesic winding on the elements of the coefficient matrix is identified, by proper coding the effect of semi-geodesic winding on the free vibration characteristics of filament wound shells of revolution can be investigated by using the multi-segment numerical integration technique in combination with the frequency trial method.

In Chapter 4 results obtained by the semi-analytical solution method is compared with the results of finite element solution for a conical shell geometry. It is shown that for the particular shell geometry studied and preset slippage tendency of 0.2, finite element solution has a maximum 3% of deviation from the solution determined by the numerical integration based solution method.

In Chapter 5 sample studies on the effect of semi-geodesic winding on the stiffness coefficients and the free vibration characteristics have been performed for truncated conical and spherical shells of revolution. Sample calculations show that the use of higher preset slippage tendency in the winding process results in higher winding angle and thickness along the whole meridian of the shell of revolution. Based on the results obtained for the truncated conical and spherical shells of revolution, it is concluded that when the preset slippage tendency is increased circumferential bending stiffness (D_{22}) also increases, and at high circumferential wave numbers circumferential bending stiffness stands out as the dominant parameter governing the natural frequencies. Therefore, when the preset slippage tendency is increased, natural frequencies of higher circumferential vibration modes also increase irrespective of the initial winding angle. However, for low circumferential wave numbers a general conclusion on the effect of preset slippage tendency on

the natural frequencies cannot be drawn. Depending on the shell type and the initial winding angle, shells manufactured with low preset slippage tendency during the winding process may have higher natural frequencies than the shells manufactured with high preset slippage tendency. Example study on the lateral displacement mode shape of the conical shell also revealed that semi-geodesic winding may have a significant effect on the mode shapes depending on the preset slippage tendency used during the filament winding process. It is shown that the increase in the bending stiffness due to the use of higher preset slippage tendency may cause significant shifts in peak displacement and nodal point locations.

The great advantage of composite materials over isotropic materials are their tailorability according to the needs for the specific application. However, traditional geodesic path dependancy of the filament winding method defined by the winding laws limited the options of the designer compared to other manufacturing techniques. Thus, each parameter improving the flexibility of the design and optimization process will allow a more optimized solution and broaden the application field. The influence of the preset slippage tendency on the natural frequencies and mode shapes makes it a new parameter to control the dynamic properties of shells of revolution. This influence shown throughout this thesis will provide more flexibility to the designer during the optimization process of the structure.

Present study shows that continuous variation of the winding angle and thickness in the meridional direction, due to the different preset slippage tendency applied during the winding process, can be handled very accurately by the multi-segment numerical integration technique because of the very reliable numerical integration routines that are available. Therefore, numerical integration based solution technique in combination with the frequency trial method provides a very powerful solution alternative to the vibration analysis of shells of revolution wound by using semi-geodesic fiber paths.

6.1 RECOMMENDATIONS FOR FUTURE WORK

The method presented can also be extended to the static problems. Thus, stress analysis of filament wound laminated composite shell of revolution which are wound along semi-geodesic fiber paths with general boundary conditions can be carried out by any linear shell theory including transverse shear deformation. The static solution under axisymmetric loading can further be extended to include the geometric and material nonlinearity effects for any available nonlinear shell theory by using the solution method outlined by Kalnins [59].

The method of solution can further be extended to higher order transverse shear deformation theories by modifying the coefficient matrix K. There is no need of using the shear correction factor when higher order transverse shear deformation theories are used.

Possibility of extending the present method of solution to the laminated shells of revolution which are modeled as layerwise rather than as an equivalent single layer can be sought.

Semi-geodesic winding pattern effect can be analysed for different conical and spherical shell geometries and effect of geometrical properties on the vibration characteristics can be investigated. Structures other than conical and spherical shapes such as paraboloidal shells of revolution can be studied.

For the present study, winding of the filaments is assumed to be starting from the small radius end of the shell of revolution. The effect of winding pattern on the vibration characteristics can be also be analyzed for the case for which the winding starts from the large radius end of the shell.

REFERENCES

[1] Jones, R. M., “Mechanics of Composite Materials”, USA, 1999, pg. 2.

[2] Stephen W. Tsai, “Theory of Composite Design”, USA, 1992, ch. 1, pg. 1-8.

[3] Daniel Gay, Suong V. Hoa, Stephen W. Tsai, “Composite Materials Design and Applications”, USA, 2003, pg. 3-27.

[4] Vinson, J. R., R. L. Sierakowski, “Behavior of Structures Composed of Composite Materials”, USA, 1987, pg. 14, pg. 149-171.

[5] Allen A. K., MSc. Thesis, “A method for winding advanced composites of unconventional shapes using continuous and aligned fibers”, Brigham Young University, 2004, pg. 4.

[6] M. Lossie, H. Van Brussel, “Design Principles in Filament Winding”, Composites Manufacturing, Volume 5, Issue 1, March 1994, Pages 5-13

[7] Cheol-Ung Kim, Ji-Ho Kang, Chang-Sun Hong, Chun-Gon Kim,” Optimal design of filament wound structures under internal pressure based on the semi-geodesic path algorithm”, Composite Structures 67 (2005) 443–452.

[8] J.G. Teng, J.F. Chen, S.T. Smith and L. Lam, FRP Strengthened RC Structures, (John Wiley and Sons. West Sussex, England, 2002), pp. 1-10, 100-108, 148-236.

[9] S. Poveromo, Fall 2003, “The Use of Fiber Reinforced Polymer Composites to Retrofit Reinforced Concrete Bridge Columns”, MATE 115 Course Paper, San Jose State University.

[10] Ochoa O. O., Salama M. M., “Offshore Composites: Transition Barriers to an Enabling Technology”, Composites Science and Technology 65(2005) 2588-2596.

[11] P. Xu, J. Y. Zheng, P.F. Liu, “Finite element analysis of burst pressure of composite hydrogen vessel”, Materials and Design 30(2009) 2295-2301.

[12] Antonio Miravete, “Processing and Manufacturing”, Composite Design Tutorial at Stanford University (September 2009).

[13] ATS Press Release, Grevenbroich, 20.11.2009.

[14] Choong-Yul Son, Keon-Hoon Kim, Kang-Su Lee, Jung-Tak Lee, Jong-Bum Won, ,”Study on Natural Frequency of Offshore Wind Turbine Tower” INHA University Department of Naval Architecture & Ocean Engineering Incheon 402-751 Korea.

[15] EWEA Offshore Report, “Oceans of Opportunity”, 2009.

[16] Ross D. K., “Hydrogen Storage: the major technical barrier to the development of hydrogen fuel cell cars”, Vacuum 2006, 80:1084-91.

[17] Baruch M., Arbocz J., and Zhang GQ., 1994, “Laminated Conical Shells-Considerations for the Variations of the Stiffness Coefficients,” Proceedings of the 36th AIAA/ASME/ASCE/AHS/ASC S.S.D.M. conference, Hilton Head, SC, USA, pp. 2505-2516.

[18] Goldfeld Y., and Arbocz J., 2004, ‘Buckling of Laminated Conical Shells Given the Variations of the Stiffness Coefficients,’ AIAA Journal, Vol. 42, No.3, pp. 642-649.

[19] Wells, G.M., and McAnulty, K.F., 1987, "Computer Aided Filament Winding Using Non-Geodesic Trajectories," Proc. 6th International Conferenceon Composite Materials-ICCM-VI, F.L. Matthews et al., eds., Elsevier Applied Science, London, 2, pp. 161-173.

[20] Lossie, M., and Van Brussel, M., 1994, "Design Principles in Filament Winding," Composite Manufacturing., 5(1), pp. 5-13.

[21] Scholliers, J., and Van Brussel, M., 1994, "Computer-Integrated Filament Winding: Computer-Integrated Design, Robotic Filament Winding and Robotic Quality Control," Composite Manufacturing., 5(1), pp. 15-23.

[22] Lossie, M., and Van Brussel, M., 1994, "Design Principles in Filament Winding" Composite Manufacturing, 5(1), pp. 5-13.

[23] Baruch M., Arbocz J., and Zhang GQ., 1994, “Laminated Conical Shells-Considerations for the Variations of the Stiffness Coefficients,” Proceedings of the 36th AIAA/ASME/ASCE/AHS/ASC S.S.D.M. conference, Hilton Head, SC, USA, pp. 2505-2516.

[24] Wells, G.M., and McAnulty, K.F., 1987, "Computer Aided Filament Winding Using Non-Geodesic Trajectories," Proc. 6th International Conferenceon Composite Materials-ICCM-VI, F.L. Matthews et al., eds., Elsevier Applied Science, London, 2, pp. 161-173.

[25] Scholliers, J., and Van Brussel, M., 1994, "Computer-Integrated Filament Winding: Computer-Integrated Design, Robotic Filament Winding and Robotic Quality Control," Composite Manufacturing., 5(1), pp. 15-23.

[26] Vinson, J. R. and T. W. Chou”Composite Materials and Their Use in Structures”, Applied Science Publishers, London, 1975.

[27] Wilkins, D. J. and T. S. Love, “Combined Compression-Torsion Buckling Tests of Laminated Composite Cylindrical Shells”, AIAA Journal of Aircraft, vol. 12, No:11, (1975): 885-889.

[28] White, J. C., “The Flexural Vibrations fo Thin Laminated Cylinders”, Journal of Engineering Industry (1961), 397-402.

[29] Dong, S. B., “ Free Vibration of Laminated Orthotropic Cylindrical Shells”, Journal of the Acoustical Society of America, vol. 44 (1968):1628-1635.

[30] Bert, C. W., V. Baker and D. Egke, “Free Vibrations of Multilayer Anisotropic Cylindrical Shells”, Journal of Composite Materials, vol. 3 (1969): 480-499.

[31] Tasi, J., “Reflection of Extension Waves at the End of a Thin Cylindrical Shell”, Journal of Acoustical Society of America, vol. 44 (1968): 291-292.

[32] Tasi, J., " Effect of Heterogeneity on the Axisymmetric Vibration of Cylindrical Shells", Journal of Sound and Vibration, vol. 14 (1971) 325-328.

[33] Mirsky, I. 'Vibration of Orthotropic, Thick, Cylindrical Shells", Journal of Acoustical Societyof America, vol. 36 (1964): 41-51.

[34] Mirsky, I. "Axisymmetric Vibrations of Orthotropic Cylinders", Journal of Acoustic Society of america, vol.36 (1964): 2106-2112.

[35] Dong, S. B. And Tso, "On a Laminated Orthotropic Shell Theory Including Transverse Shear Deformation", Journal of Applied Mechanics, vol. 39(1972): 1091-1097.

[36] Sun, C. T. And Whitney, J. M. "Axisymmetric Vibrations of Laminated Composite Cylindrical Shells", Journal of the Acoustical Society of America, vol. 55 (1974): 1238-1246.

[37] Noor, A.K., and Peters, J.M., 1987, "Vibration Analysis of Laminated Anisotropic Shells of Revolutions," Computer Methods in Applied Mechanics and Engineering, 61, pp. 277-301.

[38] Xi, Z.C., Yam, L.H., and Leung, T.P., 1996, "Semi-analytical Study of Free Vibration of Composite Shells of Revolution Based on the Reissner-Mindlin Assumption," International Journal of Solids and Structures, 33, pp. 851-863.

[39] Correia, I.F., Barbosa, J.I., Soares, C.M.M., and Soares, C.A.M., 2000, "A Finite Element Semi-analytical Model for Laminated Axisymmetric Shells: Statics, Dynamics and Buckling," Computers and Structures, 76, pp.299-317.

[40] Ferreira, A.J.M., Roque, C.M.C., and Jorge, R.M.N., 2007, "Natural Frequencies of FSDT Cross-Ply Composite Shells by Multiquadrics," Composite Structures, 77, pp.296-305.

[41] Nguyen-Van, H., Mai-Duy, N., and Tran-Cong,T., 2008, "Free Vibration Analysis of Laminated Plate/Shell Structures Based on FSDT with a Stabilized Nodal-Integrated Quadrilateral Element, " Journal of Sound and Vibration, 313, pp.205-223.

[42] Korjakin A., Rikards R., Chate A., and Altenbach H., 1998, "Analysis of Free Damped Vibrations of Laminated Composite Conical Shells, " Composite Structures, 4, pp.39-47.

[43] Park, J.S., Hong, C.S., Kim, C.G., and Kim, C.U., 2002, "Analysis of Filament Wound Composite Structures Considering the Change of Winding Angles Through the Thickness Direction, " Composite Structures, 55, pp. 63-71.

[44] Yavuzbalkan, E., 2005, "Free Vibration Analysis of Anisotropic Laminated Composite Shells of Revolution," MSc Thesis, Department of Aerospace Engineering, Middle East Technical University, Ankara, Turkey.

[45] Quatu, Mohamad S. , "Recent Research Advances in the Dynamic Behavoir of Shells: 1989-2000, Part 1: Laminated Composite Shells," Applied Mechanics Reviews, 55(4), pp. 325-349, 2002.

[46] Koiter, W. T., "A Consistent First Approximation in the General Theory of Thin Elastic Shells," Proceedings of the Symposium on the Theory of Thin Elastic Shells, Amsterdam, North Holland, pp. 12-32, 1960.

[47] Toorani, M. H. ,and Lakis, A. A., "General Equations of Anisotropic Plates and Shells Including Transverse Shear Deformations, Rotatory Inertia and Initial Curvature Effects," Journal of Sound and Vibration, 237(4), pp. 561-615, 2000.

[48] Noor, Ahmed K., and Burton, W. Scott, “Assessment of Computational Models for Multilayered Composite Shells,” Applied Mechanics Reviews, 43(4), pp. 67-97, 1990.

[49] Reddy, J. N., “Mechanics of Laminated Composite Plates-Theory and Analysis,” Boca Raton, USA, CRC Press, 1997.

[50] E.Reissner, A new derivation of the equations for the deformation of elastic shells, American Journal of Mathematics 63 (1941) 177-184.

[51] J.R. Vinson, R.L. Sierakowski, The Behaviour of Structures Composed of Composite Materials, 2nd Edition, Kluwer Academic Publishers, Dordrecht, The Netherlands, 2002.

[52] J.M. Whitney, The effect of transverse shear deformation on the bending of laminated plates, Journal of Composite Materials 3 (1969) 534-547.

[53] R.D.Mindlin, Influence of rotatory inertia and shear on flexural motions of isotropic, elastic plates, Journal of Applied Mechanics 18 (1951) 31-38.

[54] W. Soedel, Vibration of Shells and Plates, Marcel Dekker, New York, 1993.

[55] A.Kayran, J.R.Vinson, Free vibration analysis of laminated composite truncated circular conical shells, AIAA Journal 28 (1990) 1259-1269.

[56]A.Kalnins, Free vibration of rotationally symmetric shells, Journal of the Acoustical Society of America 36 (1964) 1355-1365.

[57] Kayran A., and Yavuzbalkan, E., 2009, "Semi-analytical Study of free Vibration Characteristics of Shear deformable Filament Wound Anisotropic Shells of Revolution, " Journal of Sound and Vibration, 319, pp.260-281.

[58] Arnold, R.N., and Warburton, G.B., 1949, "Flexural Vibrations of the Walls of Thin Cylindrical Shells Having Freely Supported Ends," Proceedings of the Royal Society of London, Series A, Mathematical and Physical Sciences, 197, pp. 238-256.

[59] Kalnins, A., and Lestingi, J.F., On Nonlinear Analysis of Elastic Shells of Revolution,” Journal of Applied Mechanics, March 1967, pp. 59-64.

APPENDIX A

VARIATION OF WINDING ANGLE FOR CONICAL SHELLS OF REVOLUTION

Considering the geometrical properties given in Figure 3.2, Eq. (A.1) and (A.2) are written;

$$\tan\beta = \frac{R}{x} \tag{A.1}$$

$$\left\{\begin{matrix} R = x.\tan\beta \\ R` = \tan\beta \\ R`` = 0 \end{matrix}\right\} \tag{A.2}$$

The variation of the winding angle of filament wound shells of revolution along the meridian is derived in [43] and given in the form;

$$\frac{d\alpha}{dx} = \frac{fst\left((1+R'^2)\sin^2\alpha - RR''\cos^2\alpha\right) - (1+R'^2)R'\sin\alpha}{R(1+R'^2)\cos\alpha} \tag{A.3}$$

Substitution of Eqs. (A.2) into Eq. (A.3), leads to Eq. (A.5) for a conical shell of revolution;

$$\frac{d\alpha}{dx} = \frac{fst.\sin^2\alpha - \tan\beta.\sin\alpha}{x.\tan\beta.\cos\alpha} \tag{A.4}$$

$$\frac{d\alpha}{dx} = \frac{\left(fst.\sin\alpha - \tan\beta\right)\tan\alpha}{x.\tan\beta} \tag{A.5}$$

Eq. (A.5) can be integrated as follows;

$$\frac{\tan\beta.d\alpha}{\left(fst.\sin\alpha-\tan\beta\right).\tan\alpha}=\frac{dx}{x} \tag{A.6}$$

$$\int_{\alpha_1}^{\alpha}\frac{\tan\beta}{\left(fst.\sin\alpha-\tan\beta\right).\tan\alpha}d\alpha=\int_{x_1}^{x}\frac{1}{x}dx \tag{A.7}$$

$$\tan\beta\int_{\alpha_1}^{\alpha}\frac{1}{\left(fst.\sin\alpha-\tan\beta\right).\tan\alpha}d\alpha=\ln\left(\frac{x}{x_1}\right) \tag{A.8}$$

Integrating the right hand side of the Eq. (A.7), absolute values are not used for x and x_1 as both terms are positive considering the convention shown in Figure 3.2.

Applying integration by parts;

$$\left\{\begin{matrix}\sin\alpha=u\\ \cos\alpha.d\alpha=du\end{matrix}\right\} \tag{A.9}$$

$$\tan\beta\int_{\alpha=\alpha_1}^{\alpha=\alpha}\frac{1}{u.\left(fst.u-\tan\beta\right)}du=\ln\left(\frac{x}{x_1}\right) \tag{A.10}$$

Eq. (A.10) can be represented as follows;

$$\tan\beta\int_{\alpha=\alpha_1}^{\alpha=\alpha}\left[\frac{D}{u}+\frac{E}{\left(fst.u-\tan\beta\right)}\right]du=\ln\left(\frac{x}{x_1}\right) \tag{A.11}$$

where

$$\frac{1}{u.\left(fst.u-\tan\beta\right)}=\frac{D}{u}+\frac{E}{\left(fst.u-\tan\beta\right)}$$

Considering the polynomial equivalence;

$$D.fst.u-D.\tan\beta+E.u=1$$

$$\left\{\begin{matrix}D.fst+E=0\\ -D.\tan\beta=1\end{matrix}\right\}$$

$$\left\{\begin{matrix}D=\dfrac{-1}{\tan\beta}\\ E=\dfrac{fst}{\tan\beta}\end{matrix}\right\} \tag{A.12}$$

Substituting Eq. (A.12) into Eq. (A.11) and simplifying;

$$-\int_{\alpha=\alpha_1}^{\alpha=\alpha}\frac{1}{u}du+\int_{\alpha=\alpha_1}^{\alpha=\alpha}\frac{1}{u-\dfrac{\tan\beta}{fst}}du=\ln\left(\frac{x}{x_1}\right) \tag{A.13}$$

Then, Eq. (A.13) can be integrated and Eq. (A.9) can be substituted back;

$$\ln\left(\frac{x}{x_1}\right)=-\ln\left|\sin\alpha\right|_{\alpha_1}^{\alpha}+\ln.\left|\sin\alpha-\frac{\tan\beta}{fst}\right|_{\alpha_1}^{\alpha}$$

$$\ln\left(\frac{x}{x_1}\right)=-\ln\left|\sin\alpha\right|+\ln\left|\sin\alpha_1\right|+\ln.\left|\sin\alpha-\frac{\tan\beta}{fst}\right|-\ln.\left|\sin\alpha_1-\frac{\tan\beta}{fst}\right|$$

$$\ln\left(\frac{x}{x_1}\right)=\ln\left[\frac{\left|\sin\alpha_1\right|.\left|\sin\alpha-\dfrac{\tan\beta}{fst}\right|}{\left|\sin\alpha\right|.\left|\sin\alpha_1-\dfrac{\tan\beta}{fst}\right|}\right]$$

Considering that sin α and sin α_1 have the same sign, absolute values can be eliminated from these terms;

$$\frac{x}{x_1}=\frac{\sin\alpha_1.\left|\sin\alpha-\dfrac{\tan\beta}{fst}\right|}{\sin\alpha.\left|\sin\alpha_1-\dfrac{\tan\beta}{fst}\right|} \tag{A.14}$$

There exist two solutions for Eq. (A.14):

1) $\sin\alpha-\dfrac{\tan\beta}{fst}>0$ and $\sin\alpha_1-\dfrac{\tan\beta}{fst}>0$

OR

$\sin\alpha-\dfrac{\tan\beta}{fst}<0$ and $\sin\alpha_1-\dfrac{\tan\beta}{fst}<0$

In this case the absolute value signs in Eq. (A.14) can be removed and the terms inside the absolute value signs can be taken out as they are, yielding:

$$x_1\sin\alpha_1\sin\alpha-x_1\sin\alpha_1\frac{\tan\beta}{fst}-x\sin\alpha_1\sin\alpha+x\sin\alpha\frac{\tan\beta}{fst}=0$$

$$\sin\alpha = \frac{x_1.\sin\alpha_1.\tan\beta}{fst.\sin\alpha_1.(x_1 - x) + x.\tan\beta} \tag{A.15}$$

Or in other form, if x_1 and x are substituted by $\frac{R_1}{\tan\beta}$ and $\frac{R}{\tan\beta}$ respectively, Eq. (A.15) becomes;

$$\sin\alpha = \frac{R_1.\sin\alpha_1.\tan\beta}{fst.\sin\alpha_1.(R_1 - R) + R.\tan\beta} \tag{A.16}$$

2) $\sin\alpha - \frac{\tan\beta}{fst} > 0$ and $\sin\alpha_1 - \frac{\tan\beta}{fst} < 0$

OR

$\sin\alpha - \frac{\tan\beta}{fst} < 0$ and $\sin\alpha_1 - \frac{\tan\beta}{fst} > 0$

In this case when the absolute value signs in Eq. (A.14) are removed a minus sign will show up such that after manipulations second solution will be given by Eq. (A.17).

$$-x_1\sin\alpha_1\sin\alpha + x_1\sin\alpha_1\frac{\tan\beta}{fst} - x\sin\alpha_1\sin\alpha + x\sin\alpha\frac{\tan\beta}{fst} = 0$$

$$\sin\alpha = \frac{x_1.\sin\alpha_1.\tan\beta}{fst.\sin\alpha_1.(x_1 + x) - x.\tan\beta} \tag{A.17}$$

Or in other form, if x_1 and x are substituted by $\frac{R_1}{\tan\beta}$ and $\frac{R}{\tan\beta}$ respectively, Eq. (A.17) becomes;

$$\sin\alpha = \frac{R_1.\sin\alpha_1.\tan\beta}{fst.\sin\alpha_1.(R_1 + R) - R.\tan\beta} \tag{A.18}$$

Thus, solution of Eq. (A.5) leads to two solutions as given in Eq. (A.15) and (A.17). The solution depends on the sign of $\sin\alpha - \frac{\tan\beta}{fst}$ and $\sin\alpha_1 - \frac{\tan\beta}{fst}$.

Note that initial winding angle (α_1), preset slippage tendency (*fst*), and cone angle (β) are design parameters and they do not vary for a specific design. Winding angle (α) is the only parameter changing during the winding process and this variation is according to Eq. (A.5). It should also be noted that, winding angle at any meridional location is not known a priori before the solution of Eq. (A.5). This leads to the conclusion that for specific cases (depending on β, *fst* and α_1) only Eq.

(A.15) or only Eq. (A.17), or both equations might be valid, which might give two possible positions for the winding angle for a conical shell of revolution.

However, the validity of those two solutions should be checked considering the continuity law in the solution interval. According to the continuity law, if the derivative of $\alpha(x)$ exists in the meridional axis from x_1 to x, then it must be continuous in this interval. Considering that *sin* α is a continuous function, following statement can be concluded.

For infinitely small $|x-x_1|$, α must go to α_1, and $\sin\alpha$ must go to $\sin\alpha_1$. This means that, $\sin\alpha - \frac{\tan\beta}{fst}$ and $\sin\alpha_1 - \frac{\tan\beta}{fst}$ must have the same sign to satisfy the continuity requirement.

This analysis shows clearly that Eq. (A.5) has only one solution, which is Eq. (A.15) and at any meridional location only one winding angle is possible to satisfy the semi-geodesic winding with desired preset slippage tendency.

APPENDIX B

VARIATION OF WINDING ANGLE FOR SPHERICAL SHELLS OF REVOLUTION

The variation of the winding angle of filament wound shells of revolution along the meridian is derived in [43] and given in the form;

$$\frac{d\alpha}{dx} = \frac{fst\left((1+R'^2)\sin^2\alpha - R\,R''\cos^2\alpha\right) - (1+R'^2)R'\sin\alpha}{R(1+R'^2)\cos\alpha} \tag{B.1}$$

For spherical shells of revolution or any general shell of revolution, the variation of the winding angle with respect to meridional coordinate ϕ should be obtained. Therefore, first a relationship between $\frac{\mathrm{d}\alpha}{\mathrm{d}\phi}$ and $\frac{\mathrm{d}\alpha}{\mathrm{d}x}$ will be obtained.

The term $\frac{d\alpha}{d\phi}$ can be derived as follows: Employing chain rule for $\frac{d\alpha}{dx}$,

$$\frac{\mathrm{d}\alpha}{\mathrm{d}x} = \frac{d\alpha}{d\phi}.\frac{d\phi}{dx} \tag{B.2}$$

For a spherical shell of revolution R_θ and R_ϕ is equal to the radius of the sphere R_s and R is given by R_s .sin ϕ;

$$\begin{cases} R_\phi = R_\theta = R_s \\ dx = ds\sin\phi \\ ds = R_\phi d\phi \end{cases} \tag{B.3}$$

Applying chain rule for $\frac{\mathrm{d}\phi}{\mathrm{d}x}$

$$\frac{\mathrm{d}\phi}{\mathrm{d}x}=\frac{\mathrm{d}\phi}{\mathrm{d}s}\frac{\mathrm{d}s}{\mathrm{d}x}=\frac{1}{\mathrm{R}_{\phi}}\frac{1}{\sin\phi} \tag{B.4}$$

Therefore, substituting Eq. (B.3) into Eq. (B.4);

$$\frac{d\alpha}{d\mathrm{x}}=\frac{d\alpha}{d\phi}\frac{1}{R_{\phi}\sin\phi}=\frac{d\alpha}{d\phi}\frac{1}{R_{\mathrm{s}}\sin\phi}$$

$$\frac{d\alpha}{d\phi}=\frac{d\alpha}{d\mathrm{x}}R_{\mathrm{s}}\sin\phi \tag{B.5}$$

In Eq. (B.1), there appear R' and R'', which are the derivatives of R with respect to x, axial coordinate. These derivatives also should be written with respect to the meridional coordinate.

$$\begin{cases} R=R_s\sin\phi \\ \dfrac{\mathrm{d}R}{\mathrm{d}\phi}=R_s\cos\phi \\ \dfrac{\mathrm{d}^2R}{\mathrm{d}\phi^2}=-R_s\sin\phi \end{cases} \tag{B.6}$$

Employing chain rule for $\frac{\mathrm{d}R}{\mathrm{d}x}$ and substituting Eq. (B.4) and Eq. (B.6);

$$\frac{dR}{dx}=\frac{dR}{d\phi}\frac{d\phi}{dx}=\frac{dR}{d\phi}\frac{1}{R_s\sin\phi}$$

$$\frac{dR}{dx}=\frac{R_s\cos\phi}{R_s\sin\phi}$$

$$\frac{\mathrm{d}R}{\mathrm{d}x}=\cot\phi \tag{B.7}$$

2nd derivative of R with respect to x, axial coordinate can be calculated as follows;

$$\frac{d^2R}{dx^2}=\frac{d}{dx}\left[\frac{dR}{d\phi}\frac{1}{R_s\sin\phi}\right]=\frac{d}{d\phi}\left[\frac{dR}{d\phi}\frac{1}{R_s\sin\phi}\right]\frac{d\phi}{dx} \tag{B.8}$$

Again substituting Eq. (B.4) and Eq. (B.6);

$$\frac{d}{d\phi}\left[\frac{dR}{d\phi}\frac{1}{R_s\sin\phi}\right]\frac{d\phi}{dx}=\left[\frac{d^2R}{d\phi^2}\frac{1}{R_s\sin\phi}-\frac{dR}{d\phi}\frac{\cos\phi}{R_s\sin^2\phi}\right]\frac{1}{R_s\sin\phi}$$

$$\frac{d}{d\phi}\left[\frac{dR}{d\phi}\frac{1}{R_s\sin\phi}\right]\frac{d\phi}{dx}=\left[-R_s\sin\phi\frac{1}{R_s\sin\phi}-R_s\cos\phi\frac{\cos\phi}{R_s\sin^2\phi}\right]\frac{1}{R_s\sin\phi}$$

$$\frac{d}{d\phi}\left[\frac{dR}{d\phi}\frac{1}{R_s\sin\phi}\right]\frac{d\phi}{dx}=\left[-1-\frac{\cos^2\phi}{\sin^2\phi}\right]\frac{1}{R_s\sin\phi}$$

$$\frac{d}{d\phi}\left[\frac{dR}{d\phi}\frac{1}{R_s\sin\phi}\right]\frac{d\phi}{dx}=\frac{-1}{R_s\sin\phi}\left[1+\cot^2\phi\right]$$

$$\frac{d^2R}{dx^2}=\frac{-1}{R_s\sin\phi}\left[1+\cot^2\phi\right] \qquad \text{(B.9)}$$

Once terms in Eq. (B.1) are derived, $\frac{d\alpha}{d\phi}$ can be obtained as follows;

$$\frac{\mathrm{d}\alpha}{\mathrm{d}\phi}=\frac{\mathrm{d}\alpha}{\mathrm{d}x}\mathrm{R}_s\sin\phi=R_s\sin\phi\left\{\frac{fst\left[\left(1+R'^2\right)\sin^2\alpha-RR''\right]-(1+R'^2)R'\sin\alpha}{R(1+R'^2)\cos\alpha}\right\} \qquad \text{(B.10)}$$

Substituting Eq. (B.7) and Eq. (B.9), 1st and 2nd derivative of R with respect to x, into Eq. (B.10) and simplifying;

$$\frac{\mathrm{d}\alpha}{\mathrm{d}\phi}=\frac{fst.(\sin^2\alpha+\cos^2\alpha)-\cot\phi\sin\alpha}{\cos\alpha}$$

$$\frac{\mathrm{d}\alpha}{\mathrm{d}\phi}=\frac{fst-\cot\phi\sin\alpha}{\cos\alpha} \qquad \text{(B.11)}$$

Unfortunately Eq. (B.11) cannot be explicitly integrated because ϕ and α variables cannot be separated. Therefore, it has to be integrated numerically from an initial winding angle of α_1 and the initial edge ϕ_1 to any meridional location ϕ where the winding angle will be α.

APPENDIX C

INFLUENCE OF MESH DENSITY ON FINITE ELEMENT MODEL UNDER FREE VIBRATION

Simulations with different mesh densities are realized in order to investigate the influence of mesh density on finite element model under free vibration.

Shell model is divided into 20, 50 and 70 segments in the meridional direction and natural frequency outputs are compared. For each case, 4 node quad elements are used and the global edge length is selected accordingly so that elements are close to a square shape. This lead to a greater mesh density as the number of the segments is increased.

In order to investigate the effect of mesh size, the thickness and winding angle are selected as constant along the meridional and circumferential direction. For the same truncated conical shell geometry analyzed in Chapter 4, thickness and winding angle at the mid location of the shell in meridional direction are calculated as 0.2231039 mm and 29.08485^{o} respectively. Calculated thickness and winding angle values are assigned to each and every element on the shell model.

The frequency output for three different mesh sizes are presented in Table C.1. From Table C.1, it can be seen that for all three mesh sizes, the calculated frequencies are almost the same. Only for n=0, 20 segment solution gives an output about 0.7% less than others.

Table C.1 Comparison of different mesh densities for the finite element solution

	FEM Output Fundamental Frequencies [Hz]		
n	20 Segment	50 Segment	70 Segment
0	685.54	689.19	690.20
1	660.10	660.64	660.70
2	566.38	566.54	566.59
3	455.56	455.55	455.61
4	359.86	359.83	359.89
5	284.82	284.84	284.88

Considering the presented simulation results, it is concluded that division of the shell model into 50 segments in meridional direction is a good compromise between output quality and computational cost.